TRAVEL TIME AND LOCATION PROBABILITIES FOR GROUNDWATER CONTAMINANT SOURCES

by

Jim (Jinzhong) Liu

Submitted in Partial Fulfillment of the Requirements
for the Degree of Master of Science in Hydrology

New Mexico Institute of Mining and Technology
Socorro, New Mexico

August 1995

ABSTRACT

When groundwater contamination is monitored in pumping wells or monitoring wells, the primary questions of regulatory concern are: Where did the contaminant come from and what was its release history? In order to address these questions, two types of probability are introduced in this research. The first probability is called a travel time probability. It describes how long it takes a contaminant to move from some prescribed location in the aquifer to the well. The second probability, called the location probability, helps define the origin of the contaminant observed or produced in the well. It gives the probability that the contaminant from some location in the aquifer will arrive at the well some specific time later. Both probabilities can be presented as probability density functions or cumulative distribution functions.

Wilson and his students (Wilson and Rao, 1992; Wilson and Liu, 1995) proposed the hypothesis that the probabilities for location and travel time can be directly computed by solving new backward–in–time partial differential equations with reversed flow. This method is called the backward–in–time method. We run only one single simulation and obtain the travel time or location probabilities for each possible location. Compared to previous research, the new method is more direct, faster, especially for multiple dimensions, and more economical, but it has never been tested in either theory or practice. This research is designed: (1) to examine the new method for one–dimensional advection and dispersion by formulating backward–in time partial differential equations along with appropriate boundary and initial conditions and then comparing the resulting solution to the normal forward–in–time solution; (2) to test the method's ability for use in two–dimensional domains; (3) to extend this new method to cases accounting for aquifer heterogeneity, chemical reactions, and natural recharge; and (4) to test its application in an actual field tracer test.

Using analytical solutions of one–dimensional backward–in–time partial differential equations, we have successfully tested the new hypothesis that backward problems can be formulated and solved. By proper selection of boundary and initial conditions at the well, one of two maps for travel time probability and location probabilities is obtained with only one simulation of a back-

wards–in–time partial differential equation. Travel time and location probabilities are related by Bayes theorem. Using the Laplace transform–in–time Galerkin finite element method, the simulated results show that the new method can account for dispersion, chemical reactions, heterogeneity, and natural recharge in a two–dimensional aquifer. The application of the new backward–in–time method to the capture zone tracer test at the Borden sites (Wilson and Linderfelt, 1995; Linderfelt, 1994) demonstrates that the new method, together with normalized measured tracer breakthrough, can be used to identify tracer injection sites and to delineate time–dependent capture zones for wellhead protection. The new method also can be applied to monitoring design and data interpretation, assignment of responsibility for observed contamination, and aquifer remediation.

ACKNOWLEDGEMENTS

I would like to express my appreciation to the members of my thesis committee for their support and suggestions throughout this study. I would especially like to thank Professor John Wilson, my advisor, for his guidance and encouragement, and for his generous sharing of knowledge and ideas. Professor Rob Bowman acted as technical advisor in all aspects of tracer implementation and analysis in the HPLC lab. Professor Allan Gutjahr was very helpful in dealing with the geostatistics and stochastics problems. Critical reviews by Dr. Jim McCord of the Sandia National Lab, Albuquerque, greatly improved the final version of this thesis. I also wish to thank Dr. Chia Chen, who is a former professor of New Mexico Tech, for his contributions to my graduate study and field experiment training.

I am grateful to all of the graduate students in the Hydrology Program who offered advice, assistance, or showed me how to work in the lab. and in aquifer tests. William Linderfelt worked on both the field experiment and interpretation of the tracer test in the Borden site. He showed me all the field information and his simulation results when I worked on the tracer analysis with the HPLC and performed the tracer concentration determinations. I am grateful to Rob Terberg, Monty Flishch, Chris Holmes, Jun Lin, Anil Mishra, Paul Holfmann, Tongying Shun, Lance Hughson, and Mitch Plummer.

Thanks to LuAnn Pavletich for her help in editing this thesis. Thanks to Edith Montoya and Pat Mills for their assistance.

The research was funded by the U.S. Department of Energy, through the New Mexico Waste-management Education & Research Consortium (WERC).

This thesis is dedicated to my parents who through my childhood and young adult years, have provided both financial and a great deal of moral support. Lastly, I would like to thank my wife Ying and my son Jesse, for their patience, especially during the final stages of this work.

TABLE OF CONTENTS

LIST OF TABLES

LIST OF FIGURES

LIST OF SYMBOLS

Symbol	Description
f_t	aqueous phase travel time PDF [1/T]
g_t	sorbed phase travel time PDF [1/T]
f_x	aqueous phase location PDF for one-dimension [1/L]
g_x	sorbed phase location PDF for one dimension [1/L]
f_X	aqueous phase location PDF for two dimensions [$1/L^2$]
g_X	sorbed phase location PDF for two-dimensions [$1/L^2$]
C^f	aqueous phase flux concentration [M/L^3]
C^r	aqueous phase resident concentration [M/L^3]
C^r_s	sorbed phase resident concentration [M/L^3]
D	dispersion coefficient [L^2/T]
D^*	diffusion coefficient [L^2/T]
F_t	aqueous phase travel time CDF
G_t	sorbed phase travel time CDF
F_x	aqueous phase location CDF
G_x	sorbed phase location CDF
F_X	aqueous phase location CDF
G_X	sorbed phase location CDF
K_d	distribution coefficient [L^3/M]
V	average velocity [L/T]
R	retardation factor
t	time [T]
α	mass transport coefficient [1/T]
α_L	longitudinal dispersivity coefficient [L^2]
α_T	transverse dispersivity coefficient [L^2]
ϱ_b	soil bulk density [M/L^3]
θ	porosity
λ	decay rate [1/T]
τ	travel time [T]
$\frac{\partial}{\partial t}$, $\frac{\partial}{\partial \tau}$	partial differentiation with respect to time
$\frac{\partial}{\partial x}$; $\frac{\partial}{yx}$	partial differentiation with respect to distance

δ	delta function
erf	error function
erfc	complementary error function

1. INTRODUCTION

When groundwater contamination is monitored in pumping wells or monitoring wells, the primary questions of regulatory concern are: Where did the contaminant come from and what was its release history? Answers to these questions are complicated by: (1) uncertainties about the appropriate conceptual model and its parameters; (2) aquifer heterogeneity; (3) dispersion; (4) chemical reactions; (5) natural recharge; and (6) transient flow. In order to address these questions, we introduce conditional probabilities for travel time and for contaminant location. The travel time probability describes how long it takes a contaminant to move from some prescribed location in the aquifer to the well. It can be used to delineate a wellhead protection area. The location probability defines the probability that a contaminant originating at some location in the aquifer will arrive at the pumping well some specific time later. It is useful in identifying possible sources of past contamination and for monitoring design. Both probabilities can be presented as a probability density function (PDF) or a cumulative distribution function (CDF) (Wilson and Liu, 1994, 1995; Liu and Wilson, 1994). Each probability can be written in terms of the other, and each can be derived independently by solving one or more partial differential equations backward in time and space (Wilson, and Liu, 1995).

As an example, Figure 1.1 and 1.2 present, respectively, a two-dimensional travel time probability map and a location probability map. The ambient flow is from right to left at an average velocity of 1 m/d (porosity=0.3), with the well pumping at 5 m^3/day at location (20, 25). Figure 1.1a describes the travel time cumulative probability that groundwater contamination at various points in the aquifer will take 20 or fewer days to be captured by the pumping well. For example, at position A, there is a 20 percent probability that groundwater contamination will take less than 20 days to move from the prescribed location A in the aquifer to the well. Figure 1.1b describes the probability for a travel time less than 40 days. It shows that the capture zone extends in an upstream direction. Figure 1.2a illustrates the location

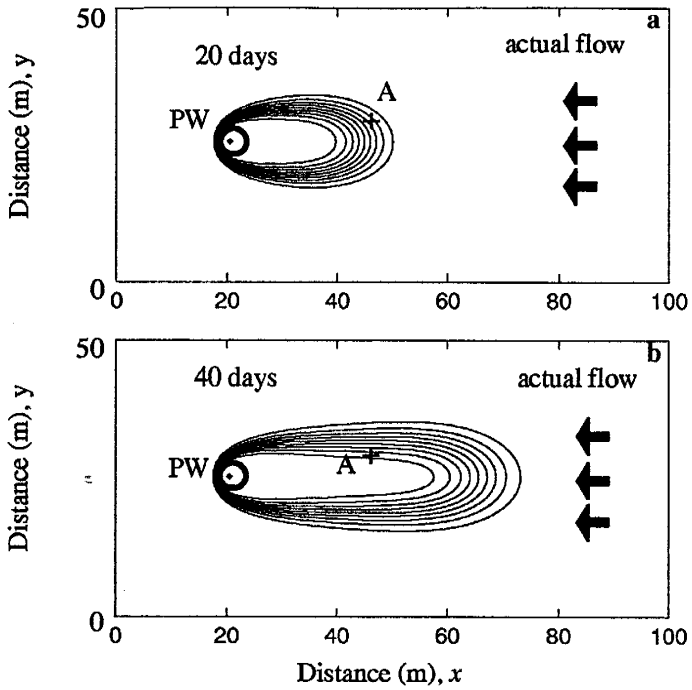

Figure 1.1. Two-dimensional travel time probability map constructed from a backward-in-time model. The actual flow is from right to left at velocity V_x=1.0 m/day, V_y=0; longitudinal dispersivity α_L=0.4 m, transverse dispersivity α_T=0.1 m. The actual pumping well (PW) is located at (20,25). The outermost contour line represents 0.1, and the contour interval value is 0.1. a. For 20 days; b. For 40 days

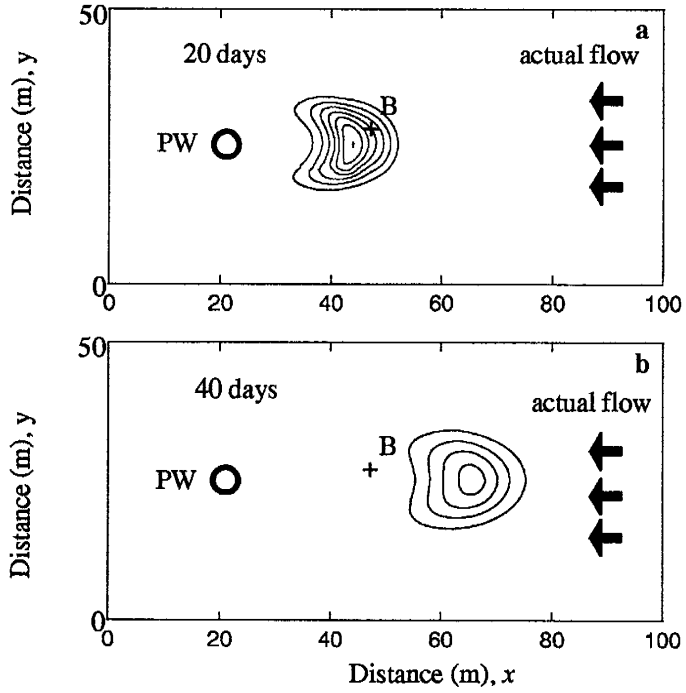

Figure 1.2. Two-dimensional location probability map constructed from a backward-in-time model. The outermost contour line represents 0.001, and the contour interval value is 0.001. a. For 20 days; b. For 40 days.

probability for a given time 20 days in the past. Suppose a single sample of contamination is observed in the well. Then this plot describes the location of that contamination 20 days earlier. For example, at position B, the probability is about 0.004 that the contaminant was located at position B. The highest probability for the contaminant's former location is located approximately 22 meters upstream of the well. Figure 1.2b illustrates the location probability for 40 days in the past. Over time, this location of the greatest probability has moved to 45m upstream of the well. Figures 1.1 and 1.2 represent fairly simple examples. The question then becomes: How can we accurately produce maps to represent increasingly complex cases of contamination?

1.1 Background

For the forward–in–time problem, a migrating plume of the contamination spreads and becomes diluted in the flowing groundwater. The plume is characterized by two measures of concentration: resident concentration and flux concentration. The resident concentration, $C^r(x,t)$, is the instantaneous mass density of contaminant in a fixed volume of pore space. It is defined as the mass of contaminant per unit volume of water. The flux concentration, $C^f(x,t)$, is defined as the ratio of the contaminant mass flux to the groundwater flux. It is the inflow or outflow concentration that moves through the fixed planes forming the boundaries of a transport volume. The flux concentration is linearly proportional to dispersivity and the gradient of resident concentration (Parker and Van Genuchten, 1984; Jury and Roth, 1990). In the standard forward–in–time problem, the normalization of the flux concentration describes an arrival time probability for a contaminant to arrive at a particular observation location from a prescribed source location (Jury and Roth, 1990; Henley and Kumamoto, 1992). When the source location is unknown, we may construct a travel time probability map by rerunning the forward–in–time simulations for each possible source location and computing arrival times for each one. This method takes much computation time and becomes very expensive.

Uffink (1988, 1989) developed a random walk particle transport code for the forward-in-time advection-dispersion problem. He ran it backward-in-time, with a reversed velocity field, to yield location probability. In this model, particles were injected into a pumping well and then moved away by advection and dispersion. This approach indicated that the advective part of the transport model is reversed while the dispersive part is left positive, as provided by a Chapman-Kolmogorov backward stochastic process (Uffink, 1989). The principle difference between this model and classical advective particle and front backtracking (Shafer, 1987a,b; EPA, 1990; Schafer-Perini and Wilson, 1991; Wilson and Linderfelt, 1990) is the incorporation of dispersion. In principle the dispersion can be hydrodynamic or macro. Wilson and Linderfelt (1991), Bagtzoglou et al. (1992), and Chin and Chittaluru (1994) also constructed location probability maps from the backward-in-time problem using similar random walk methods. Backward-in-time solutions for location probability have been limited to the random walk particle method.

Chin and Chittaluru (1994) and Wilson and Liu (1995) pointed out that the relationship between travel time and location probabilities can be described by the Bayes theorem, and this relationship can be used to translate one to the other. Chin and Chittaluru (1994) demonstrated this method by computing the travel time probability from the location probability. In this approach, the random walk model is used to determine the probability distribution of particle locations as a function of travel time to a pumping well; then the Bayes theorem is used to compute the travel time probability. Chin and Chittaluru's approach is limited to the random walk model.

Can we figure out a simpler and more direct method to address backward-in-time problems? Wilson and his students (Wilson and Rao 1992; Wilson and Liu, 1994) proposed a new hypothesis, in which the probabilities for location and travel time can be directly formulated by solving a new partial differential equation (PDE) for advection-dispersion. To implement this approach the flow problem is run backwards-in-time, with inflow and outflows reversed. Groundwater pumping becomes groundwater injection and distributed natural re-

charge becomes a prescribed discharge. The advection–dispersion code is then run backwards in time, with "concentration" representing a probability. This backward–in–time PDE model requires a single simulation run for either travel time or location probabilities for an entire domain. This new approach is a simple, fast, and economical method, but it has never been tested in either theory or practice.

1.2 Objectives and Scope

Compared to previous research, the new hypothesis proposed by Wilson and others (Wilson and Rao 1992; Wilson and Liu, 1994) is more direct, faster, especially for multiple dimensions, and more economical. Can we use the new hypothesis to address the travel time and location probabilities in either one– or two–dimensional backward–in–time problems? How can we utilize this model in applications, for example, to manage a tracer test interpretation? The purposes of this report are: (1) To examine the new hypothesis for one–dimensional advection and dispersion by formulating backward–in–time PDEs along with the appropriate boundary and initial conditions for both travel time and location probabilities. (2) To extend this new hypothesis to the cases accounting for linear equilibrium sorption, non–equilibrium sorption, first order decay, and natural recharge in a one–dimensional domain. (3) To test its ability with respect to heterogeneity, natural recharge, linear equilibrium sorption, and non–equilibrium sorption in a two–dimensional domain. (4) To test its application in an actual field tracer test at the Borden site in Ontario, Canada.

Chapter 2 and Chapter 3 illustrate the one–dimensional backward–in–time model. First, new analytical solutions of travel time and location probabilities are directly solved using double Laplace transforms with new boundary and initial conditions proposed by this research. Analytical solutions from backward–in–time models are compared to solutions for equivalent forward–in–time models. The relationship between travel time probability and location probability is explored. Having proved the backward–in–time method in one dimension, it is trivial to argue that the method also works in two dimensions. Section 4 mainly

presents the examples of the two-dimensional backward-in-time method. Travel time and location probability are directly simulated for two dimensions, employing new boundary and initial conditions, using the Laplace transform-in-time Galerkin finite element method (Sudicky and McLaren, 1992). The numerical simulations are computed by the code, FRAC-TRAN (Sudicky and McLaren, 1991), which we have modified for non-equilibrium sorption, natural recharge, and third type boundary condition at wells in this research. Simulations from the two-dimensional backward-in-time method are employed to compare to the simulations from a forward-in-time model. Chapter 5 presents an application of the two-dimensional backward-in-time model to a tracer test at the Borden site. The travel time probability density function simulated by the new method is used to interpret normalized tracer concentration breakthrough curves observed at the pumping well. Then, travel time cumulative distributions simulated by the new method are compared to empirically determined time-dependent capture zones for the test.

2. THE ONE-DIMENSIONAL BACKWARD-IN-TIME MODEL FOR THE CASE OF ADVECTION-DISPERSION

For a one-dimensional model, contamination transport can be illustrated by the pumping system in Figure 2.1. The contamination is introduced into an aquifer at a source location (CS), and it moves downstream to the pumping well (PW) by advection and dispersion. This process is described by a forward-in-time (FIT) model. In this section we mainly demonstrate the backward-in-time (BIT) method for the case of advection-dispersion only, before we can test its application in more complex cases.

2.1 Groundwater Contaminant Transport to a Pumping Well

In the pumping well system shown in Figure 2.1, the contaminant is initially located at x_o=100 m, the pumping well is located at the position x=0, and the groundwater flow average velocity, V, is in the negative x direction. Contaminant concentration in the aquifer is described by the FIT advection-dispersion equation:

$$\frac{\partial C^r}{\partial t} = D\frac{\partial^2 C^r}{\partial x^2} + V\frac{\partial C^r}{\partial x} \tag{2.1}$$

where C^r=$C^r(x,t)$ is the aqueous phase resident concentration [M/L^3] (mass of dissolved solute/fluid volume), V is the average (seepage) velocity [L/T], D is the dispersion coefficient [L^2/T], t is time [T], and x is the direction coordinate [L]. For the pumping well, the boundary condition is assumed by $\partial C^r/\partial x = 0$. In this research, in order to examine the backward-in-time model, the contamination released at a source location is assumed to be a Dirac delta function. The new boundary and initial conditions for (2.1) are given by:

$$\frac{\partial C^r}{\partial x} = 0, \qquad at\ x = 0\ ; \tag{2.2a}$$

$$C^r = 0, \qquad as\ x \to \infty; \tag{2.2b}$$

$$C^r(x,t) = \frac{M}{\theta}\delta(x-x_o),\ for\ t = 0 \tag{2.2c}$$

where $\delta(x-x_o)$ is a Dirac delta function for a pulse input of dissolved contaminant mass, M, and θ is the porosity of the aquifer of which the cross sectional area is equal to unit one.

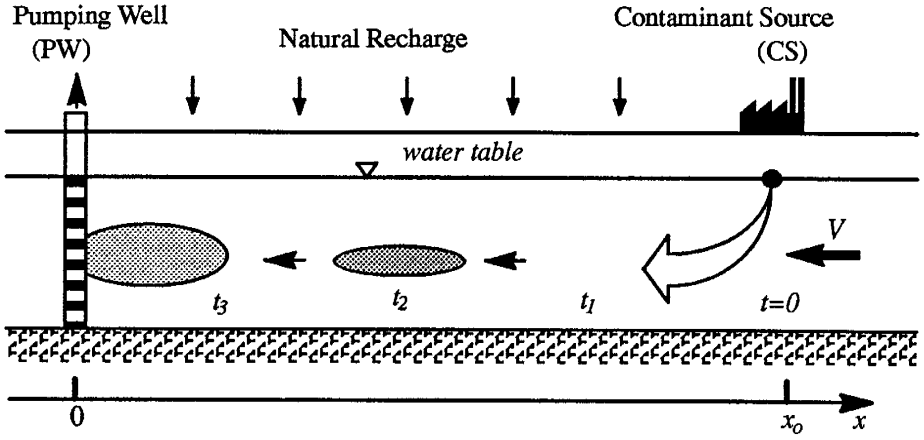

Figure 2.1. Sketch of geometry representing the basic one-dimensional forward-in-time problem. A pumping well (PW) is located at x=0, and the dissolved contamination source (CS) is located at x_o. The groundwater flows from right to left in the negative x-direction.

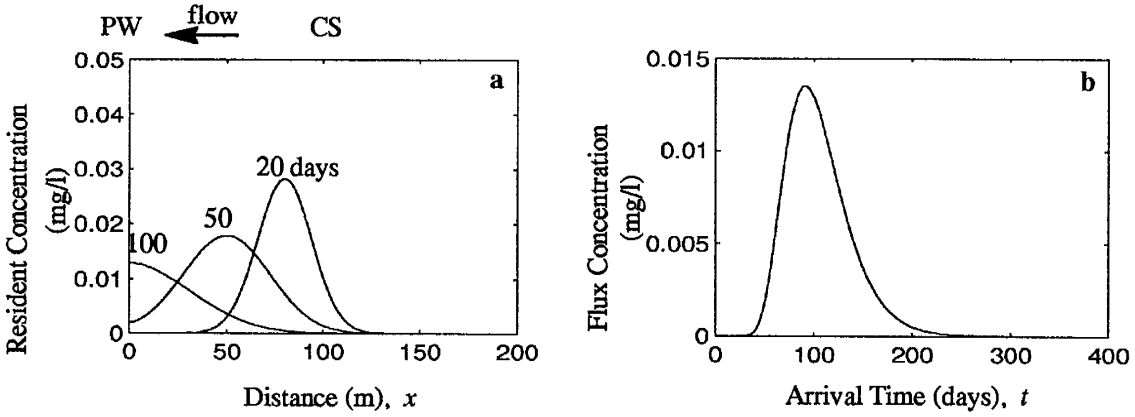

Figure 2.2. Space-time solution of the contaminant concentration (mg/l) for the case of advection-dispersion. **a.** Plots shows resident concentration from a contamination source (CS) at x_o=100 m to a pumping well (PW) at x=0, for V=1.0 m/day, D=5.0 m/day, θ=0.35, and M=0.34 g; **b.** The contaminant flux concentration (mg/l) breakthrough curve at PW with arrival time.

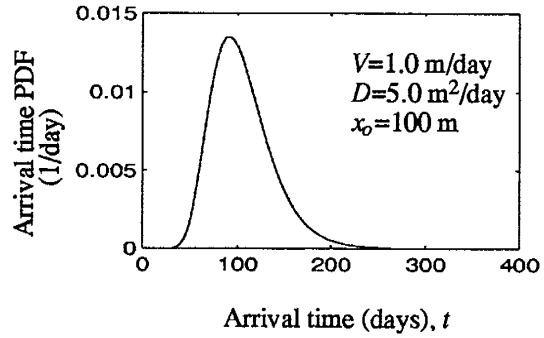

Figure 2.3. The arrival time probability density function (PDF) at the pumping well (x=0), for particles released at point x_o.

The analytical solution for the resident concentration shown in equations (2.1)–(2.2) is derived using double Laplace Transforms in time and space, as shown in Appendix A1. The solution is written as:

$$C^r(x,t) = \frac{1}{\sqrt{4\pi Dt}}\frac{M}{\theta} exp\left[\frac{-(x-x_o + Vt)^2}{4Dt}\right]\left\{1 + exp\left(\frac{-x_o x}{Dt}\right)\right\}$$

$$-\frac{V}{2D}\frac{M}{\theta} exp\left[\frac{Vx_o}{D}\right] erfc\left[\frac{(x + x_o + Vt)}{\sqrt{4Dt}}\right] \qquad (2.3)$$

This analytical solution was first derived by Wilson and Rao (1992). Figure 2.2a shows the results for x_o=100 m, V=1 m/day, and D=5.0 m^2/day. The relatively high value of the dispersion coefficient, D=5 m^2/day, is intended to illustrate the consequences of dispersion. In Figure 2.2a the contaminant distributions for t=20, 50, and 100 days illustrate how the plume expands, disperses, and dilutes with increasing time. Figure 2.2a also represents the fact that the contaminant plume has moved downstream and been extracted by the pumping well, with the concentration breakthrough shown in Figure 2.2b.

2.2 The Forward-in-time Model for Arrival Time Probability

The outflow concentration at the pumping well is defined as a flux concentration, or the ratio of the contaminant mass flux to the water flux. The flux concentration, C^f=$C^f(x,t)$, is related to the resident concentration by: $C^f = C^r + (D/V)\,\partial C^r/\partial x$ (Parker and van Genuchten, 1984; Jury and Roth, 1990). At the pumping well, since $\partial C^r/\partial x = 0$, the aqueous phase flux concentration is equal to the aqueous phase resident concentration:

$$C^f(x = 0,t) = \frac{1}{\sqrt{\pi Dt}}\frac{M}{\theta} exp\left[\frac{-(x_o - Vt)^2}{4Dt}\right] - \frac{V}{2D}\frac{M}{\theta} exp\left[\frac{Vx_o}{D}\right] erfc\left[\frac{x_o + Vt}{\sqrt{4Dt}}\right] \qquad (2.4)$$

The arrival time probability density function (PDF), $f_t(t|x_o)$ describes the probability that a non-reacting contaminant particle, released at location x_o and time t=0, will reach the pumping well in time t. It is obtained from the normalized flux concentration (Jury and Roth, 1990; Chin and Chittaluru, 1994):

$$f_t(t|x_o) = \frac{\dot{m}}{M} \tag{2.5}$$

where $\dot{m}=V/\theta C^f(x=0,t)$ is the mass flux at the pumping well, V is the average velocity [L/T] at the pumping well, $x=0$, and θ is the porosity of the aquifer. M is the total mass released at the source location, $x_o=100$ m. When Equation (2.4) is inserted into Equation (2.5), the solution of the FIT arrival time PDF can be rewritten as:

$$f_t(t|x_o) = \frac{V}{\sqrt{\pi D t}} \exp\left[\frac{-(x_o-Vt)^2}{4Dt}\right] - \frac{V^2}{2D} \exp\left[\frac{Vx_o}{D}\right] erfc\left[\frac{x_o + Vt}{\sqrt{4Dt}}\right] \tag{2.6}$$

Figure 2.2b shows a diagram of the flux concentration (in mg/l) vs. arrival time (in days) from the source location x_o to the pumping well. The mean arrival time taken by the contaminant from the source location to the pumping well is about 100 days. The flux concentration is normalized and replotted as the diagram of the arrival time probability density function vs. the arrival time in Figure 2.3.

What happens if we do not know where the source is located? Supposed all we observe is the contamination concentration in the pumping well. This problem can be addressed using the arrival time probabilities for each possible contamination source location, x_o, to find the travel time probability density function. These probabilities are given by equation (2.6). In a multidimensional numerical model, we would have to rerun the code for each x_o, a potentially expensive undertaking. Figure 2.4a shows five arrival time probability density functions for possible source locations at x_o=50 m, 75 m, 100 m, 125 m, and 150 m. The probability at t=100 days is graphically taken from Figure 2.4a, and replotted in Figure 2.4b as the x's, along with equation (2.6) for t=100 days, and variable x_o. This plot is the travel time probability density function. In multidimensional systems, we would have to run many simulations to approximate the continuous curve of $f_t(t=100|x_o)$ in Figure 2.4b. As we can see, in practical multidimensional applications, with many potential source locations, x_o, it is expensive to get. Is there a better method?

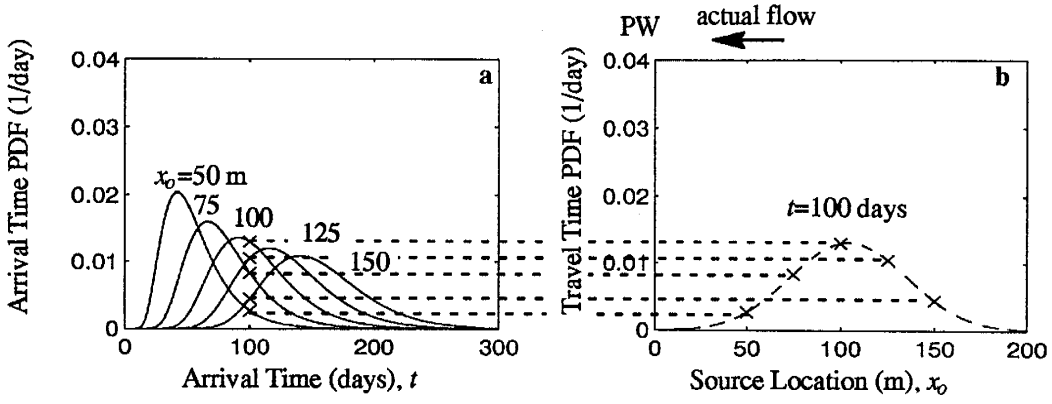

Figure 2.4. Graphic view of the FIT construction of the travel time probability density function for various contaminant source locations, x_o, from the forward problem solution. a. Arrival time probability at x=0 and given values of x_o=50 m, 75 m, 100 m, 125 m, 150 m; b. Travel time PDF of 100 days.

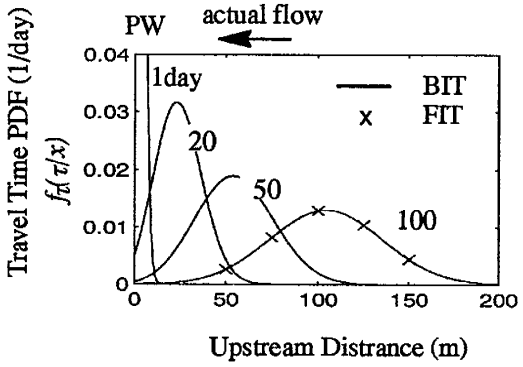

Figure 2.5. Diagram of the travel time probability density function (PDF) for advection-dispersion. The plots represent the probability density function of contamination that was observed in the well 1, 20, 50, 100, and 150 days later, at V=1.0 m/day, D=5.0 m^2/day. Solid lines show the travel time PDF computed by the backward-in-time (BIT) PDEs model, and crosses show the arrival time PDFs computed from the forward-in-time (FIT) construction method.

2.3 The Backward-in-time Model for Travel Time Probability

In the backward-in-time problem, the travel time probability density function (PDF), $f_\tau(\tau|x)$, states how long it takes a contaminant to move to the pumping well from a former location x. The travel time PDF can be directly formulated from the advection-dispersion model when the flow problem is run backwards-in-time with "concentration" representing a probability (Wilson and Rao, 1992; Wilson and Liu, 1994). If we take equation (2.1), and run it backwards in advection ($V \rightarrow -V$) we can get the following, familiar advection-dispersion equation:

$$\frac{\partial f_\tau}{\partial \tau} = D\frac{\partial^2 f_\tau}{\partial x^2} - V\frac{\partial f_\tau}{\partial x} \tag{2.7}$$

where $f_\tau = f_\tau(\tau|x)$ is the travel time probability density function [1/T], x is a given variable for the former location, and $\tau = t - t_o$ is the travel time from the former location at time t_o to the pumping well at later time t. For the backward-in-time problem in Figure 2.1, the travel time PDF for the location x should be zero at $\tau=0$. For the pumping well, we can describe the boundary condition at the pumping well by "injecting" a unit of travel time probability at the pumping well. The new appropriate boundary and initial conditions for the backward-in-time model are expressed as:

$$Vf_\tau - D\frac{\partial f_\tau}{\partial x} = V\delta(\tau), \quad at\ x = 0 \tag{2.8a}$$

$$f_\tau = 0, \quad at\ x \rightarrow \infty \tag{2.8b}$$

$$f_\tau = 0, \quad for\ \tau = 0 \tag{2.8c}$$

where $f_\tau = f_\tau(\tau|x)$ is the travel time probability density function. The new solution of the probability density function is derived from (2.7) and (2.8) by double Laplace Transforms (see Appendix A2):

$$f_\tau(\tau|x) = \frac{V}{\sqrt{\pi D\tau}}\ exp\left[\frac{-(x-V\tau)^2}{4D\tau}\right] - \frac{V^2}{2D}exp\left[\frac{Vx}{D}\right]erfc\left[\frac{x+V\tau}{\sqrt{4D\tau}}\right] \tag{2.9}$$

This solution is identical to the arrival time probability described by equation (2.6), except for notations on distance (x or x_o) and time (τ or t).

For the example in Figure 2.1, Figure 2.5 shows the BIT travel time probability density functions vs. upstream distance, for four selected travel times: τ=1day, 20 days, 50 days and 100 days. Its distribution for τ=100 days is matched by the arrival time probability previously derived in Figure 2.4b. We get the probability distribution at τ=1 day, 20 days, and 50 days, directly from equation (2.7), instead of solving equation (2.6) for many different values of x_o.

The travel time cumulative distribution function (CDF), $F_\tau(\tau|x)=P(\tau'<\tau|x)$ is the probability that the contaminant takes time less than τ to reach the pumping well from the location x. The travel time CDF can also be computed by the backward-in-time method. The boundary condition at the pumping well is like a continuous "injection" of probability one, while the initial probability elsewhere is set to zero. The unit value represents a probability of one that the contamination immediately around the well will be captured. For the contamination transport shown in equations (2.1)-(2.2), the cumulative distribution can be solved by equation (2.7) replacing f_τ with F_τ along the new appropriate boundary and initial conditions:

$$VF_\tau - D\frac{\partial F_\tau}{\partial x} = V, \quad at\ x = 0 \tag{2.10a}$$

$$F_\tau = 0, \quad at\ x \to \infty \tag{2.10b}$$

$$F_\tau = 0, \quad for\ \tau = 0 \tag{2.10c}$$

where $F_\tau=F_\tau(\tau\,|\,x)$ is the travel time cumulative distribution function. The new analytical solution is derived from the double Laplace transforms (see Appendix A.2):

$$F_\tau = \frac{V\tau}{\sqrt{\pi D\tau}}\ exp\left[\frac{(x-V\tau)^2}{4D\tau}\right] + \frac{1}{2}\left\{erfc\left[\frac{(x-V\tau)}{\sqrt{4D\tau}}\right]\right\}$$

$$-\left[\frac{D + Vx + V^2\tau}{2D}\right]\left\{exp\left[\frac{Vx}{D}\right]erfc\left[\frac{(x + V\tau)}{\sqrt{4D\tau}}\right]\right\} \qquad (2.11)$$

Based on the definition of the cumulative distribution, the travel time CDF can also be expressed as the integration of the travel time PDF, $f_\tau(\tau|x)$ (Jury and Roth, 1990; Henley and Kumamoto, 1992; Chin and Chittaluru, 1994):

$$F_\tau(\tau|x) = P(\tau' < \tau|x) = \int_0^\tau f_\tau(\tau'|x)d\tau' \qquad (2.12)$$

If we insert the equation (2.9) into (2.12), we can get the same solution of the travel time CDF shown in equation (2.11). The relation of the travel time PDF and CDF shown in equation (2.12) can be employed to obtain one from the other.

Figure 2.6 shows the hypothesized time dependent cumulative distribution maps for the pumping well in Figure 2.1, for travel times less than 1 day, 20 days, 50 days, and 100 days. For the time less than 50 days, the cumulative distribution extends almost 100 meters upstream, with a better than fifty percent chance of capture for the contamination within 53 meters of the well. As time increases, the capture zone expands, disperses, and extends in an upstream direction.

2.4 The Backward-in-time Model for Location Probability

The location probability density function, $f_x(x|\tau)$, is the probability that the contaminant observed in the pumping well was located at a position x, for a given travel time τ. For the contamination transport shown in Figure 2.1, the location PDF is expressed by the same governing equation (2.7) replacing $f_\tau(\tau|x)$ with $f_x(x|\tau)$. The initial PDF is set to unity around the pumping well at travel time τ=0, and the location PDF is not injected into the pumping

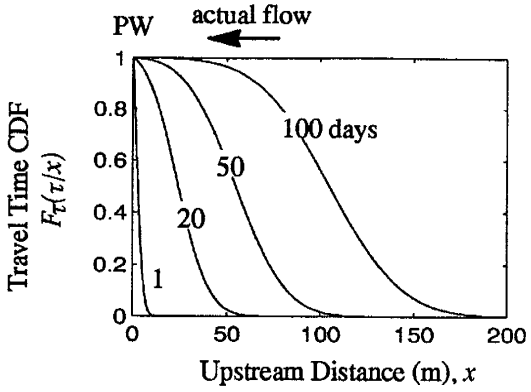

Figure 2.6. Diagram of the travel time cumulative distribution function (CDF) for advection–dispersion. The plots represent the travel time CDFs for travel times: τ=1day, 20 days, 50 days, and 100 days.

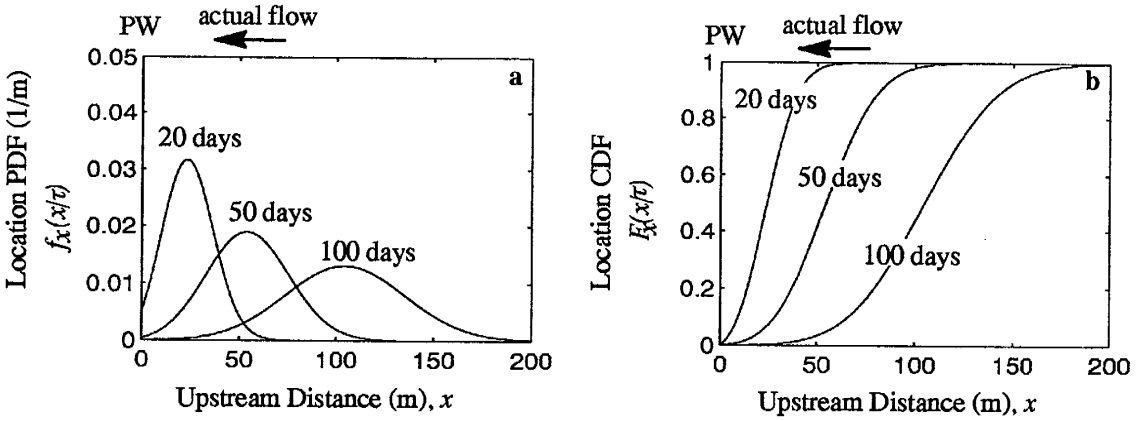

Figure 2.7. Diagram of the location probability for advection–dispersion vs. upstream distance. a. The plots represent the location probability density function of contamination for three exact times: τ=20, 50, and 100 days, at V=1.0 m/day, D=5.0 m^2/day. b. The plots represent cumulative probability distribution.

well. The new initial and boundary conditions are described by:

$$Vf_x - D\frac{\partial f_x}{\partial x} = 0, \quad at\ x = 0 \tag{2.13a}$$

$$f_x = 0, \quad at\ x \to \infty \tag{2.13b}$$

$$f_x = \delta(x), \quad for\ \tau = 0 \tag{2.13c}$$

where f_x=$f_x(x|\tau)$ is location probability density function [1/L]. $\delta(x)$ is the Dirac delta function. The new analytical solution for the location PDF is derived from equations (2.7) and (2.13) using double Laplace transforms (see Appendix A3) and is written as:

$$f_x(x|\tau) = \frac{1}{\sqrt{\pi D\tau}}\ exp\left[\frac{-(x-V\tau)^2}{4D\tau}\right] - \frac{V}{2D}exp\left[\frac{Vx}{D}\right]erfc\left[\frac{x+V\tau}{\sqrt{4D\tau}}\right] \tag{2.14}$$

For the previous example, Figure 2.7a shows the location probability density function for the travel time: τ=20 days, 50 days, and 100 days. The location PDF distribution moves in an upstream direction and spreads with increasing travel time. If we move the origin point to 100 m in Figure 2.7a, we can see that the location PDFs and the concentration distributions in Figure 2.2a are symmetric with respect to x=100 m. This result is also demonstrated by Uffink (1989). The solutions for location PDF and travel time PDF demonstrate that, in this case, they are related by $f_x(x|\tau)$=$f_\tau(\tau|x)/V$.

In the one-dimensional backward-in-time model, the location cumulative distribution function, $F_x(x|\tau)$=P(x'<$x|\tau$), can also be directly found from the BIT method. For the previous example, the location cumulative distribution can be formulated by equation (2.7), replacing f_τ with F_x. The cumulative distribution function is set to unit one for the initial condition, and the cumulative distribution function is equal to zero in the pumping well. The appropriate new boundary and initial conditions can be written as:

$$F_x = 0, \quad at\ x = 0 \tag{2.15a}$$

$$F_x = 0, \quad at\ x \to \infty \tag{2.15b}$$

$$F_x = 1, \quad for\ \tau = 0 \tag{2.15c}$$

where F_x=$F_x(x|\tau)$ is the location cumulative distribution function. The analytical solution

is derived in Appendix A3, and the result is expressed as:

$$F(x|\tau) = 1-\frac{1}{2}\left\{erfc\left[\frac{(x-V\tau)}{\sqrt{4D\tau}}\right] + exp\left[\frac{Vx}{D}\right]erfc\left[\frac{(x+V\tau)}{\sqrt{4D\tau}}\right]\right\} \tag{2.16}$$

The location cumulative distribution function (CDF) can also be computed by the integration of the location probability density functions, $f_x(x|\tau)$, along the distance from the pumping well to location x:

$$F_x(x|\tau) = P(x' < x|\tau) = \int_0^x f_x(x'|\tau)dx' \tag{2.17}$$

After inserting equation (2.14) into (2.17), we obtain the same solution shown in equation (2.16). The analytical solution for the cumulative distribution function, $F_x(x|\tau)$, is confirmed by the integration of location PDF.

Figure 2.7b shows the diagram of the location cumulative distribution function vs. the upstream distance for the travel time: τ=20 days, 50 days and 100 days. The location CDF for travel time, say τ=50 days, illustrates the probability that the contamination observed from the pumping well is located within a distance less than 100 m. The location cumulative distribution of the contamination spreads and extends in an upstream direction with increasing travel time.

2.5 Relation of Travel Time and Location Probabilities

The travel time and location probability density functions are directly determined from the backward-in-time method, with the analytical solutions shown in equations (2.9) and (2.14), respectively. The relation of travel time PDF, $f_\tau(\tau|x)$, and location PDF, $f_x(x|\tau)$, can be expressed as:

$$f_\tau(\tau|x) = Vf_x(x|\tau) \tag{2.18}$$

where V is the average velocity at the pumping well.

The travel time and location probability are both conditional probabilities in the backward–in–time problem. The relation of both probabilities can also be expressed through Bayes theorem (Henley and Kumamoto, 1992):

$$f_x(x|\tau) = \frac{f_\tau(\tau|x)g(x)}{\int_0^\infty f_\tau(\tau|x)g(x)dx} \tag{2.19}$$

where $g(x)$ is the location probability density function. In a one–dimensional model, all contaminants released from the source location are captured by the pumping well in complete time. If the location g(x) is described by a uniform function, the relation in equation (2.13) can be rewritten as:

$$f_x(x|\tau) = \frac{f_\tau(\tau|x)}{\int_0^\infty f_\tau(\tau|x)dx} \tag{2.20}$$

After inserting the analytical solutions of equations (2.9) and (2.14) into equation (2.20), equation (2.18) is obtained.

3. THE ONE-DIMENSIONAL MODEL FOR CASES OF CHEMICAL REACTIONS AND NATURAL RECHARGE

Contaminant transport in the aquifer is usually complicated by chemical reactions and natural recharge. How do we extend the new backward-in-time (BIT) hypothesis to these more complex cases? To examine the extensions of the new model, the pumping well system in Figure 2.1 is used to describe forward-in-time (FIT) contaminant transport models addressing first order decay, linear equilibrium sorption, non-equilibrium sorption, and natural recharge. These contaminant transport models are used, respectively, to formulate the backward-in-time (BIT) models for each case.

3.1 The One-dimensional Backward-in-time Model in the Case of First Order Decay

In the case of first order decay, contaminants in the aquifer decay with time, usually through either biodegradation or radioactivity. The contaminant concentration in governing equation (2.1) must be modified, and aqueous phase resident concentration is then described by:

$$\frac{\partial C^r}{\partial t} = D\frac{\partial^2 C^r}{\partial x^2} + V\frac{\partial C^r}{\partial x} - \lambda C^r \tag{3.1}$$

where $C^r=C^r(x,t)$ is resident concentration [M/L^3], and λ is the first order decay rate [1/T]. For the example shown in Figure 2.1, this equation is solved with the same boundary and initial conditions given in equation (2.2), yielding:

$$C^r(x,t) = exp(-\lambda t)C^r(x,t;\ \lambda = 0) \tag{3.2}$$

where $C^r(x,t;\ \lambda=0)$ is the resident concentration for $\lambda=0$ as given in equation (2.3). Figure 3.1 shows the aqueous phase resident concentration for $\lambda=0.01$ day^{-1} (time constant is 100 days) for time t=20 days, 50 days, and 100 days. Compared to the resident concentration without first order decay in Figure 2.2a, Figure 3.1 demonstrates that the resident concentration decays as time increases.

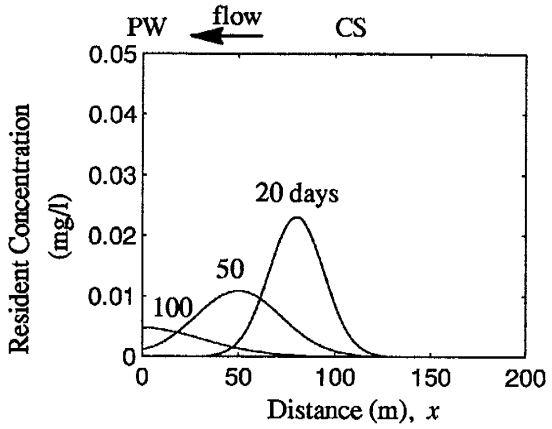

Figure 3.1. Diagram of the aqueous resident concentration for the case of first order decay vs. upstream distance. The source location x_0=100 m, V=1.0 m/day, D=5.0 m^2/day, and λ=0.01 day^{-1}.

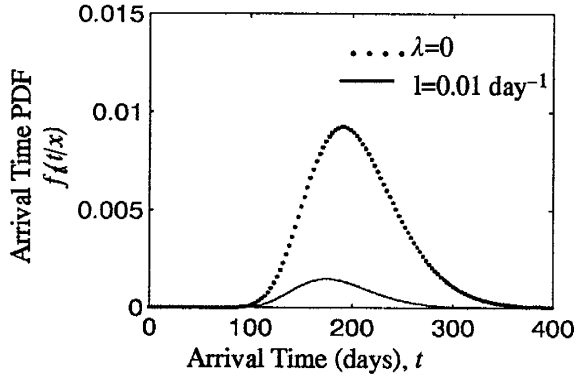

Figure 3.2. Diagram of the arrival time PDF for the case of the first order decay vs. arrival time from the source location at x_0=100 m, at V=1.0 m/day, D=5.0 m^2/day. The dotted line shows advection dispersion only, at λ=0.0; the solid line shows advection-dispersion within first order decay, at λ=0.01 day^{-1}.

3.1.1 The Forward-in-time Model for Arrival Time Probability

The aqueous phase flux concentration observed in the pumping well at x=0, where $C^f(x=0,t)=C^r(x=0,t)$, is also affected by first order decay. The normalized flux concentration, i.e. arrival time PDF is:

$$f_t(t|x_o) = exp(-\lambda t) f_t(t|x_o;\ \lambda = 0) \tag{3.3}$$

where $f_t(t\,|\,x_o;\,\lambda=0)$ is the arrival time PDF for the non-decay case given in Equation (2.6). Figure 3.2 shows arrival time PDF for both first order decay and no decay. The arrival time probability for first order decay is smaller, suffering exponentially decays as time increases. The influence of first order decay is dependent on the decay rate, velocity, and the distance from the source location to the pumping well. The decay of arrival time probability increases with the decay rate, the distance, and decreases with velocity.

3.1.2 The Backward-in-time Model for Travel Time Probability

For the backward-in-time model, the travel time PDF, $f_\tau(\tau\,|\,x)$, should exponentially decay as time increases. The probability density function can be expressed as:

$$\frac{\partial f_\tau}{\partial \tau} = D\frac{\partial^2 f_\tau}{\partial x^2} - V\frac{\partial f_\tau}{\partial x} - \lambda f_\tau \tag{3.4}$$

The solution of the travel time PDF is derived along the same boundary and initial conditions given in equation (2.8):

$$f_\tau(\tau|x) = exp(-\lambda\tau) f_\tau(\tau|x;\lambda = 0) \tag{3.5}$$

where $f_\tau(\tau\,|\,x;\lambda=0)$ is the travel time PDF for no decay which is given in equation (2.9). Equation (3.5) is the same as (3.3) except for (x_o or x). The travel time CDF can be computed by the integration of travel time PDF:

$$F_\tau(\tau|x) = \int_0^\tau f(\tau|x)d\tau = \int_0^\tau e^{-\lambda\tau} f(\tau|x;\ \lambda = 0)d\tau \tag{3.6}$$

where $F_\tau(\tau\,|\,x)$ is travel time CDF for first order decay, $f_\tau(\tau\,|\,x;\,\lambda=0)$ is the travel time PDF for non first order decay.

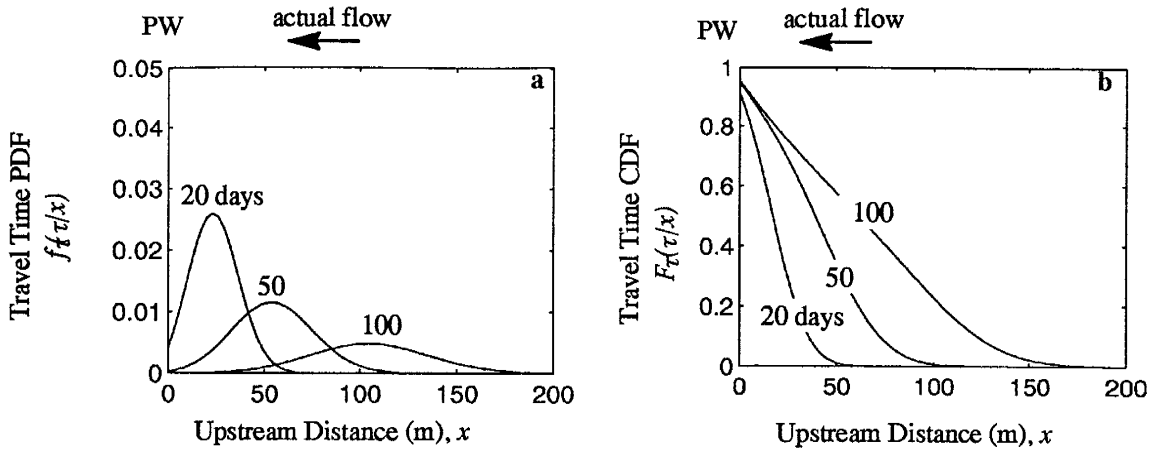

Figure 3.3. Diagram of the travel time probability for the case of first order decay vs. upstream distance. The plots represent probabilities of the former locations for contamination that was observed in the well 20, 50, and 100 days later at V=1.0 m/day, D=5.0 m^2/day, and λ=0.01 day^{-1}. **a.** Travel time PDF; **b.** Travel time CDF.

Using the previous example in Figure 2.1, Figure 3.3 shows the travel time probability for three times: τ=20 days, 50 days, and 100 days, at λ=0.01 day^{-1} (time constant 100 days). Figure 3.3a indicates that the travel time probability density reduces exponentially with time. This reflects reduced probability due to the fact that some of the dissolved contaminant will decay before it reaches the pumping well. Figure 3.3b describes travel time cumulative distribution. The capture zone of the contamination reduces as time increases under the case of first order decay.

3.1.3 The Backward-in-time Model for Location Probability

For the case of first order decay, the estimation of location PDF, $f_x(x|\tau)$, is not affected by the decay of the contaminant. The location probability for a given travel time is the same as the solution for non-first order decay:

$$f_x(x|\tau) = f_x(x|\tau;\ \lambda = 0) \tag{3.7}$$

where $f_x(x|\tau;\ \lambda=0)$ is the location PDF for non first order decay in (2.14).

If we insert equation (3.5) into (2.20), we can get the same solution as equation (3.7). This result further demonstrates that the relationship between travel time and location probabilities is given by the Bayes theorem.

3.2 The One-dimensional Backward-in-time Model in the Case of Linear Equilibrium Sorption

In the case of linear equilibrium sorption, the resident concentration can be described as being in the aqueous phase, sorbed phase, or both the aqueous and sorbed phase. The aqueous phase resident concentration of contamination, $C^r(x,t)$, is then described by:

$$R\frac{\partial C^r}{\partial t} = D\frac{\partial^2 C^r}{\partial x^2} + V\frac{\partial C^r}{\partial x} \tag{3.8}$$

where $C^r=C^r(x,t)$ is the aqueous phase resident concentration [M/L^3], and $R=(1 + K_d\varrho_b/\theta)$ is the retardation factor due to linear equilibrium sorption with distribution coefficient K_d [L^3/M], bulk density ϱ_b [M/L^3], and porosity θ. The sorbed phase resident concentration, $C^r_s(x,t)$, is described by $[(R-1)/R]C^r(x,t)$, and the total resident concentration, $C^r_{\text{total}}(x,t)$, is described by $C^r_{\text{total}}=RC^r(x,t)$. Equation (3.8) is solved with the same forward problem boundary and initial condition given in (2.2). The resident concentration is solved and described as:

$$C^r(x,t) = \frac{1}{R}\, C^r(x,\frac{t}{R};\ R = 1) \tag{3.9a}$$

$$C^r_s(x,t) = \frac{R-1}{R}\, C^r(x,\frac{t}{R};\ R = 1) \tag{3.9b}$$

$$C^r_{total}(x,t) = C^r(x,t) + C^r_s(x,t) = C^r(x,\frac{t}{R};\ R = 1) \tag{3.9c}$$

where $C^r(x,t/R;\ R=1)$ is the aqueous phase resident concentration for the $R=1$ non-sorption case (2.3) but at time t/R ($R>1$).

For the example in Figure 2.1, Figure 3.4 shows the resident concentrations for $R=2$ vs. upstream distance. Compared to the non-sorption in Figure 2.2a, Figure 3.4 shows that the concentrations are retarded by $R=2$. Figure 3.4a indicates that the aqueous phase resident concentration is reduced by $R=2$. Figure 3.4c demonstrates that total resident concentration

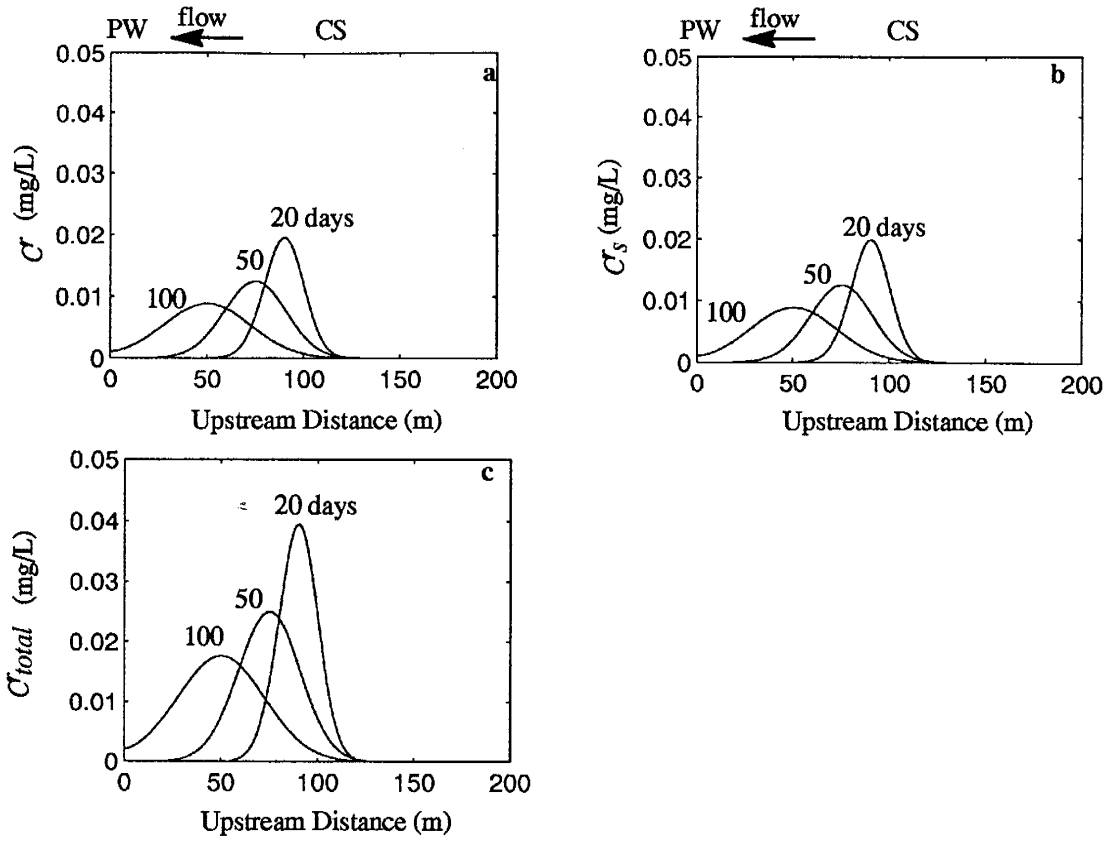

Figure 3.4. Diagram of the resident concentration (mg/l) with linear equilibrium sorption vs. upstream distance. The plots represent plumes of contamination in the aquifer 20, 50, and 100 days later. V=1.0 m/day, D=5.0 m^2/day, ϱ_b=1.5 mg/cm^3, θ=0.3, R=2.0. **a.** Aqueous phase concentration; **b.** Sorbed phase concentration; **c.** Total concentration.

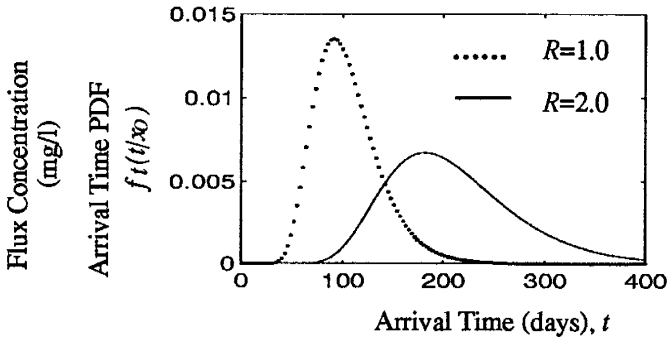

Figure 3.5. Diagram of the aqueous phase flux concentration observed in PW or normalized concentration (arrival time PDF) for linear equilibrium sorption. Plots describe arrival time PDF vs. arrival time from the source location x_o=100 m, at V=1.0 m/day, D=5.0 m^2/day. The dotted line and solid line represent R=1.0 and R=2.0, respectively.

is equal to the aqueous phase resident concentration for non-sorption at time t/R. The total concentration in the time t=100 days is the same as the concentration for the non-sorption case in the time t=50 days.

3.2.1 The Forward-in-time Model for Arrival Time Probability

For linear equilibrium sorption, the aqueous phase flux concentration observed in the pumping well at x=0 is described by the aqueous phase resident concentration, $C^f(x=0,t)=C^r(x=0,t)$. Then the normalized flux concentration represents aqueous phase arrival time PDF:

$$f_t(t|x_o) = \frac{1}{R} f_t(\frac{t}{R}|x_o;\ R = 1) \tag{3.10}$$

where $f_t(t|x_o)$ is the aqueous phase arrival time probability, $f_t(t/R|x_o; R=1)$ is arrival time probability (2.6) for the non-sorption case at time t/R (R>1). Figure 3.5 presents the arrival time probability for linear equilibrium sorption with R=2 and for non-sorption with R=1. Figure 3.5 shows that the arrival time probability is retarded and reduced by the retardation factor R=2. The integration of the arrival time probability over the time domain is equal to one.

3.2.2 The Backward-in-time Model for Travel Time Probability

For the case of sorption, the travel time probability can also be described as being in the aqueous phase, sorbed phase, or the combined aqueous phase and sorbed phase. The aqueous phase travel time PDF, $f_\tau(\tau|x)$, is directly solved from the backward-in-time model:

$$R\frac{\partial f_\tau}{\partial \tau} = D\frac{\partial^2 f_\tau}{\partial x^2} - V\frac{\partial f_\tau}{\partial x} \tag{3.11}$$

with the same initial and boundary conditions presented in equation (2.8):

$$f_\tau(\tau|x) = \frac{1}{R} f_\tau(\frac{\tau}{R}|x;\ R = 1) \tag{3.12}$$

where $f_\tau(\frac{\tau}{R}|x;\ R = 1)$ is the aqueous phase travel time PDF for the non-sorption case but at travel time, τ/R, as given in equation (2.9). The BIT travel time PDF, $f_\tau(\tau|x)$, is the same as the arrival time PDF computed from the forward-in-time model (3.10). The total travel

time PDF for the combined aqueous phase and sorbed phase, $f_{\tau,\,\text{total}}(\tau|x)$, is illustrated by the travel time PDF for the aqueous phase, $f_{\tau,\,\text{total}}(\tau|x)=Rf_\tau(\tau|x)$, i.e. $f_{\tau,\,\text{total}}(\tau|x)=f_\tau(\tau/R|x;\ R=1)$.

The travel time CDF for the aqueous phase, $F_\tau(\tau|x)$, can also be directly computed from a backward-in-time partial differential equations (3.11) and (2.10) with f_τ replacing F_τ. The new analytical solution is:

$$F_\tau(\tau|x) = F_\tau(\frac{\tau}{R}|x;\ R = 1) \tag{3.13}$$

$F_\tau(\frac{\tau}{R}|x;\ R = 1)$ is the travel time CDF for the non-sorption case at time, τ/R, as given in equation (2.11). This analytical solution is also obtained from the integration of the travel time PDF, $f_\tau(\tau|x)$.

For the previous example, the analytical solution for travel time PDF with R=2 is shown in Figure 3.6. Compared to the aqueous phase travel time PDF for non-sorption in Figure 2.5, Figure 3.6 demonstrates that the aqueous phase travel time PDF for various locations x is retarded and reduced by retardation factor R. However, in applications of the retardation equilibrium model, we are not interested in the aqueous phase alone, but rather the total probability. It is given by multiplying the curves in Figure 3.6 by R=2, or retarding the curves in Figure 2.5 by $1/R$=0.5. Then, the probabilities are distributed the same in space but simply take longer to the pumping well. Figure 3.7 shows diagrams of the aqueous phase travel time CDF for travel time: τ=40 days, 100 days, and 200 days. Compared to the aqueous phase travel time CDF for the non-sorption case in Figure 2.6, this distribution is retarded by the retardation factor R. The capture zone of the contamination for a travel time of 100 days is the same as that for non-sorption at 50 days.

3.2.3 The Backward-in-time Model for Location Probability

A location probability can also be described for the aqueous phase, sorbed phase, or the combined aqueous phase and sorbed phase. The location probability density function (PDF) for the aqueous phase, $f_x(x\,|\,\tau)$, is determined by the backward-in-time PDE in (3.11) and (2.13) except that the initial condition is $f_x(x, \tau = 0) = \delta(x)/R$. The analytical solution of

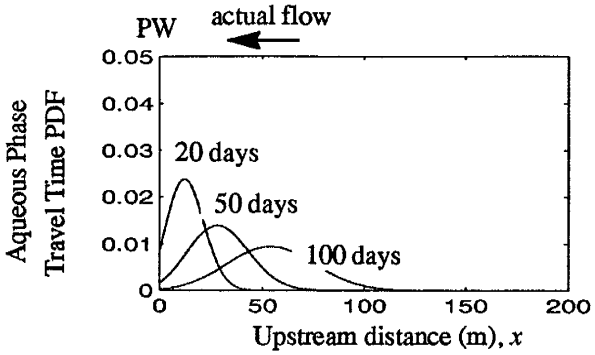

Figure 3.6. Diagram of the aqueous phase travel time PDF for the case of linear equilibrium sorption. The plots represent the travel time PDF for three times: τ=20 days, 50 days, and 100 days at V=1.0 m/day, D=5.0 m^2/day, and R=2.0.

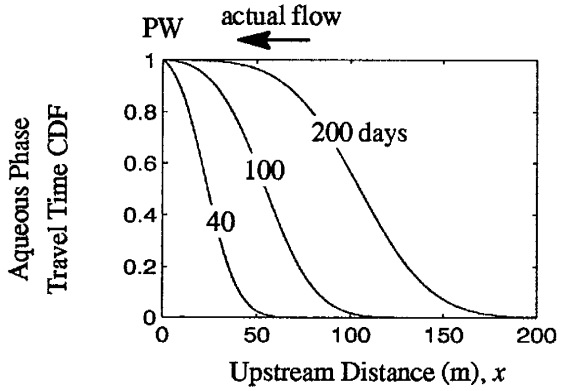

Figure 3.7. Diagram of the travel time cumulative distribution function (CDF) for linear equilibrium sorption. The plots represent the travel time CDF vs. upstream distance for travel times: τ=40 days, 100 days, and 200 days at V=1.0 m/day, D=5.0 m^2/day, and R=2.0.

the location PDF is:

$$f_x(x|\tau) = \frac{1}{R} f_x(x|\frac{\tau}{R};\ R = 1) \tag{3.14a}$$

where $f_x(x|\frac{\tau}{R};\ R = 1)$ is the location PDF for the non-sorption case at τ/R, which is given in equation (2.14). The sorbed phase location PDF, $g_x(x|\tau)$, is expressed by:

$$g_x(x|\tau) = \frac{(R-1)}{R} f_x(x|\frac{\tau}{R};\ R = 1) \tag{3.14b}$$

The total location PDF for combined aqueous and sorbed phases, $f_{x,\text{total}}(x|\tau)$, is given by:

$$f_{x,total}(x|\tau) = f_x(x|\frac{\tau}{R};\ R = 1) \tag{3.14c}$$

Figure 3.8 represents location PDFs for linear equilibrium sorption with R=2.0. Figure 3.8a shows that the PDF for the aqueous phase is retarded and reduced by retardation factor R=2; Figure 3.8b shows the PDF for the sorbed phase is retarded and reduced by retardation

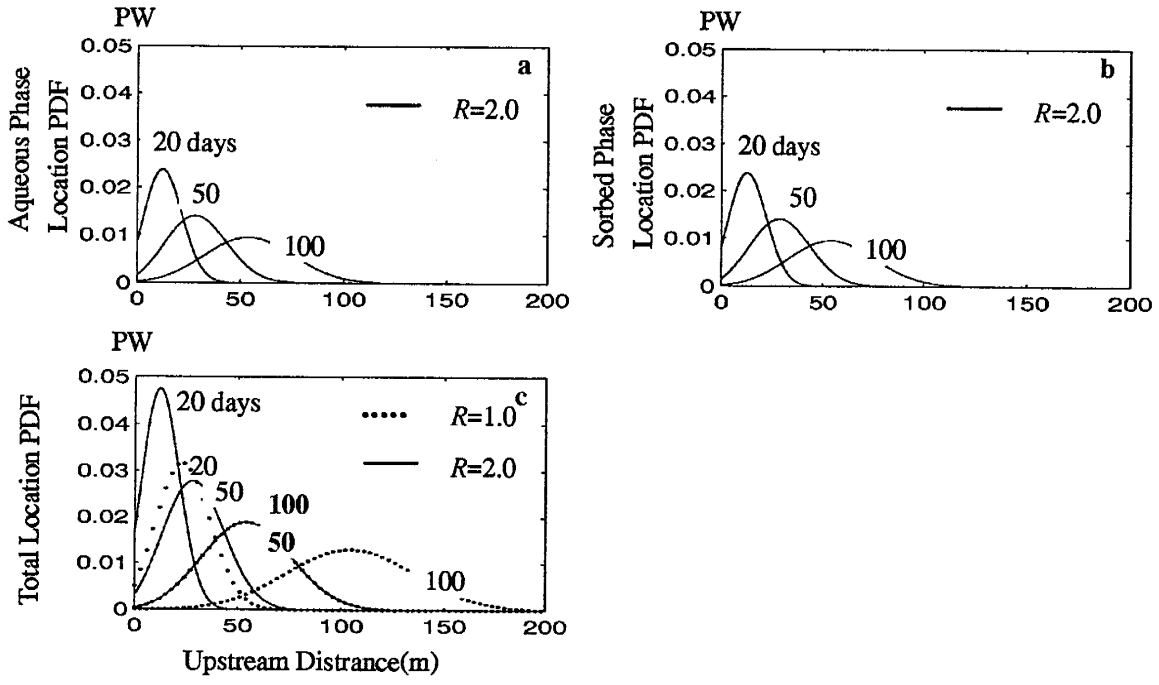

Figure 3.8. Diagram of the location PDFs for linear equilibrium. a. The plots represent the aqueous phase PDF for three times: τ=20 days, 50 days, 100 days later, at V=1.0 m/day, D=5.0 m^2/day, R=2.0. b. Sorbed phase location PDF. c. Total location PDF for two cases: R=1.0 and R=2.0.

factor $R/(R-1)=2$, which, in this case is identical to the aqueous phase probability. Figure 3.8c shows that the total location PDF is retarded by $R=2$, but not reduced.

For linear equilibrium sorption, the relation of total travel time probability and the total location probability can be expressed as:

$$f_{x,total}(x|\tau) = \frac{f_{\tau,total}(\tau|x)}{\int_0^\infty f_{\tau,total}(\tau|x)dx} \tag{3.15}$$

This relation is easily proved by inserting the total PDF for travel time and location into equation (3.15). We can obtain the relation of both probabilities, $f_{x,\text{total}}(\tau|x)=f_{\tau,\text{total}}(\tau|x)/V$, after integrating the total location PDF in equation (3.15).

3.3 The One-dimensional Model in the Case of Non-Equilibrium Sorption

In contaminant transport within non-equilibrium sorption, the resident concentrations for the aqueous phase, $C^r(x,t)$, and the sorbed phase, $C_s{}^r(x,t)$, can be described by (Van Genuchten and Wierenga, 1976; Van Genuchten and Alves, 1982; Parker and Jardine, 1986; Bruesseau, al et., 1992; Jury and Roth, 1990):

$$\frac{\partial C^r}{\partial t} + \frac{\partial C_s^r}{\partial t} = D\frac{\partial^2 C^r}{\partial x^2} - V\frac{\partial C^r}{\partial x} \tag{3.16a}$$

$$\frac{\partial C_s^r}{\partial t} = \alpha\left[\frac{K_d\varrho_b}{\theta}C^r - C_s^r\right] \tag{3.16b}$$

where $C^r=C^r(x,t)$ is aqueous phase resident concentration [M/L^3], $C_s{}^r(x,t)$ is sorbed phase resident concentration [M/L^3]. ϱ_b is the bulk density of the aquifer material [M/L^3], θ is the porosity of the aquifer, K_d is the equilibrium sorption coefficient [L^3/M], and α is the mass transfer coefficient [1/T]. For the previous example in Figure 2.1, the boundary and initial conditions for the aqueous phase are shown in (2.2), and the initial condition for the sorbed phase is $C_s{}^r(x,t)=0$. A new analytical solution of (3.16) is derived using the double Laplace transforms in time and space (see Appendix A4). After inverting the space transform, the Laplace transform of the concentration in time ($t\rightarrow p$) is described by:

$$\hat{C}^r = \frac{M}{\theta}\frac{exp(s_2(x-x_o))}{V\xi}\left[1-U_{(x-x_o)}\right]-\frac{M}{\theta}\frac{exp(s_1(x-x_o))}{V\xi}\left[\frac{s_2}{s_1}exp(\frac{-V\xi x_o}{D})-U_{(x-x_o)}\right] \quad (3.17a)$$

$$\hat{C}_s^r = \frac{\alpha K_d \varrho_b}{(\alpha + p)\theta}\hat{C}^r \quad (3.17b)$$

$$U_{(x-x_o)} = \begin{cases} 0 \ at \ x \le x_o \\ 1 \ at \ x > x_o \end{cases}$$

$$s_1 = -\frac{V}{2D}(1+\xi) \qquad s_2 = -\frac{V}{2D}(1-\xi)$$

$$A = \left(1 + \frac{\varrho K_d \alpha}{\theta(p+\alpha)}\right)p \qquad \xi = \sqrt{\frac{V^2 + 4AD}{V^2}}$$

where $\hat{C}^r = \hat{C}^r(x,p)$ is the Laplace transform of the aqueous phase resident concentration with respect to time ($t \rightarrow p$). $\hat{C}_s^r = \hat{C}_s^r(x,p)$ is the Laplace transform of the sorbed phase resident concentration. Using numerical inversion of the Laplace transform (e.g. Jury and Roth, 1990), we can inverse the p to t, and get the solution for the resident concentration. For the case ϱ=1.5g/cm^3, porosity θ=0.3, and K_d=0.0 (R=1), the solution represents the non-sorption case we have been studying, verifying the numerical inversion of the Laplace transform with the analytical solution in equation (2.3). For the aqueous phase resident concentration and sorbed phase resident concentration, Figure 3.9 shows the resident concentration for: aqueous phase, sorbed phase and the combined phases, with K_d=0.2 (R=2) and α=0.02 day^{-1} (time constant is 50 days). Compared to that for non-sorption, the resident concentration for the aqueous phase is retarded and reduced by non-equilibrium sorption.

3.3.1 The Forward-in-time Model for Arrival Time Probability

For non-equilibrium sorption, the arrival time PDF, $f_t(t|x_o)$, is derived from the normalization of the aqueous phase flux concentration, and its Laplace transform:

$$\hat{f}_t = \frac{2exp(-s_2 x_o)}{(1+\xi)} \quad (3.18a)$$

$$\hat{g}_t = \frac{\alpha \varrho_b K_d}{\theta(\alpha + p)}\hat{f}_t \quad (3.18b)$$

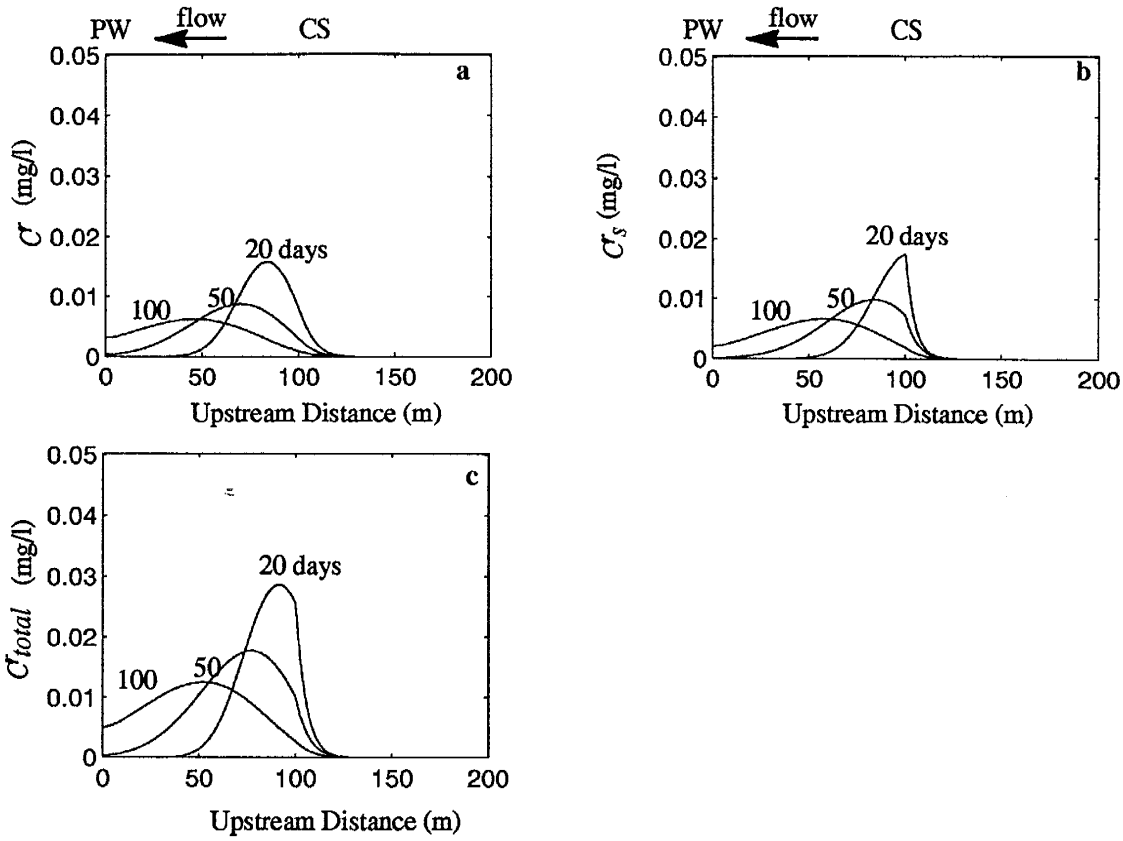

Figure 3.9. Diagram of the resident concentration (mg/l) for non-equilibrium sorption. The plots represent contaminant concentration in the aquifer 50, 100, and 200 days later. V=1.0 m/day, D=5.0 m^2/day, ϱ_b=1.5g/cm^3, θ=0.3, K_d=0.2cm^3/g, and α=0.02/day (time constant=50 days). **a.** Aqueous phase concentration; **b.** Sorbed phase concentration; **c.** Total concentration.

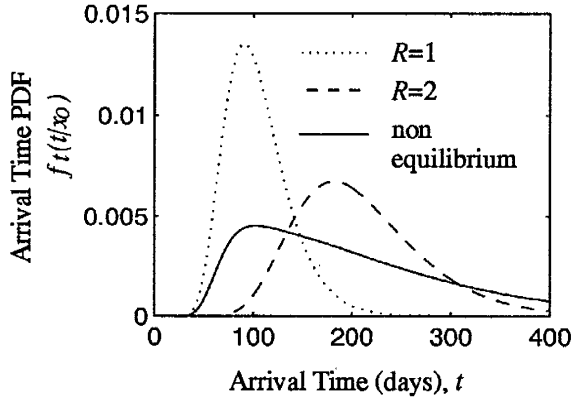

Figure 3.10. Diagram of arrival time PDF for non-equilibrium sorption. Plots give arrival time PDF for the aqueous phase for the three cases: non-sorption, linear equilibrium sorption (R=2.0), and non-equilibrium sorption (K_d=0.2cm^3/g, α=0.02 day^{-1}) for the source location, x_o=100 m, V=1.0 m/day, D=5.0 m^2/day.

where $\hat{f}_t = \hat{f}_t(x_o, p)$ is the Laplace transform of arrival time probability density function for the aqueous phase with respect to time ($t \rightarrow p$), and $\hat{g}_t = \hat{g}_t(x_o, p)$ is the Laplace transform of arrival time PDF for the sorbed phase. The constant coefficient, A and ξ are given in equation (3.17). Figure 3.10 shows diagrams of the arrival time PDFs for the aqueous phase. Compared to the cases for non-sorption (R=1) and linear equilibrium sorption (say R=2), the arrival time PDF with non-equilibrium sorption is characterized by its long tail. The integration of the arrival time PDF over the time domain is equal to one.

3.3.2 The Backward-in-time Model for Travel Time Probability

For the backward-in-time problem, the travel time PDFs for aqueous phase and sorbed phase are described by:

$$\frac{\partial f_\tau}{\partial \tau} + \frac{\partial g_\tau}{\partial \tau} = D\frac{\partial^2 f_\tau}{\partial x^2} - V\frac{\partial f_\tau}{\partial x} \tag{3.19a}$$

$$\frac{\partial g_\tau}{\partial \tau} = \frac{\alpha \varrho_b K_d}{\theta} f_\tau - \alpha g_\tau \tag{3.19b}$$

where $f_\tau = f_\tau(\tau|x)$ is the travel time PDF for the aqueous phase, and $g_\tau = g_\tau(\tau|x)$ is the travel time PDF for the sorbed phase. For the previous example shown in Figure 2.1, the appropriate boundaries and initial conditions for the aqueous phase travel time PDF are given in equation (2.8), and the initial condition for the sorbed phase travel time PDF is equal to zero, g_τ=0. The new analytical solution is derived in Appendix A5. The Laplace transform of the travel time PDFs with respect to time ($\tau \rightarrow p$) is described by:

$$\hat{f}_\tau(x, p) = \frac{2exp(-s_2 x)}{(1 + \xi)} \tag{3.20a}$$

$$\hat{g}_\tau(x, p) = \frac{\alpha \varrho_b K_d}{\theta(\alpha + p)} \frac{2exp(-s_2 x)}{(1 + \xi)} \tag{3.20b}$$

where $\hat{f}_\tau = \hat{f}_\tau(x, p)$ is the Laplace transform of travel time PDF for the aqueous phase with respect to time ($\tau \rightarrow p$), and $\hat{g}_\tau = \hat{g}_\tau(x, p)$ is the Laplace transform of travel time PDF for the sorbed phase. The constant coefficients, s_2 and ξ, are given in equation (3.17). Compared to the arrival time PDF, $\hat{f}_t = \hat{f}_t(x_o, p)$ in equation (3.18), the travel time PDF, $f_\tau(\tau \,|\, x)$, is iden-

tical. The total travel time for the aqueous phase and sorbed phase, $f_{\tau,\,\text{total}}(\tau|x)$, is given by:

$$\hat{f}_{\tau,total}(x,p) = \left[\frac{\alpha\varrho_b K_d}{\theta(\alpha + p)} + 1\right]\frac{2exp(-s_2 x)}{(1+\xi)} \tag{3.20c}$$

The cumulative distribution of travel time for the aqueous phase, $F_\tau(\tau\,|\,x)$, can be directly solved from (3.19) and (2.10) with initial condition $G_\tau(\tau\,|\,x)=0$ at $\tau=0$. The analytical solution of the Laplace transform in time is:

$$\hat{F}_\tau(x,p) = \frac{2exp(-s_2 x)}{p(1+\xi)} \tag{3.21}$$

Figure 3.11a shows the travel time probability density function for the aqueous phase for K_d=0.2 cm^3/g (R=2) and α=0.02 day^{-1} (time constant=50 days), for the three times: τ=20 days, 50 days, and 100 days. Compared to the travel time PDF for the non-sorption case in Figure 2.5a, Figure 3.11a indicates that the aqueous phase travel time PDF is retarded and reduced by the non-equilibrium sorption. Figure 12b describes the cumulative distribution of travel time for the aqueous phase. The capture zone in Figure 12b becomes smaller than that for non-sorption in Figure 2.6.

3.3.3 The Backward-in-time Model for Location Probability

The location PDFs for non-equilibrium sorption are expressed in equation (3.19) by replacing f_τ with f_x, and g_τ with g_x. The solution is derived by using double Laplace transforms in time and space along with boundary and initial conditions from equation (2.13) and initial condition g_τ=0 at τ=0. After inverting the space transform, the Laplace transform of the location PDF in time ($t\rightarrow p$) is described by:

$$\hat{f}_x = \frac{2exp(-s_2 x)}{V(1+\xi)} \tag{3.22a}$$

$$\hat{g}_x = \frac{\alpha\varrho_b K_d}{\theta(\alpha + p)}\hat{f}_x \tag{3.22b}$$

$$\hat{f}_{x,\text{total}} = \left(\frac{\alpha\varrho_b K_d}{\theta(\alpha + p)} + 1\right)\hat{f}_x \tag{3.22c}$$

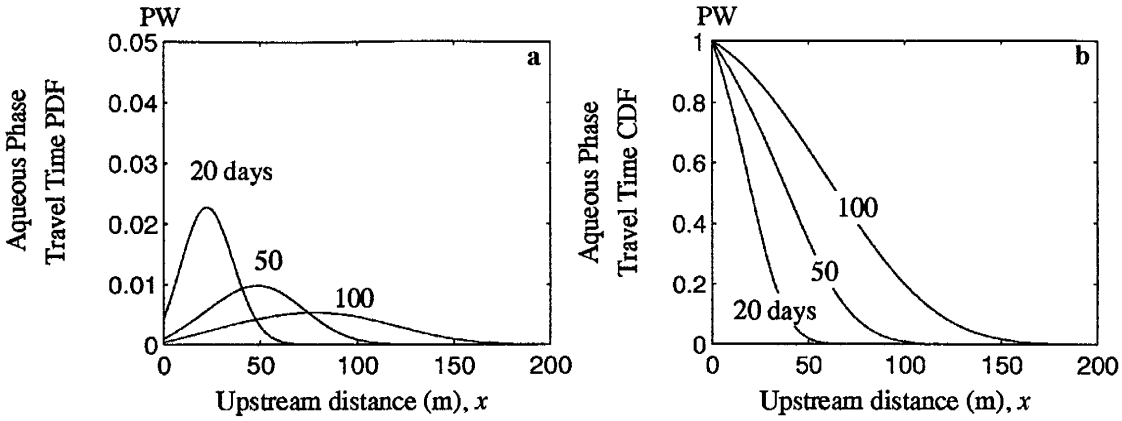

Figure 3.11. Diagram of the travel time probability for non-equilibrium sorption. **a.** The plots represent travel time PDFs for three times: τ=20 days, 50 days, and 100 days, at V=1.0 m/day, D=5.0 m^2/day, K_d=0.2 cm^3/g (R=2), and α=0.02 day^{-1} (time constant=50 days); **b.** For the aqueous phase travel time CDF.

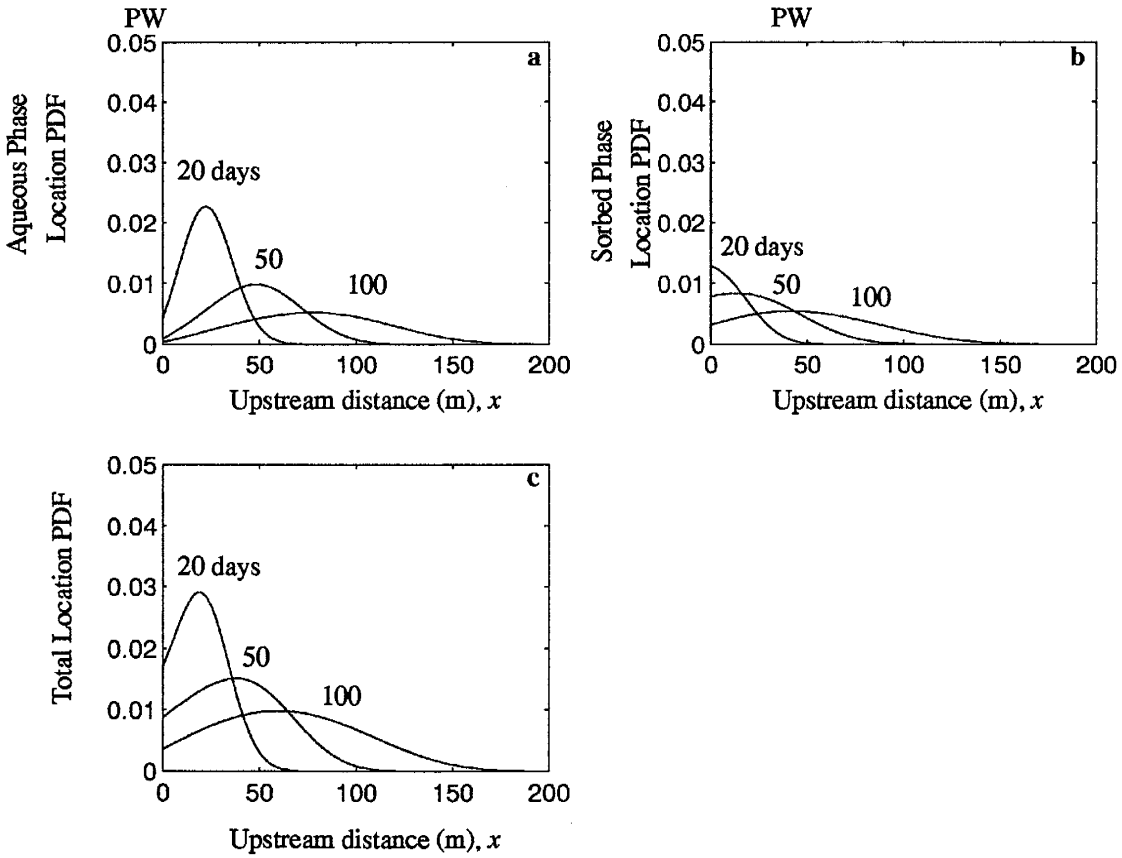

Figure 3.12. Diagram of the location PDF for non-equilibrium sorption vs. upstream distance. The plots represent location PDF for three times: τ=20, 50, 100 days, at V=1.0 m/day, D=5.0 m^2/day, K_d=0.2cm^3/g (R=2), and α=0.02 day^{-1} (time constant=50 days). **a.** Location PDF for the aqueous phase; **b.** Location PDF for the sorbed phase; **c.** Total location PDF for both the aqueous and sorbed phases.

where $\hat{f}_x = \hat{f}_x(x,p)$ is the Laplace transform of location PDF for the aqueous phase, $\hat{g}_x = \hat{g}_x(x,p)$ is the Laplace transform of location PDF for the sorbed phase. $\hat{f}_{x,\text{total}} = \hat{f}_{x,\text{total}}(x,p)$ is location PDF for the combined aqueous phase and sorbed phase.

For the previous example, Figure 3.12 shows the location probability density functions for three times: τ=20 days, 50 days, and 100 days. Figure 3.12a presents the aqueous phase location PDF. The location PDF is retarded and reduced by non-equilibrium sorption. Figure 3.12b shows that the sorbed phase location PDF. The probabilities are closer to the well. Figure 3.12c describes the total location probability density function. The three types of location PDFs are affected by the mass transport coefficient α (or time constant $1/\alpha$): For the large α, the location PDFs tend to equilibrium sorption; for the small α, the location PDFs tend to non-sorption.

For non-equilibrium sorption, the relation of total travel time probability and the total location probability can also be described by a relationship analogous to that in (3.15).

3.4 The One-dimensional Model in the Case of Natural Recharge

For a one-dimensional aquifer with natural recharge, the average velocity and dispersion are spatially variable. Contaminant transport is different than in the previous cases. When clean water is regionally recharged into the aquifer shown in Figure 2.1, the aqueous resident concentration of the contamination, $C^r(x,t)$, must be expressed as:

$$\frac{\partial C^r}{\partial t} = \frac{\partial}{\partial x}\left(D\frac{\partial C^r}{\partial x}\right) + \frac{\partial (VC^r)}{\partial x} \tag{3.24}$$

where C^r=$C^r(x,t)$ is the aqueous phase resident concentration. D=$\alpha_L V$+D^* is the dispersion coefficient [L^2/T], D^* is the diffusion coefficient, and α_L is the dispersivity. Assume that the average velocity V_o at the pumping well, x=0, is constant. The average velocity V in the aquifer can be described by:

$$V = V_o - \frac{Nx}{B\theta} \tag{3.25}$$

for uniform recharge, where N is the natural recharge rate [L/T], B is the thickness of the aquifer [L], and θ is the porosity. For the pumping system in Figure 2.1, the boundary and initial conditions are the same as those in equation (2.2).

We could not find a convenient closed form solution for the resident concentration for (3.24) and (2.2). Instead this case was simulated by an implicit finite difference method with Δt=0.1 and Δx=1.0. Figure 3.13a represents a diagram of the resident concentration vs. up-stream distance for three times: t=20days, 50days and 100 days, while V_o=1.0m/day, α_L=5m, N=0.001 m/day, and θ=0.3. Because the average velocity, V, and the dispersion coefficient, D, linearly decrease in the x direction, the contaminant concentration distributions are not symmetric in the aquifer, a significant difference from the the concentration distributions for no recharge in Figure 2.2.

3.4.1 The Forward-in-time Model for Arrival Time Probability

In the forward-in-time problem, since $\partial C^r/\partial x = 0$ at the pumping well, the aqueous phase flux concentration is equal to the resident concentration simulations. The arrival time PDF can be obtained from the normalization of the simulated concentrations at the pumping well. Figure 3.13b shows the arrival time PDF for natural recharge. It is delayed by the lower velocities intrinsic to this aquifer, and is somewhat spread out by the higher velocities at the head of the plume, relative to the tail.

3.4.2 The Backward-in-time Model for Travel Time Probability

The backward-in-time model can also be extended to the case of natural recharge. The flow problem is run backward-in-time, and the distributed natural recharge becomes a pre-scribed discharge. For the pumping well in Figure 2.1, the travel time PDF, $f_\tau = f_\tau(\tau \mid x)$, can be computed from:

$$\frac{\partial f_\tau}{\partial \tau} = \frac{\partial}{\partial x}\left(D\frac{\partial f_\tau}{\partial x}\right) + \frac{\partial(-Vf_\tau)}{\partial x} - \frac{N}{B\theta}f_\tau \tag{3.26}$$

After inserting equation (3.25) into equation (3.26), we can obtain:

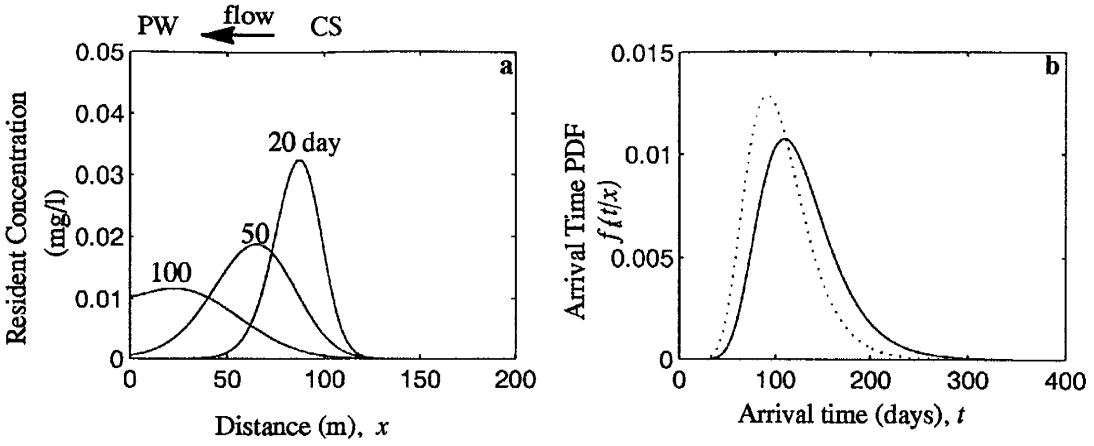

Figure 3.13. **a.** Space-time solution of the contaminant concentration (mg/l) for the case of uniform natural recharge. The contamination source (CS) is located at x_o=100 m, and the pumping well (PW) is located at x=0. The average velocity at the pumping well V_o=1.0 m/day, natural recharge rate N=0.001m/day, the dispersivity α_L=5.0 m. **b.** Normalized flux concentration or arrival time PDF at the pumping well vs. arrival time. Solid line represents the natural recharge with N=0.001 m/day; dotted line represents the non natural recharge case.

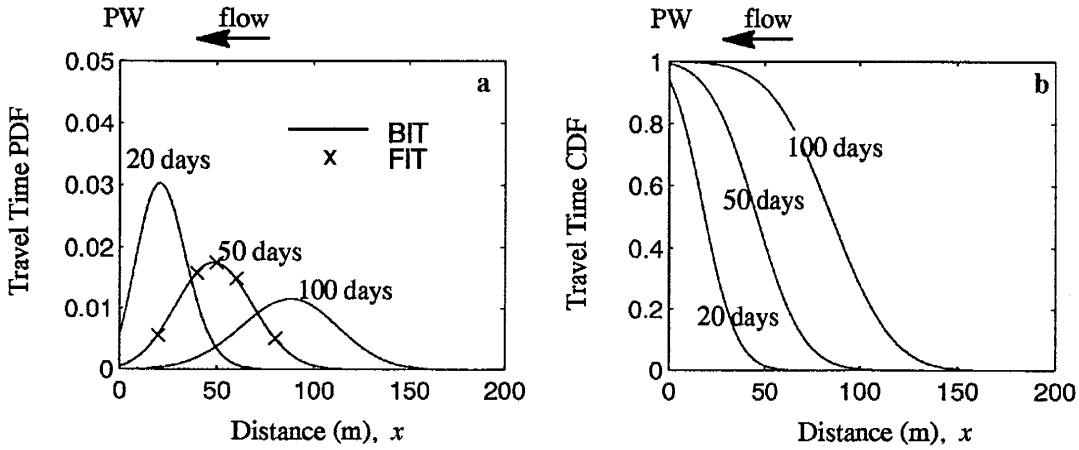

Figure 3.14. Diagram of travel time probability for the case of natural recharge. **a.** The plots represent travel time PDF for three travel times: τ=20, 50, and 100 days at V_o=1.0 m/day, α_L=5.0 m, and N=0.001m/day. Solid lines represent BIT PDE solutions and crosses represent FIT solutions. **b.** The plots represent travel time CDF.

$$\frac{\partial f_\tau}{\partial \tau} = \frac{\partial}{\partial x}\left(D\frac{\partial f_\tau}{\partial x}\right) - V\frac{\partial f_\tau}{\partial x} \tag{3.27}$$

For natural recharge, the initial and boundary conditions are the same as in equation (2.8).

The solution of the travel time PDF is simulated by the implicit finite difference method. Figure 3.14a represents a diagram of the travel time PDF vs. upstream distance for three times: τ=20 days, 50 days and 100 days in the past. Figure 3.14a also presents five arrival time PDFs for τ=50 days, computed from the forward-in-time method for five different source locations. Comparison of travel time PDFs and the five arrival time PDF values confirms the travel time PDFs from the backward-in-time model. Figure 3.15a states the influence of the natural recharge rate on the travel time PDFs. The travel time PDF decreases as the recharge rate increases.

The travel time cumulative distribution function (CDF), $F_\tau(\tau \mid x)$, can be obtained from integration of the travel time PDFs, or can be directly solved from the equations (3.27) and (2.10). Figure 3.14b shows the distributions of travel time CDF vs. upstream distance for travel times: τ=20 days, 50 days, and 100 days. Figure 3.15b represents the influence of the natural recharge rate on the capture zone. The capture zone reduces as the recharge rate increases.

3.4.3 The Backward-in-time Model for Location Probability

In the case of natural recharge, the location probability can also be determined from the backward-in-time PDE. Because we assume that the contaminant did not come from natural recharge but an independent contaminant source at x_o, the backward-in-time PDE does not involve the "discharging" of the location probability while the groundwater flow is reversed. The location PDF, f_x=$f_x(x \mid \tau)$, *is* described by:

$$\frac{\partial f_x}{\partial \tau} = \frac{\partial}{\partial x}\left(D\frac{\partial f_x}{\partial x}\right) - \frac{\partial (V f_x)}{\partial x} \tag{3.28}$$

The initial and boundary conditions are the same as in equation (2.13).

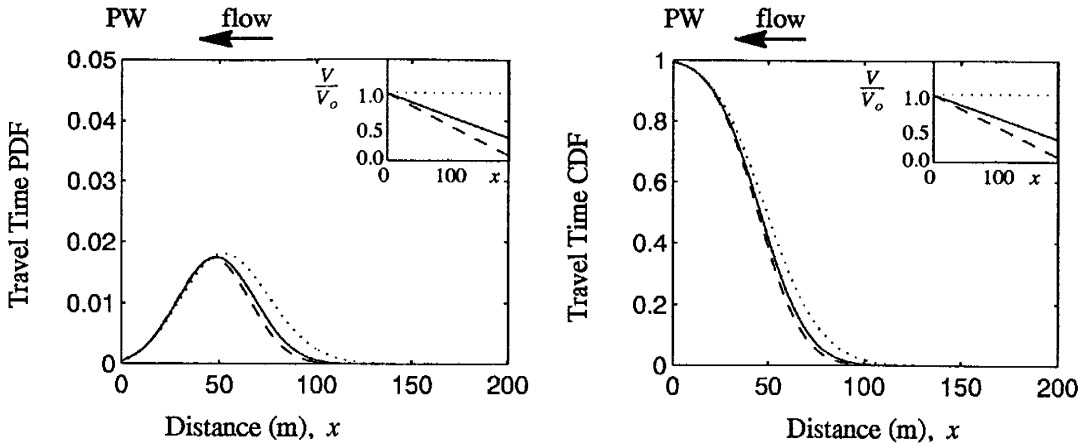

Figure 3.15. Impact of natural recharge on the travel time probability. **a.** The plots represent travel time PDF for τ=50 days at V_o=1.0 m/day, α_L=5.0 m. Solid lines represent the natural recharge rate, N=0.001 m/day; the dashed line represents the natural recharge rate N=0.0014 m/day; the dotted line represents the natural recharge rate N=0. **b.** The plots represent the cumulative probability distribution function.

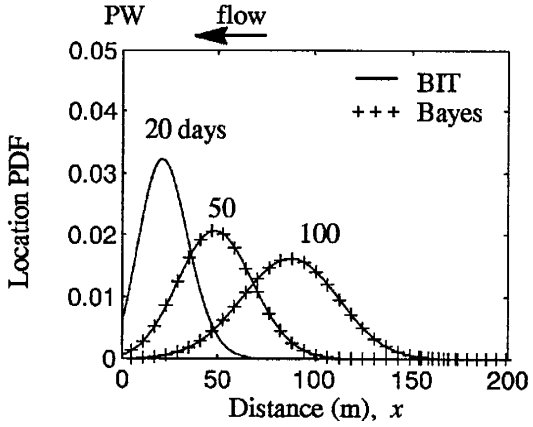

Figure 3.16. Diagram of location probability vs. upstream distance. The plots represent location PDF for three times: τ=20, 50, and 100 days, at V_o=1.0 m/day, α_L=5.0 m, and N=0.001 m/day. Solid lines show backward-in-time (BIT) PDEs solution; The crosses show solutions obtained using the Bayes theorem.

For the previous example, the numerical solutions of location probabilities from equations (3.28) and (2.13) are shown in Figure 3.16. Figure 3.16 shows the location PDFs for three times: τ=20 days, 50 days and 100 days in the past. Due to the velocity linearly decreasing along the direction x, the greatest location probability is located at about 90 m in 100 days. The capture zone of the contamination is reduced by natural recharge.

For the case of natural recharge, the travel time PDF and location PDF can also be described by equation (2.20), such that we can compute the location PDFs from the travel time PDFs through the Bayes theorem shown in equation (2.20). Figure 3.16 shows the location PDFs computed from the travel time simulation using the Bayes theorem for time τ=50 days, and 100 days. Compared to the location PDF simulations from equation (3.28), the location PDFs from the Bayes theorem are in close agreement to the location PDF simulations.

4. THE TWO-DIMENSIONAL BACKWARD-IN-TIME MODEL FOR TRAVEL TIME AND LOCATION PROBABILITIES

In the previous sections, one-dimensional models have been used to successfully study the backward-in-time approach, accounting for dispersion, chemical reactions, and natural recharge. In this section we extend the new method to a two-dimensional domain, shown in Figure 4.1, and demonstrate how to create travel time and location probability maps for it. The aquifer consists of two sub-domains: high hydraulic conductivity and low hydraulic conductivity. The groundwater flows from right to left. In the pumping well system, the pumping well is located at the downstream location, $\boldsymbol{X}_1=(x_1,y_1)$, and the contamination was introduced into the aquifer from an upstream location, $\boldsymbol{X}_o=(x_o, y_o)$. The contamination plume moves downstream, spreads, dilutes, and finally is extracted by the pumping well. This model is used to examine the new method for cases of aquifer heterogeneity, linear equilibrium sorption, non-equilibrium sorption, and natural recharge. The FIT solute transport, and backward-in-time probability models are simulated by the Laplace transform-in-time Galerkin finite element method (Sudicky and McLaren, 1992). The computer code, FRACTRAN (Sudicky and McLaren, 1991), is modified for cases of natural recharge, non-equilibrium sorption, and third type boundary conditions for sinks and sources.

4.1 The Two-dimensional Backward-in-time Model in a Heterogeneous Aquifer

4.1.1 Contaminant Transport in a Two-dimensional Heterogeneous Aquifer

In the pumping well system in Figure 4.1, the hydraulic head is expressed by the governing equation for steady state flow with a point sink:

$$\frac{\partial}{\partial x_i}\left(T_{ij}\frac{\partial h}{\partial x_j} \right) - \delta(\boldsymbol{X}-\boldsymbol{X}_1)Q_o = 0 \qquad (4.1)$$

where h is hydraulic head [L], T_{ij} is the second order aquifer transmissivity [L^2/T] tensor with i, j=1, 2, Q_o is the pumping rate[L^3/T] at a location, and $\boldsymbol{X}_1=(x_1,y_1)$. $x_{i,j}$ are the coordinates of the domain, x, y, and $\boldsymbol{X}=(x,y)$. The governing equation accounts for heterogeneous and

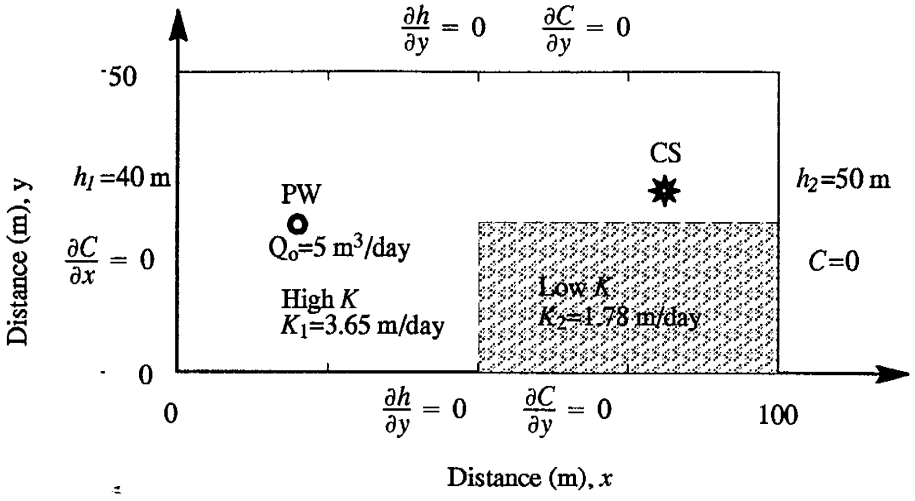

Figure 4.1 Illustration of the physical dimensions of a basic steady state flow, two-dimensional mass transport model. The heterogeneous domain is about 100 m in length and 50 m in width. A pumping well (PW) is located at (20,25), and the dissolved contamination source (CS) is located at (80,30). For the groundwater flow, the boundary conditions are illustrated as a constant head along the left and right sides with impermeable boundaries on the top and bottom. The hydraulic conductivity: K_1=3.56 m/day, K_2=1.78 m/day. For the mass transport, second type boundary conditions are used except for a first-type boundary condition on the right side.

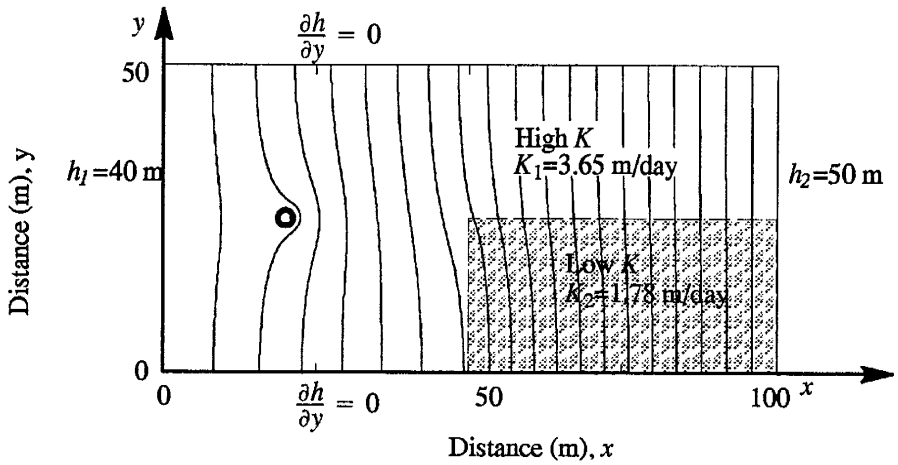

Figure 4.2. Two-dimensional hydraulic head contour in a heterogeneous aquifer. The pumping well (PW) is located at (20,25) with pumping rate Q_o=5.0 m^3/day. The contour interval is 0.5 m.

isotropic aquifer conditions, and for a steady state flow with sources or sinks. The boundary conditions in Figure 4.1 are described as a constant head on the left and right boundary, and no flow through the top and bottom boundary:

$$h = h_1, \text{ at } x = 0; \; h = h_2, \text{ at } x = L_x \tag{4.2a}$$

$$\frac{\partial h}{\partial y} = 0, \text{ at y} = 0; \; y = L_y \tag{4.2b}$$

where L_x and L_y are the length and width of the domain, and Q_o is the pumping rate at the pumping well. The hydraulic head solution for the steady state from equations (4.1)–(4.2) is numerically simulated by the Galerkin finite element method (Sudicky and McLaren, 1992). The average velocity of the groundwater is computed by Darcy's law. The parameters for groundwater flow in Figure 4.1 are shown in Table 4.1. Figure 4.2 shows the simulated hydraulic head. The groundwater flow direction is normal to the contour of the hydraulic head.

For contaminant transport in the two–dimensional heterogeneous domain shown in Figure 4.1, the contaminant was introduced into the aquifer at contamination source (CS), $\boldsymbol{X_o}=(x_o, y_o)$, at time t=0. The aqueous phase resident concentration $C^r(\boldsymbol{X},t)$ can be expressed as (Dagan, 1984; Dagan and Nauyen, 1989; Sudicky and McLaren, 1992):

$$\frac{\partial C^r}{\partial t} = \frac{\partial}{\partial x_i}\left(D_{ij}\frac{\partial C^r}{\partial x_j} \right) - V_i \frac{\partial C^r}{\partial x_i} \tag{4.3}$$

where $C^r=C^r(\boldsymbol{X},t)$ is the resident concentration, $V_i(i=1,2)$ is a first–order velocity tensor, and D_{ij} $(i,j=1,2)$ is a second–order dispersion tensor. For the example in Figure 4.1, the boundary and initial conditions for the mass transport are expressed as:

$$\frac{\partial C^r}{\partial x} = 0, \text{ at } x = 0; \quad C^r = 0, \text{ at } x = L_x \tag{4.4a}$$

$$\frac{\partial C^r}{\partial y} = 0, \text{ at y} = 0; \quad \frac{\partial C^r}{\partial y} = 0, \text{ at y} = L_y \tag{4.4b}$$

$$\lim_{r \to 0} \int_S \frac{\partial C^r}{\partial r} dS = 0, \text{ at pumping well } (x_1, y_1) \tag{4.4c}$$

$$C^r = \frac{M}{\theta B}\delta(\boldsymbol{X}-\boldsymbol{X}_o), \quad \text{for } t = 0 \tag{4.4d}$$

where $C^r=C^r(\boldsymbol{X},t)$ is the resident concentration, M is the released mass of 0.356 grams at $\boldsymbol{X}_o=(x_o,y_o)$, S is the boundary around the pumping well at radius, r. For the pumping well, the Newman solute flux is equal to zero. For the initial condition, $\delta(\boldsymbol{X}-\boldsymbol{X}_o)=\delta(x-x_o, y-y_o)$ is a Dirac function at point (x_o,y_o).

Table 4.1. The parameters for the groundwater flow and mass transport model:

Parameters	Description
Domain	100 m x 50 m rectangle
Heterogeneous and isotropic hydraulic conductivity	$K_x=K_y=3.56$ m/day in high K sub-domain $K_x=K_y=1.78$ m/day in low K sub-domain
Longitudinal dispersivity	α_L =0.4 m
Lateral dispersivity	α_T =0.2 m
Diffusion coefficient	D^*=3.0E-4 m^2/day
Porosity	θ=0.35
Porous medium bulk density	ϱ_b=1.5g/cm^3
Pumping well location	x=20, y=25m
Pumping rate	Q_o=5.0 m^3/day
Boundary conditions for groundwater flow	h_1=40 m at x=0 m, h_2=50 m at x=50 m $\partial h/\partial y$=0 on top and bottom boundaries
Boundary conditions for contaminant transport	C^r=0 at the right boundary $\partial C^r/\partial x_i$=0; otherwise
Initial condition for mass transport	$C^r=[M/(B\theta)]\ \delta(\boldsymbol{X}-\boldsymbol{X}_o)$ for t=0
Grid characteristics	Δx=0.5m, Δy=0.5m; 20,000 square elements and 20,301 nodes.

The parameters for contaminant transport are listed in Table 4.1. For the contamination source at (80,30), the resident concentration simulations from equations (4.3)–(4.4) are shown in Figure 4.3. Figure 4.3 represents resident concentration contours for three travel times: t=30 days, 40 days, and 60 days. The contaminant plume moves downstream, spreads,

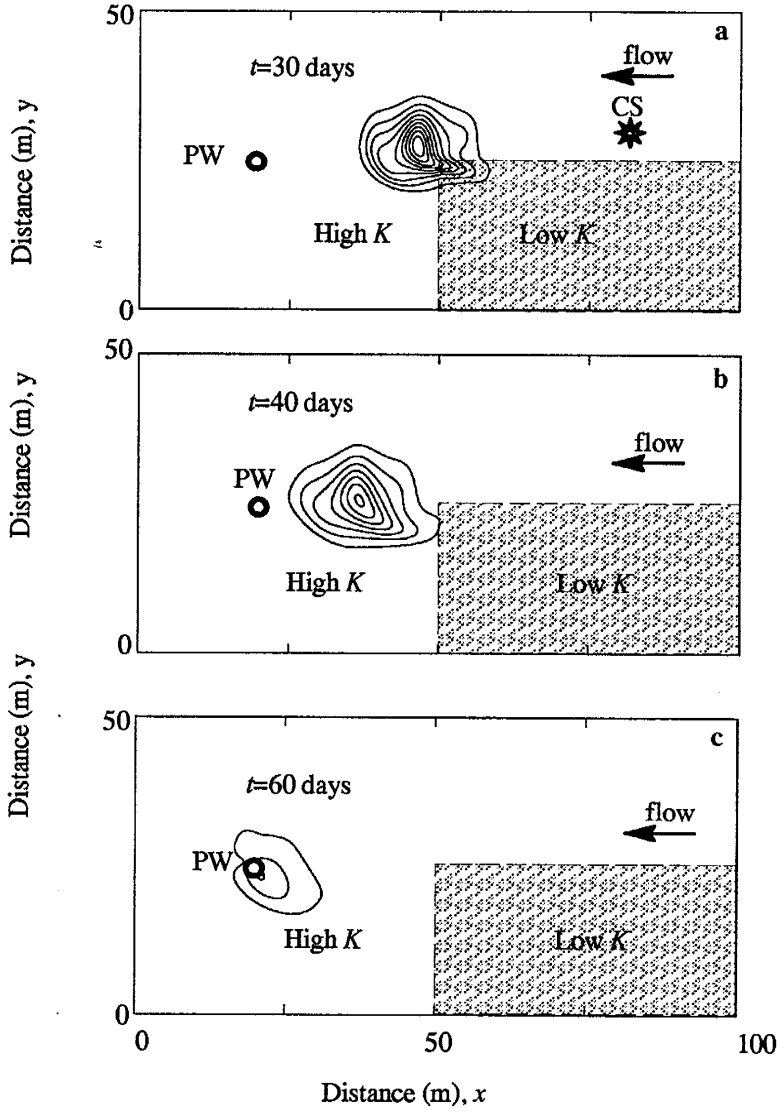

Figure 4.3. Two-dimensional transport of a contaminant plume in a heterogeneous aquifer. The contaminant source (CS) is located at (80,30), and the pumping well (PW) is located at (20,25). The outermost contour line represents 0.004 (mg/l), the contour interval is 0.004 (mg/l). a–c show the plumes for 30 days, 40 days, and 60 days, respectively.

and dilutes. This figure shows the combined effects of advection, dispersion, and aquifer heterogeneity.

4.1.2 The Forward-in-time Model for Arrival Time Probability

We can apply equations (4.3)-(4.4) to the problem of determining the contaminant flux-concentration arriving at the pumping well. In the pumping well the arriving aqueous phase flux concentration, $C^f(\boldsymbol{X},t)$, is equal to the resident concentration, $C^f(\boldsymbol{X},t)=C^r(\boldsymbol{X},t)$, as is shown by equation (4.4c). The arrival time probability density function, $f_t(t\,|\,\boldsymbol{X}_o)$ describes the probability that a non-reacting contaminant particle, released at location (x_o, y_o) at time, t=0, will reach the pumping well at (x_1, y_1) in time t. The arrival time PDF is obtained from the normalized flux concentration:

$$f_t(t|\boldsymbol{X}_o) = \frac{Q_o C^f(\boldsymbol{X}_1, t)}{M} \tag{4.5}$$

here $f_t(t\,|\,\boldsymbol{X}_o)$ is the arrival time PDF for a given source location, $\boldsymbol{X}_o=(x_o, y_o)$. Q_o is the pumping rate at the pumping well, located at $\boldsymbol{X}_1=(x_1, y_1)$. M is the total mass released at the source location.

We can compute the arrival time PDF for a given source location, $\boldsymbol{X}_o$. What happens if we don't know where the source is located? Suppose all we observe is the contamination concentration in the pumping well. It is possible to simulate the arrival time PDF numerically for each possible source location, but if there are a large number of these it would be very expensive in terms of time and computational resources. Worse, what if we do not know where the possible sources are?

4.1.3 The Backward-in-time Model for Travel Time Probability

In the new method, the travel time PDF can be directly formulated using the backward-in-time method. The two-dimensional travel time PDF, $f_\tau(\tau\,|\,\boldsymbol{X})$, for a travel time, τ, from some location $\boldsymbol{X}=(x, y)$ to pumping well location (x_1, y_1), can be expressed with the standard advection-dispersion equation by replacing the concentration with $f_\tau(\tau\,|\,\boldsymbol{X})$, and replacing V in the forward problem by $-V$:

$$\frac{\partial f_\tau}{\partial \tau} = \frac{\partial}{\partial x_i}\left(D_{ij}\frac{\partial f_\tau}{\partial x_j} \right) + V_i \frac{\partial f_\tau}{\partial x_i} \tag{4.6}$$

where $f_\tau = f_\tau(\tau \mid \boldsymbol{X})$ is travel time PDF, and $i, j = 1, 2$. In this example, the boundary and initial conditions are as follows:

$$\frac{\partial f_\tau}{\partial x} = 0, \text{ at } x = 0; \qquad f_\tau = 0, \text{ at } x = L_x \tag{4.7a}$$

$$\frac{\partial f_\tau}{\partial y} = 0, \text{ at } y = 0; \qquad \frac{\partial f_\tau}{\partial y} = 0, \text{ at } y = L_y \tag{4.7b}$$

$$\lim_{r\to 0}\int_S \left[-V_r f_\tau - D_r \frac{\partial f_\tau}{\partial r} \right] dS = \frac{Q_o}{\theta B}\delta(\tau), \text{ at pumping well } (x_1, y_1) \tag{4.7c}$$

$$f_\tau = 0, \quad \text{at } \tau = 0 \tag{4.7d}$$

where the V_r and D_r are the average velocity, and dispersion coefficient along the normal direction of the pumping well, S is the boundary of the pumping well as $r \to 0$, and Q_o is the pumping rate. Figure 4.4 shows the boundary conditions in the domain. The travel time PDF for each possible location can be obtained by running only one simulation from equations (4.6)–(4.7).

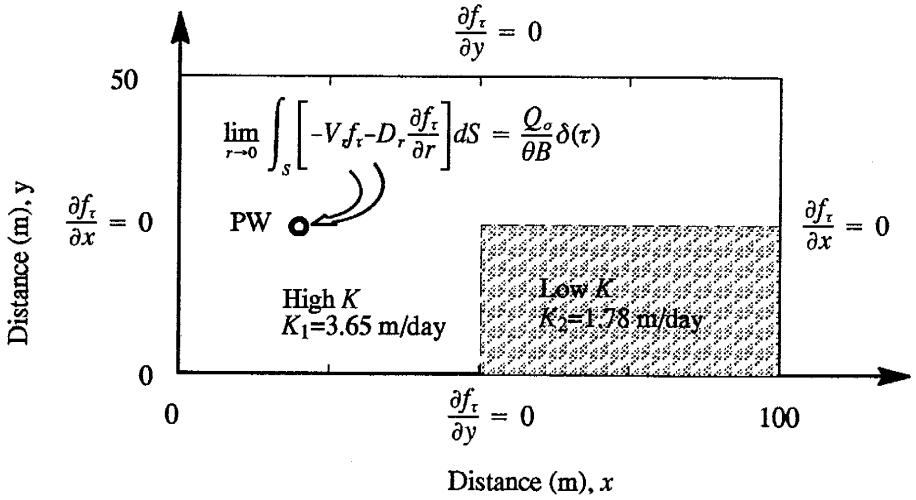

Figure 4.4. Illustration of the physical dimensions of a two-dimensional backward-in-time model. The heterogeneous domain is about 100 m in length and 50 m in width. The pumping well (PW) represents an "injected well" in the backward-in-time problem. A third type boundary condition is used at the pumping well, and second type boundary conditions are used on the other boundary.

The simulated result for the example is shown in Figure 4.5. Figure 4.5 represents the travel time PDF map for three times: τ=30 days, 40 days, and 60 days in the past. It shows that the capture zone moves in an upstream direction and spreads. Figure 4.5 also shows reduced probability as time progresses in a backward direction. The travel time PDF distribution is affected by the heterogeneity of the aquifer, and a high travel time PDF tends to occur in the high conductivity area.

Can we compare the backward-in-time (BIT) solution to the forward-in-time (FIT) solutions? Figure 4.6a and Figure 4.6b represent the travel time PDF, $f_\tau(\tau \mid \boldsymbol{X})$, (in solid line) vs. arrival times for locations (80,30) and (80, 20), simulated with the forward-in-time method (in dotted line). The small difference is due to the numerical simulation technique. The arrival time PDFs and travel time PDFs demonstrate that the travel time from the aquifer to the pumping well can be estimated using either the BIT solution or the FIT solution, but the BIT approach is more efficient. The travel time PDF for a location in the higher conductivity area is higher than that for a location in the lower conductivity area. Figure 4.7 shows the travel time PDF for 60 days along a cross section through both locations (80, 20) and (80, 30), from a single backward-in-time solution, and the arrival time PDFs from five forward-in-time solutions, further confirming the validity and efficiency of the method.

The travel time cumulative distribution function (CDF), $F_\tau(\tau \mid \boldsymbol{X})$, describes the probability that a contaminant is captured by the pumping well in a period of time less than τ, from a given location, $\boldsymbol{X}$=(x,y). The travel time CDF, $F_\tau(\tau \mid \boldsymbol{X})$, can be obtained by integrating the travel time PDF, $f_\tau(\tau \mid \boldsymbol{X})$:

$$F_\tau(\tau|\boldsymbol{X}) = \int_0^\tau f_\tau(\tau'|\boldsymbol{X})d\tau' \tag{4.8}$$

In the new method, the travel time CDF can also be formulated from equation (4.6) by replacing f_τ with F_τ, along the boundary conditions:

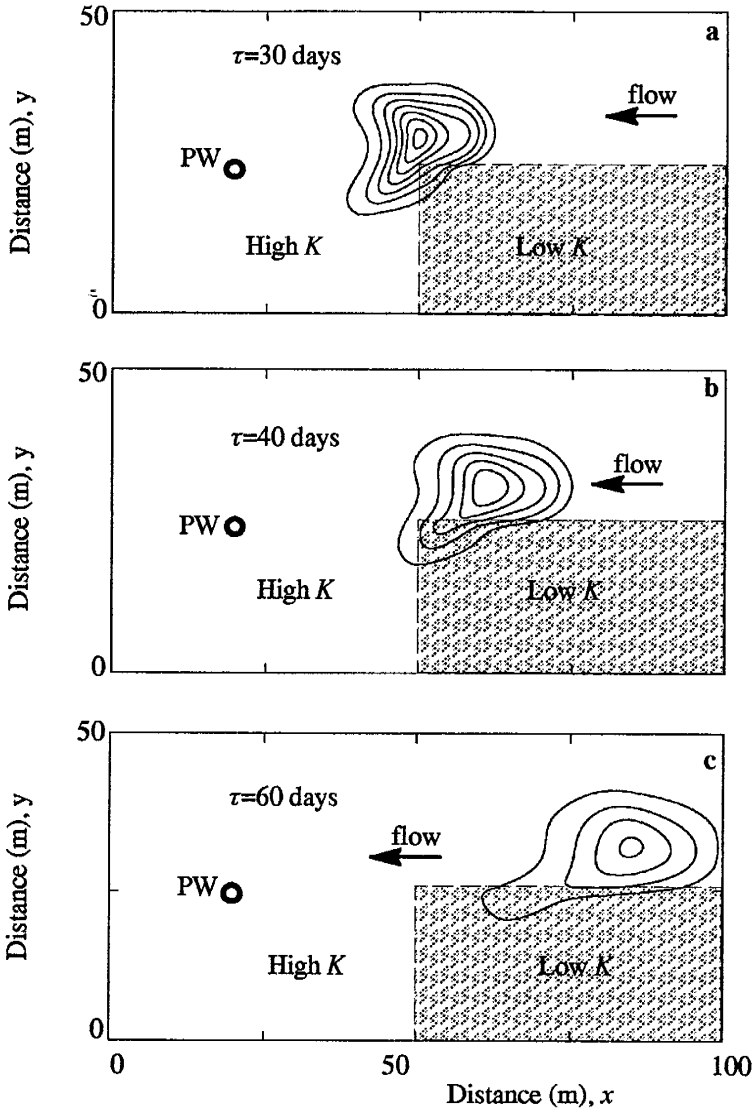

Figure 4.5. Two-dimensional travel time PDF in a heterogeneous aquifer. The outermost contour line represents 0.02, and the contour interval is 0.02, in units of 1 day^{-1}. a–c show the travel time PDF for 30 days, 40 days, and 60 days, respectively.

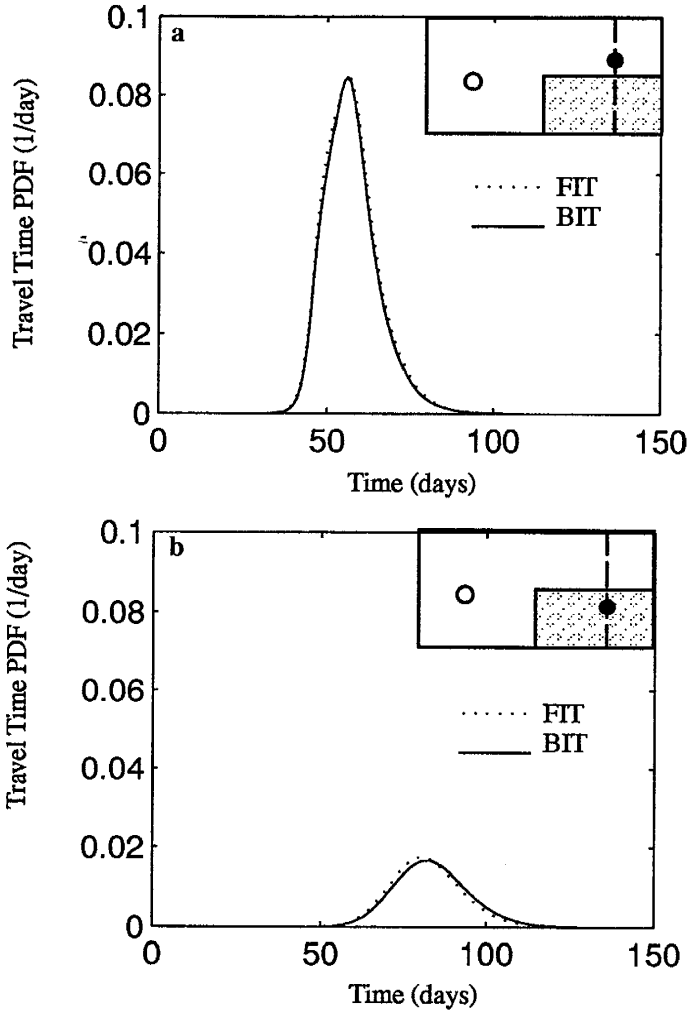

Figure 4.6. Diagram of the travel time PDF, $f_\tau(\tau|X)$ vs. travel time. **a.** Travel time PDF for the source location at (80,30), in which the dotted line shows the forward-in-time (FIT) solutions, and the solid line shows the backward-in-time (BIT) solution. **b.** Travel time PDF for the source location at (80,20). Two FIT simulations are required to construct this figure, but only one BIT simulation.

$$\frac{\partial F_\tau}{\partial x} = 0, \text{ at } x = 0; \qquad F_\tau = 0, \text{ at } x = L_x \tag{4.9a}$$

$$\frac{\partial F_\tau}{\partial y} = 0, \text{ at } y = 0; \qquad \frac{\partial F_\tau}{\partial y} = 0, \text{ at } y = L_y \tag{4.9b}$$

$$\lim_{r \to 0} \int_S \left[- V_r F_\tau - D_r \frac{\partial F_\tau}{\partial r} \right] dS = \frac{Q_o}{\theta B}, \text{ at pumping well } (x_1, y_1) \tag{4.9c}$$

$$F_\tau = 0 \quad \text{at } \tau = 0 \tag{4.9d}$$

where $F_\tau = F_\tau(\tau \mid \boldsymbol{X})$ is travel time CDF.

The travel time CDF can be computed by the following methods: 1) integration of the forward-in-time PDF, 2) integration of the backward-in-time PDF, and 3) direct computation using the backward-in-time method. The solutions from all three methods are in very close agreement, differing only by a small amount attributable to numerical approaches. Figure 4.8 shows the travel time CDF, $F_\tau(\tau \mid x,y)$, for times: τ=30 days, 40 days and 60 days. The capture zone of the contaminant extends in an upstream direction as the time increases. For the forward problem, the travel time CDF in this example had to be reconstructed by running many simulations to approximate the continuous curve of $F_\tau(\tau \mid \boldsymbol{X})$. In practical multidimen-

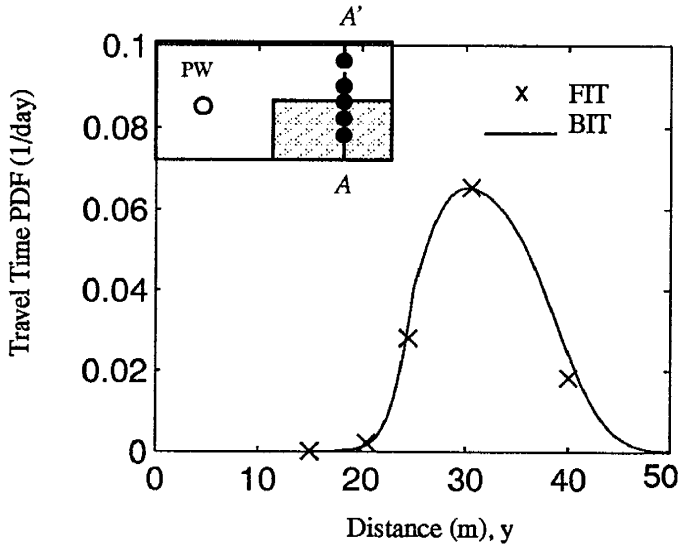

Figure 4.7. Diagram of the travel time PDF vs. distance along the cross section A-A' at x=80 m. The crosses represent the travel time PDF from five forward-in-time solutions for source locations: y=15 m, 20 m, 25 m, 30 m, and 40 m. The solid line shows one backward-in-time solution along the cross section.

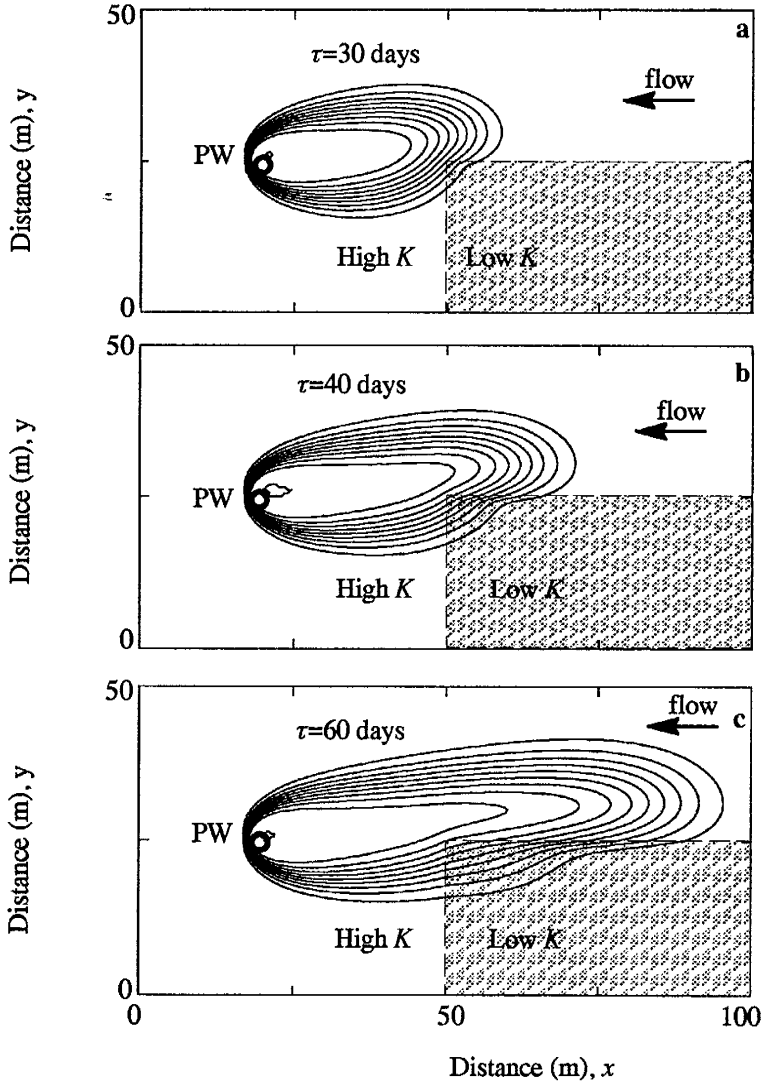

Figure 4.8. Two-dimensional travel time CDF in the heterogeneous aquifer. The outermost contour line represents 0.1, and the contour interval value is 0.1. a–c show the travel time CDFs for travel time less than 30 days, 40 days, and 50 days, respectively.

sional applications, with many potential source locations, it is unrealistic to obtain the CDF in this manner. In the backward-in-time method, the travel time CDF is easily obtained by running one numerical simulation.

4.1.4 The Backward-in-time Model for Location Probability

The location probability density function, $f_X(\boldsymbol{X}|\tau)$ describes the probability that a non-reacting contaminant particle observed from the pumping well was located at the position, $\boldsymbol{X}=(x,y)$, at a given travel time, τ. In the new method, the location PDF can be formulated by the backward-in-time PDE:

$$\frac{\partial f_X}{\partial \tau} = \frac{\partial}{\partial x_i}\left(D_{ij}\frac{\partial f_X}{\partial x_j} \right) + V_i\frac{\partial f_X}{\partial x_i} \tag{4.10}$$

where $f_X=f_X(\boldsymbol{X}|\tau)$ is the location probability density function. A unit probability is "introduced" into the aquifer at the pumping well in $\tau=0$. The boundary conditions and initial conditions are:

$$\frac{\partial f_X}{\partial x} = 0, \text{ at } x = 0; \qquad f_X = 0, \text{ at } x = L_x \tag{4.11a}$$

$$\frac{\partial f_X}{\partial y} = 0, \text{ at } y = 0; \qquad \frac{\partial f_X}{\partial y} = 0, \text{ at } y = L_y \tag{4.11b}$$

$$\lim_{r\to 0}\int_S \left[-V_r f_X - D_r\frac{\partial f_X}{\partial r} \right] dS = 0, \text{ at pumping well } (x_1, y_1) \tag{4.11c}$$

$$f_X = \delta(\boldsymbol{X}-\boldsymbol{X}_1), \text{ at } \tau = 0 \tag{4.11d}$$

where the V_r and D_r are the average velocity and dispersion coefficients along the normal direction of the pumping well, and S is the boundary of the pumping well at $r\to 0$.

For the same domain and the contaminant transport model in the previous example, the simulated location PDF, computed from equations (4.10)-(4.11), is shown in Figure 4.9 for three times: τ=30 days, 40 days, and 60 days in the past. It shows that the location distribution moves in an upstream direction, and spreads. The location PDF is affected by the heterogeneity of the aquifer, and a high location PDF tends to occur in the high conductivity area.

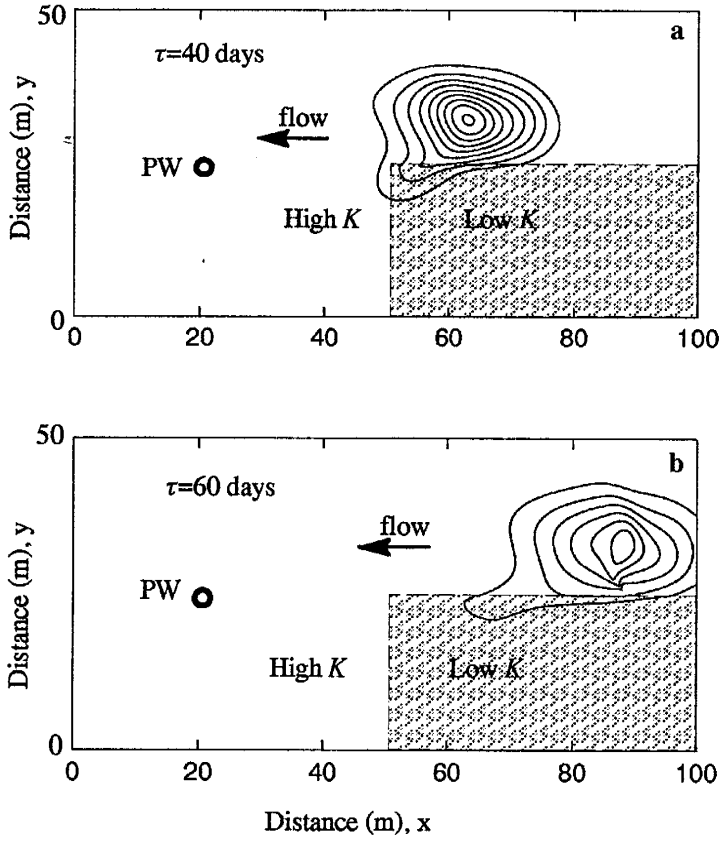

Figure 4.9. Two-dimensional location PDF in a heterogeneous aquifer. The outermost contour line represents 5.0E-4, and the contour interval is 5.0E-4 in units of 1 m^{-2}. **a-b** show the location PDFs for travel times of 40 and 60 days, respectively.

In a one–dimensional model, the relationship between the travel time and location probabilities has been described by the Bayes theorem. In a two–dimensional model, the relationship of the travel time and location probabilities is also derived from their simulations using the backward–in–time models. It is confirmed by the Bayes Theorem:

$$f_X(X|\tau) = \frac{f_\tau(\tau|X)g(X)}{\int_0^\infty f_\tau(\tau|X)g(X)dxdy} \tag{4.12}$$

where $f_X(X \mid \tau)$ is a conditional location PDF, and $g(X)$ is a uniform probability density function. $f_\tau(\tau|X)$ is the travel time probability density function. In the case of advection–dispersion only, equation (4.12) can be rewritten:

$$f_X(X|\tau) = \frac{\theta B}{Q_o} f_\tau(\tau|X) \tag{4.13}$$

For a two–dimensional heterogeneous aquifer, the travel time probability can be directly determined using the backward–in–time method, and is in close agreement with the simulation results from traditional forward–in–time methods. The examples in this research demonstrate that the backward–in–time method can be applied in a two–dimensional aquifer. For the pumping well system, the appropriate boundary condition for the travel time PDF in the backward–in–time PDE is a delta function third type boundary condition at the pumping well and the proper boundary condition for travel time CDF is a third type boundary condition. The proper initial condition for the location PDF is a delta function at the pumping well.

The travel time and location probabilities are affected by the heterogeneity of the aquifer. The backward–in–time simulations demonstrate that high probabilities tend to locate in high permeable sub–domains, and small probabilities tend to locate in low permeable sub–domains.

4.2 The Two-dimensional Backward-in-time Model for the Case of Linear Equilibrium Sorption

In the case of sorption in the domain shown in Figure 4.1, it is supposed that the groundwater flow conditions are the same as in the previous example. Two cases of sorption will be considered in this report: linear equilibrium sorption and non-equilibrium sorption.

For linear equilibrium sorption, the aqueous phase resident concentration $C^r(\boldsymbol{X},t)$ can be expressed as:

$$R\frac{\partial C^r}{\partial t} = \frac{\partial}{\partial x_i}\left(D_{ij}\frac{\partial C^r}{\partial x_j}\right) - V_i\frac{\partial C^r}{\partial x_i} \tag{4.14}$$

where $C^r = C^r(\boldsymbol{X},t)$ is the aqueous phase resident concentration in the aquifer, and R is the retardation coefficient. For the example shown in Figure 4.1, the boundary and initial conditions for mass transport are expressed by equation (4.4).

For the previous example, it is supposed R=1.5 in the high K sub-domain, and R=2.0 in the low K sub-domain. The results of the simulations from equations (4.14) and (4.4) are shown in Figure 4.10 and Figure 4.11. Figure 4.10 shows the aqueous phase resident concentration contours for three times: t=40 days, 60 days, and 90 days after release at source location, (80, 30). Compared to the aqueous resident concentration contours of non-sorption in Figure 4.3, Figure 4.10 demonstrates that the contaminant plumes are retarded by the sorption, and the retardation in the low K sub-domain is larger than that in the high K sub-domain. Figure 4.11 demonstrates that the sorbed phase resident concentration is also retarded by the sorption.

4.2.1 The Backward-in-time Model For Travel Time Probability

In the new method, the travel time PDF for the sorption case can be directly solved by applying the backward-in-time PDEs. The travel time PDF can be expressed as:

$$R\frac{\partial f_\tau}{\partial \tau} = \frac{\partial}{\partial x_i}\left(D_{ij}\frac{\partial f_\tau}{\partial x_j}\right) + V_i\frac{\partial f_\tau}{\partial x_i} \tag{4.15}$$

where $f_\tau = f_\tau(\tau \mid \boldsymbol{X})$ is the aqueous phase travel time PDF, and R is the retardation factor.

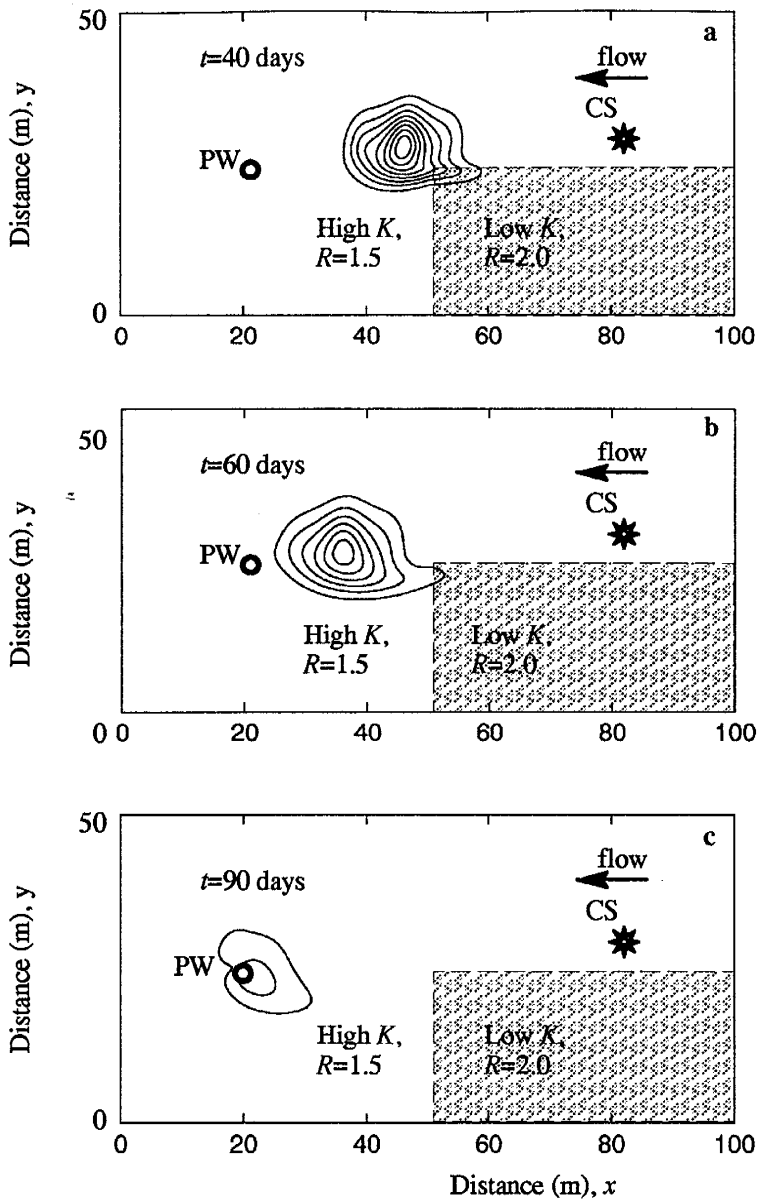

Figure 4.10. Two-dimensional aqueous phase resident concentration contour for the case of linear equilibrium sorption in a heterogeneous aquifer. The contaminant source (CS) is located at (80, 30). The outermost contour line represents 0.004 (mg/l), the contour interval is 0.004 (mg/l). a–c show the plumes for 40 days, 60 days, and 90 days, respectively.

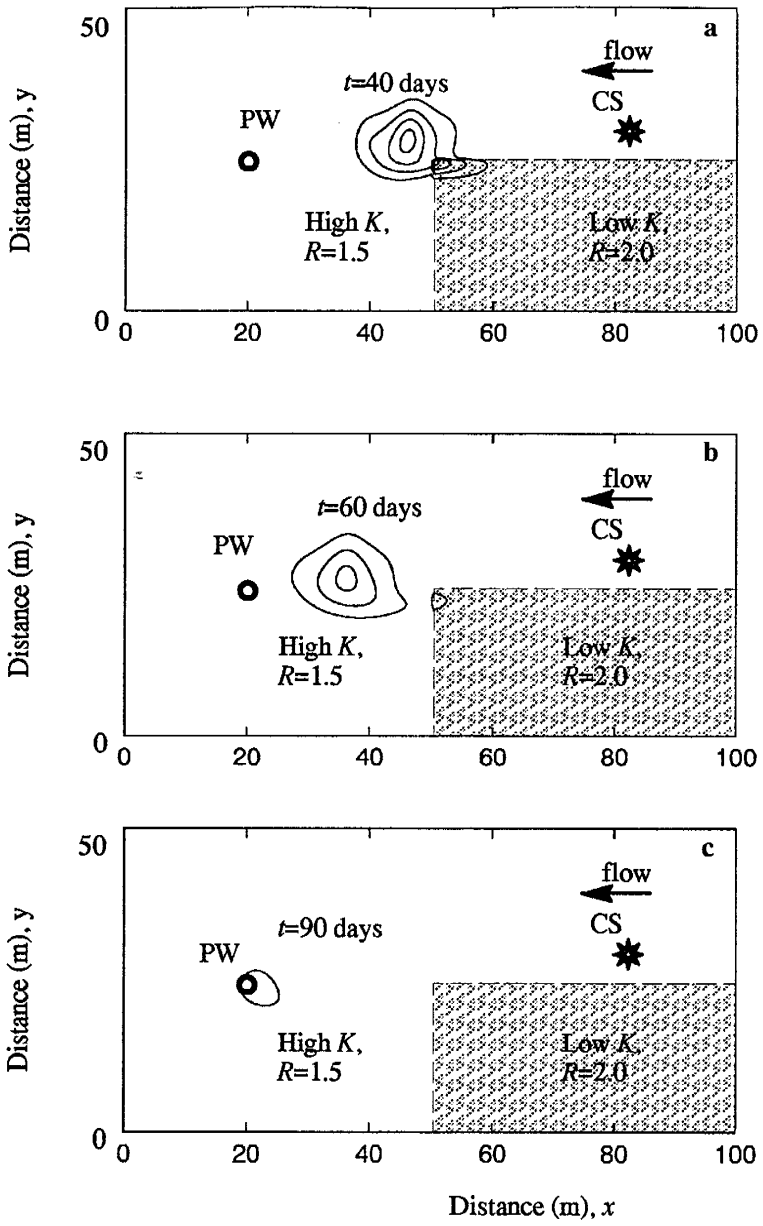

Figure 4.11. Two-dimensional sorbed phase resident concentration contour of contaminant transport in the case of linear equilibrium sorption in a heterogeneous aquifer. The contaminant source (CS) is located at (80, 30), and the pumping well (PW) is located at (20, 25). The outermost contour line represents 0.004 (mg/l), the contour interval is 0.004 (mg/l). a-c show the plumes for 40 days, 60 days, and 90 days, respectively.

Compared to the non-sorption case in equation (4.6), the travel time PDF in linear sorption is retarded by R. In this example, the boundary and initial conditions are given in equation (4.7).

The simulated travel time PDF's for the previous example are shown in Figure 4.12 and Figure 4.13. Figure 4.12 shows travel time PDFs for source locations at (80, 30) and (80, 20) vs. travel time. The simulation results from the single BIT simulation are confirmed by the two FIT solutions. Compared to the travel time PDF without sorption, the travel time PDF is retarded by the sorption. Figure 4.13 represents the travel time PDF for three travel times: τ=40 days, 60 days, and 90 days in the past. Compared to the non-sorption case in Figure 4.5, the travel time PDF distributions are closer to the pumping well.

For linear equilibrium sorption, the travel time CDF for the aqueous phase can be expressed as equation (4.15) by replacing f_τ with F_τ along the same boundary and initial conditions shown in equation (4.9). For the same example as Figure 4.13, the simulated results of the travel time CDF for the two times τ= 40 days, and 60 days are shown in Figure 4.14. Compared to the non-sorption case in Figure 4.8, the travel time CDF demonstrates that the capture zones are reduced by the sorption.

4.2.2 The Backward-in-time Model For Location Probability

For the linear equilibrium sorption case, the location PDF for the aqueous phase, $f_{\boldsymbol{X}}(\boldsymbol{X}|\tau)$ can be expressed as:

$$R\frac{\partial f_{\boldsymbol{X}}}{\partial \tau} = \frac{\partial}{\partial x_i}\left(D_{ij}\frac{\partial f_{\boldsymbol{X}}}{\partial x_j} \right) + V_i\frac{\partial f_{\boldsymbol{X}}}{\partial x_i} \tag{4.16}$$

where $f_{\boldsymbol{X}}=f_{\boldsymbol{X}}(\boldsymbol{X}|\tau)$ is the location PDF for the aqueous phase, and R is the retardation factor.

For the same domain in Figure 4.1, the boundary and initial conditions for the aqueous phase location PDF can also be expressed by equation (4.11), except that the initial condition is replaced by $\delta(\boldsymbol{X}-\boldsymbol{X}_1)/R$. The simulated location PDF for the aqueous phase is shown in Figure 4.15 for two times: τ=40days, and 60 days in the past. The greatest location PDF for

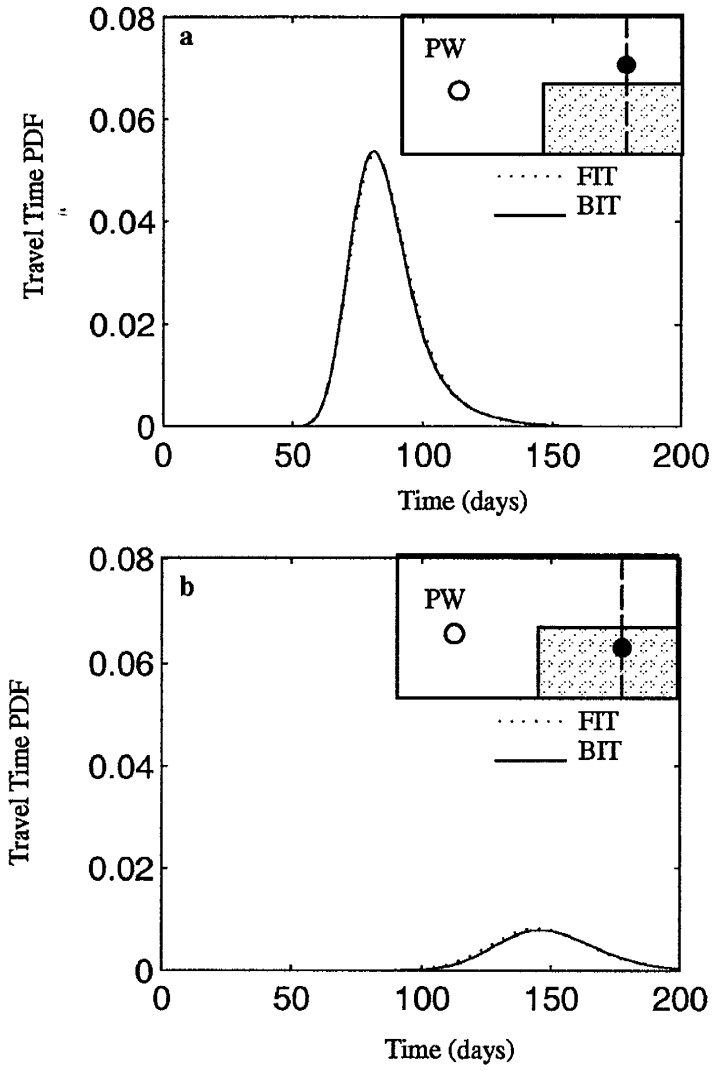

Figure 4.12. Diagram of the travel time PDF, $f_t(\tau|X)$ for linear equilibrium sorption vs. travel time. a. Travel time PDF for the source location at (80,30), in which the dotted line shows the forward-in-time (FIT) solution, and the solid line shows the backward-in-time (BIT) solution. b. Travel time PDF for the source location at (80, 20).

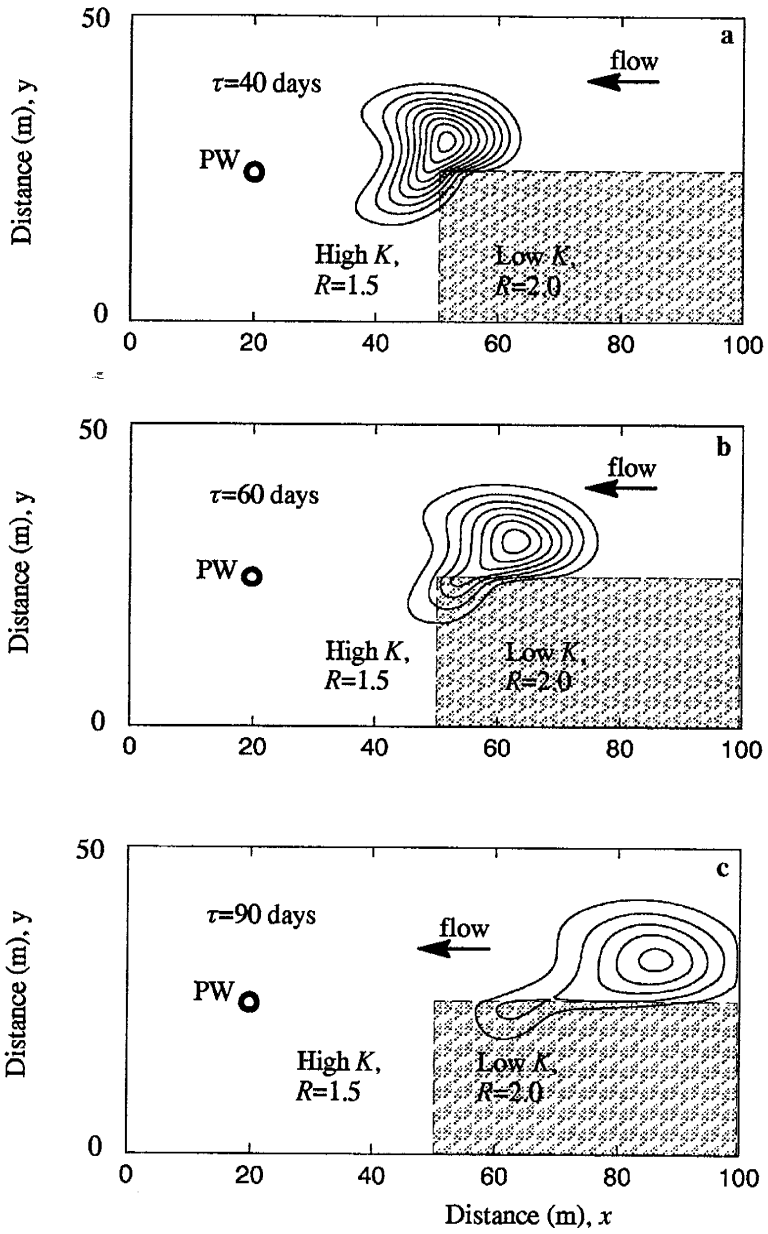

Figure 4.13. Two-dimensional travel time PDF contour for the aqueous phase in the case of linear equilibrium sorption. The pumping well (PW) is located at (20,25). The outermost contour line represents 0.01, the contour interval is 0.01. a-c show the plumes for 40 days, 60 days, and 90 days, respectively.

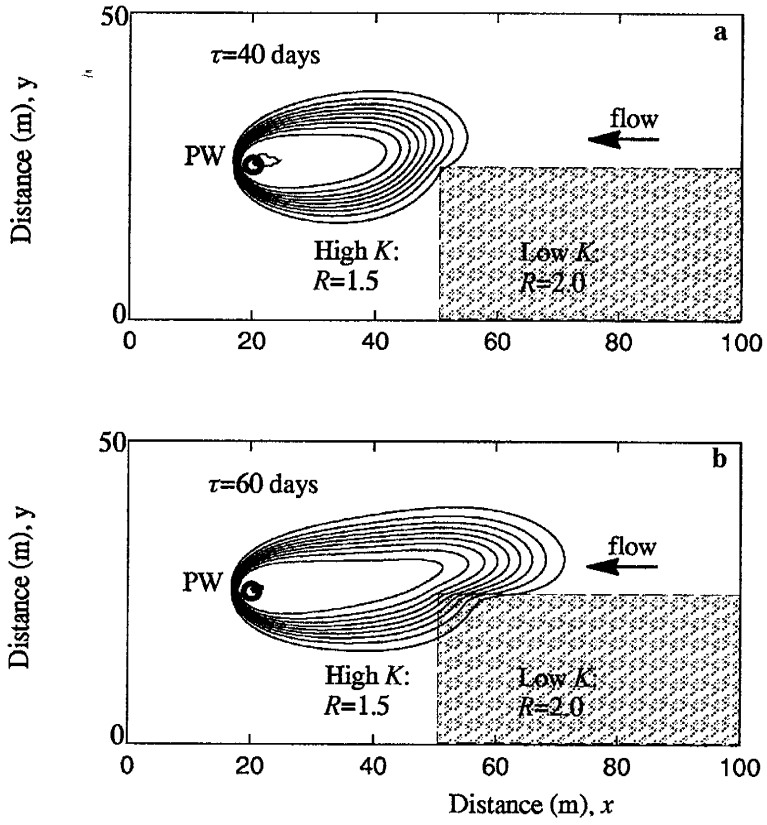

Figure 4.14. Two-dimensional travel time CDFs for linear equilibrium sorption. The retardation factor R=1.5 in the high K sub-domain, and R=2.0 in the low K sub-domain. The outermost contour line represents 0.1, and the contour interval value is 0.1. **a.** The travel time probability distribution for time less than 40 days. **b.** The travel time probability distribution for time less than 60 days.

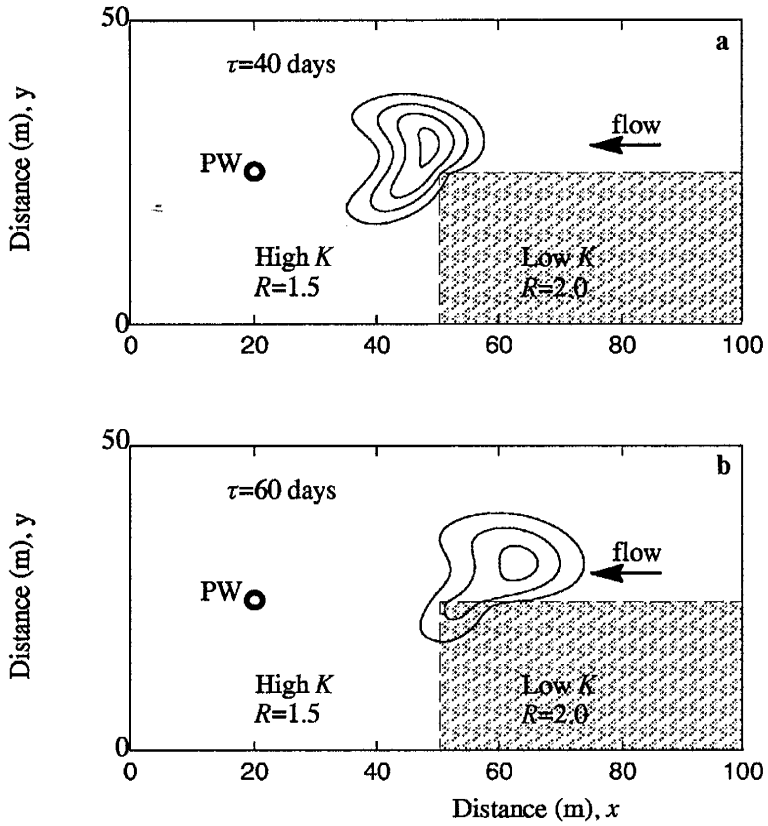

Figure 4.15. Two-dimensional location PDFs for the aqueous phase in linear equilibrium sorption. The retardation factor R=1.5 in the high K sub-domain, and R=2.0 in the low K sub-domain. The outermost contour line represents 5.0E-4, and the contour interval value is 5.0E-4. **a.** The location PDFs for the travel time, τ=40 days. **b.** The location PDFs for the travel time, τ=60 days.

τ=60 days is located around the position (60, 30). The greatest location PDF moves in an upstream direction as time progresses in a backward direction. As the result of the retardation, the location PDF distribution is closer to the pumping well than in the non-sorption case.

The location PDF for the sorbed phase, $g_X=g_X(\boldsymbol{X}|\tau)$, and the total location PDF for the combined aqueous phase and sorbed phase, $g_{X,total}=g_{X,total}(\boldsymbol{X}|\tau)$, can be computed through the aqueous phase location PDF: $g_X=f_X(R-1)/R$, $g_{X,total}=f_X R$. The total location PDF simulation is shown in Figure 4.16. Compared to the non-sorption in Figure 4.9, the total location PDF is retarded by linear equilibrium sorption.

4.3 The Two-dimensional Backward-in-time Model for the Case of Non-equilibrium Sorption

For the case of non-equilibrium sorption in the same domain shown in Figure 4.1, the resident concentrations can be expressed as:

$$\frac{\partial C^r}{\partial t}+\frac{\partial C_s^r}{\partial t}=\frac{\partial}{\partial x_i}\left(D_{ij}\frac{\partial C^r}{\partial x_j}\right)-V_i\frac{\partial C^r}{\partial x_i} \tag{4.17a}$$

$$\frac{\partial C_s^r}{\partial t}=\frac{\alpha K_d \varrho_b}{\theta}C^r-\alpha C_s^r \tag{4.17b}$$

where $C^r=C^r(\boldsymbol{X},t)$ is the aqueous phase resident concentration in the aquifer, and $C^r_s=C^r_s(\boldsymbol{X},t)$ is the sorbed phase resident concentration in the aquifer. The boundary and initial conditions for the aqueous phase resident concentration are the same as those in equation (4.4), and the initial condition for the sorbed phase concentration is expressed as:

$$C_s^r=0, \quad \text{for } t=0 \tag{4.16}$$

where $C^r_s=C^r_s(\boldsymbol{X},t)$ is the resident concentration for the sorbed phase.

For the example, it is supposed that K_d=0.12 cm^3/g (R=1.5), α=0.1 day^{-1} (time constant=10 days) in the high K sub-domain, and K_d=0.24 cm^3/g (R=2), α=0.1 day^{-1} (time constant = 10 days) in the low K sub-domain. The result of simulations for the aqueous phase concentration and sorbed phased concentration are shown in Figures 4.17 and 4.18, respec-

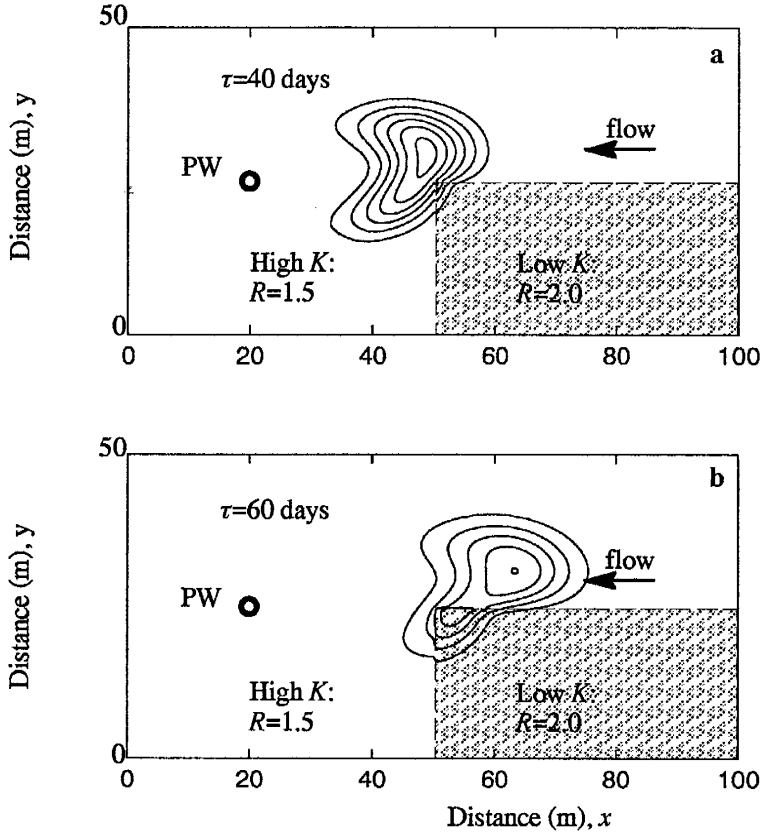

Figure 4.16. Two-dimensional total location PDFs for the aqueous phase and sorbed phase in linear equilibrium sorption. The retardation factor R=1.5 in the high K sub-domain, and R=2.0 in the low K sub-domain. The outermost contour line represents 5.0E-4, and the contour interval value is 5.0E-4. **a.** The location PDF for the travel time, τ=40 days. **b.** The location PDF for the travel time, τ=60 days.

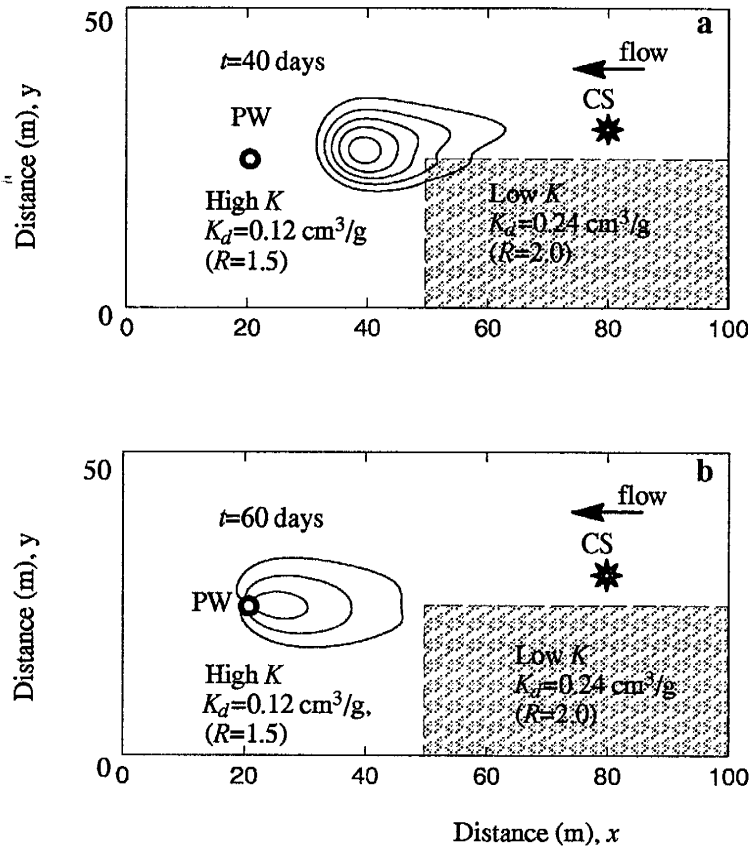

Figure 4.17. Two-dimensional aqueous phase resident concentration contour for the case of non-equilibrium sorption. The contaminant source (CS) is located at (80,30), and the pumping well (PW) is located at (20,25). The outermost contour line represents 0.004 (mg/l), the contour interval is 0.004 (mg/l). a–b show the plumes for 40 days and 60 days, respectively.

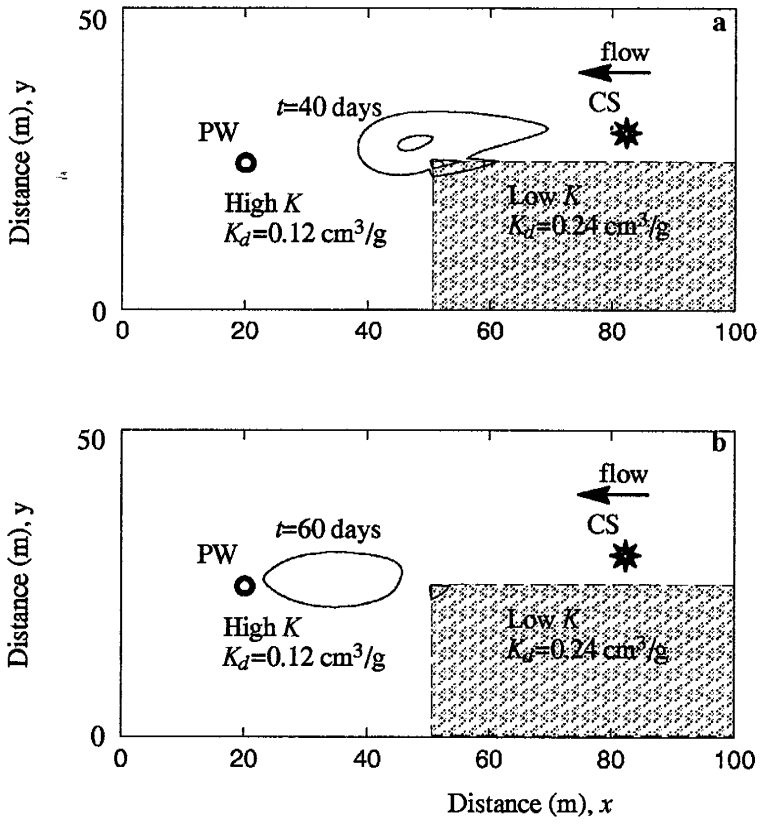

Figure 4.18. Two-dimensional sorbed phase resident concentration contour for the case of non-equilibrium sorption in a heterogeneous aquifer. The contaminant source (CS) is located at (80,30), and the pumping well (PW) is located at (20,25). The outermost contour line represents 0.004 (mg/l), the contour interval is 0.004 (mg/l). a–b show the plumes for 40, 60 days, respectively.

tively. Figure 4.17 shows the aqueous phase concentration contour for two times: t= 40 days and 60 days, after contaminants were released at source location (80, 30). Compared to the linear equilibrium sorption, Figure 4.17 indicates that the aqueous phase concentration plume is retarded within a long "tail" from the source location. Figure 4.18 shows that the concentration for the sorbed phase is less than that for linear equilibrium sorption.

4.3.1 The Backward-in-time Model For Travel Time Probability

In the backward-in-time model, the travel time PDFs for non-equilibrium sorption can be expressed as:

$$\frac{\partial f_\tau}{\partial \tau} + \frac{\partial g_\tau}{\partial \tau} = \frac{\partial}{\partial x_i}\left(D_{ij}\frac{\partial f_\tau}{\partial x_j} \right) + V_i\frac{\partial f_\tau}{\partial x_i} \tag{4.19a}$$

$$\frac{\partial g_\tau}{\partial \tau} = \frac{\alpha K_d \varrho_b}{\theta} f_\tau - \alpha g_\tau \tag{4.19b}$$

where $f_\tau = f_\tau(\tau \mid \boldsymbol{X})$ is the travel time PDF in the aqueous phase, and $g_\tau = g_\tau(\tau \mid \boldsymbol{X})$ is the travel time PDF for the sorbed phase. The boundary and initial conditions for the aqueous phase travel time PDF are the same as those in equation (4.7), and the initial condition for the sorbed phase travel time PDF is shown as:

$$g_\tau = 0, \quad \text{at } \tau = 0 \tag{4.21}$$

where $g_\tau = g_\tau(\tau \mid \boldsymbol{X})$.

The simulated results of the travel time PDFs for the aqueous phase for the example are shown in Figures 4.19 and 4.20. Figure 4.19a and Figure 4.19b show the travel time PDFs given the source locations at (80, 30) and (80, 20), respectively. Due to the non-equilibrium sorption, the travel time PDFs present long "tails" along the travel time. The simulation results from the backward-in-time (BIT) model (solid lines) are also confirmed by the two FIT solutions (dotted lines). Figure 4.20 represents the aqueous phase travel time PDF for two travel times: τ=40 days and 60 days in the past. Compared to the non-sorption case in Figure 4.5, the travel time PDF distributions have been retarded by sorption, and have a long tail pointing toward the well.

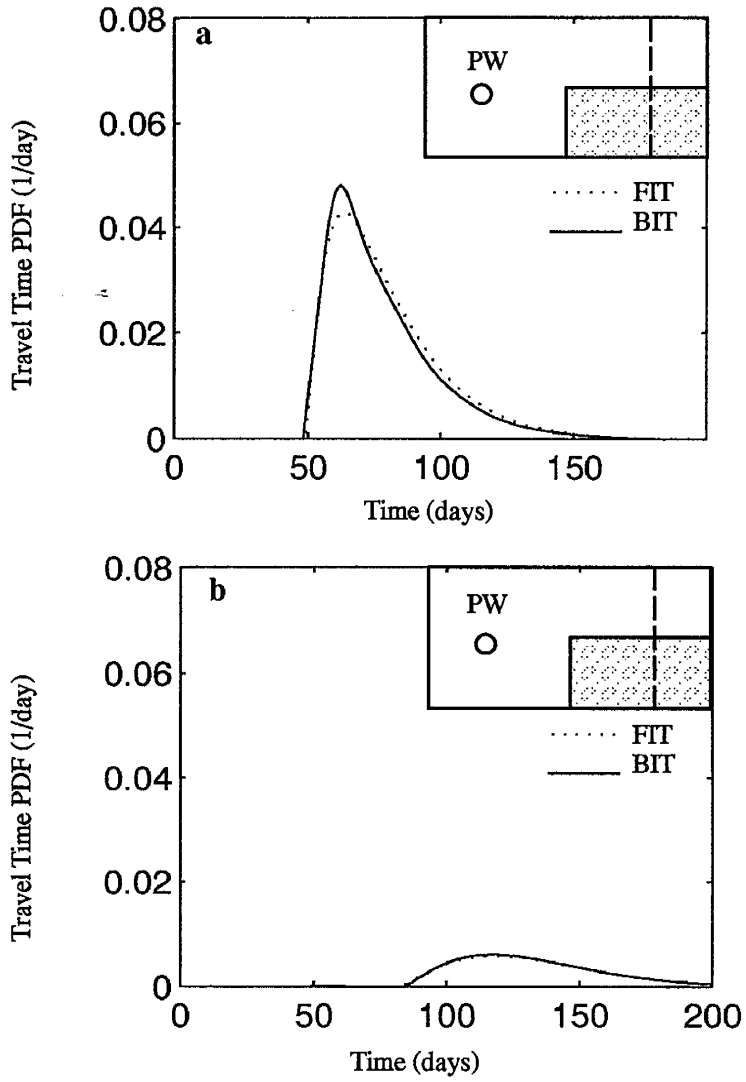

Figure 4.19. Diagram of the travel time PDF, $f_\tau(\tau|X)$ for non-equilibrium sorption vs. travel time. **a.** Travel time PDF for the source location at (80, 30), in which the dotted lines show the first of two forward-in-time (FIT) solutions, and the solid line shows the same for the single backward-in-time (BIT) solution. **b.** Travel time PDF for the source location at (80,20).

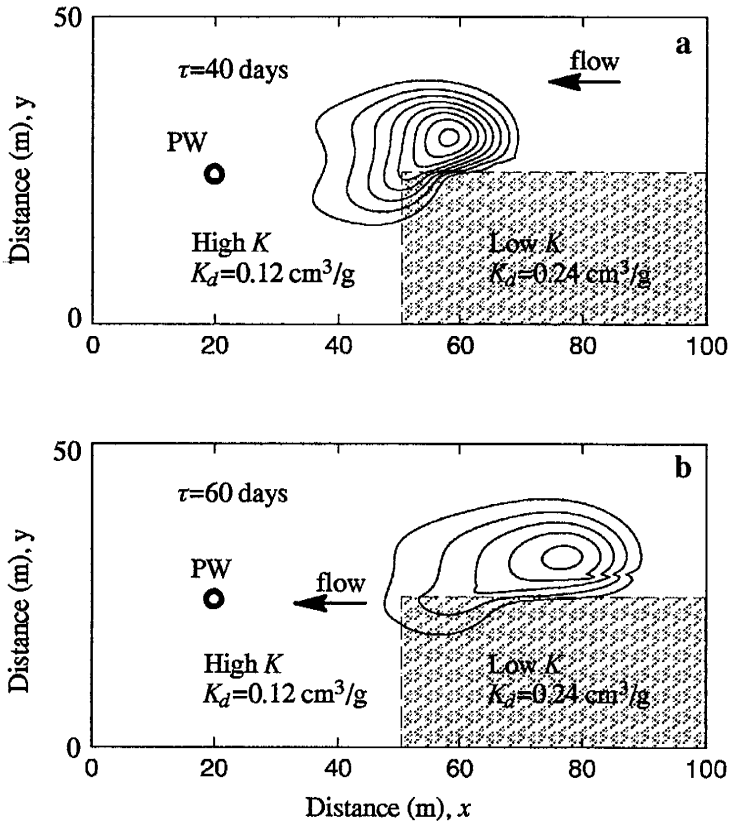

Figure 4.20. Two-dimensional aqueous phase travel time PDF in a heterogeneous aquifer with non-equilibrium sorption. In the high K sub-domain: K=3.56 m/day, K_d=0.12 cm^{-3}/g (R=1.5), α=0.1 day^{-1} (time constant=10 days). In the low K sub-domain: K_2=1.78 m/day, K_d=0.24 cm^{-3}/g (R=2.0), α=0.1 day^{-1} (time constant=10 days). The outermost contour line represents 0.01, and the contour interval is 0.01. a-b show the travel time PDF for 40 days and 60 days, respectively.

For non-equilibrium sorption, the travel time CDF can be formulated from the equation (4.19) by replacing f_τ with F_τ along with the same boundary and initial conditions shown in equation (4.9). The simulated results of the travel time CDF for the two times τ= 40 days and 60 days are shown in Figure 4.21. Compared to the non-sorption case in Figure 4.8, the travel time CDF demonstrates that the capture zones are retarded and reduced by the sorption. The front area of CDF distributions is larger than those for non-sorption or linear equilibrium sorption.

4.3.2 The Backward-in-time Model for Location Probability

In the case of non-equilibrium sorption, the location probabilities for the two phases: the aqueous and sorbed phase, can be expressed as:

$$\frac{\partial f_X}{\partial \tau} + \frac{\partial g_X}{\partial \tau} = \frac{\partial}{\partial x_i}\left(D_{ij}\frac{\partial f_X}{\partial x_j} \right) + V_i\frac{\partial f_X}{\partial x_i} \tag{4.20a}$$

$$\frac{\partial g_X}{\partial \tau} = \frac{\alpha K_d \rho_b}{\theta} f_X - \alpha g_X \tag{4.20b}$$

where $f_X = f_X(X|\tau)$ is the location PDF for the aqueous phase, and $g_X = g_X(X|\tau)$ is the location PDF for the sorbed phase. The boundary and initial conditions for the aqueous phase location PDF are the same as those in equation (4.11), and the initial condition for the sorbed phase location PDF is:

$$g_X(X|\tau) = 0, \quad \text{at } \tau = 0 \tag{4.21}$$

The total location PDF for the aqueous phase and sorbed phase, $g_{X,total} = g_{X,total}(X|\tau)$, can be computed by:

$$f_{X,total} = f_X + g_X \tag{4.22}$$

where $f_X = f_X(X|\tau)$ is the location PDF for the aqueous phase, $g_X = g_X(X|\tau)$ is the location PDF for the sorbed phase.

The simulated results of location PDF are shown in Figures 4.22 and 4.23. Figure 4.22 represents the location PDF for the aqueous phase for two times: τ=40days and 60 days in the past. The greatest location PDF for τ=60 days is located around the position (75, 30).

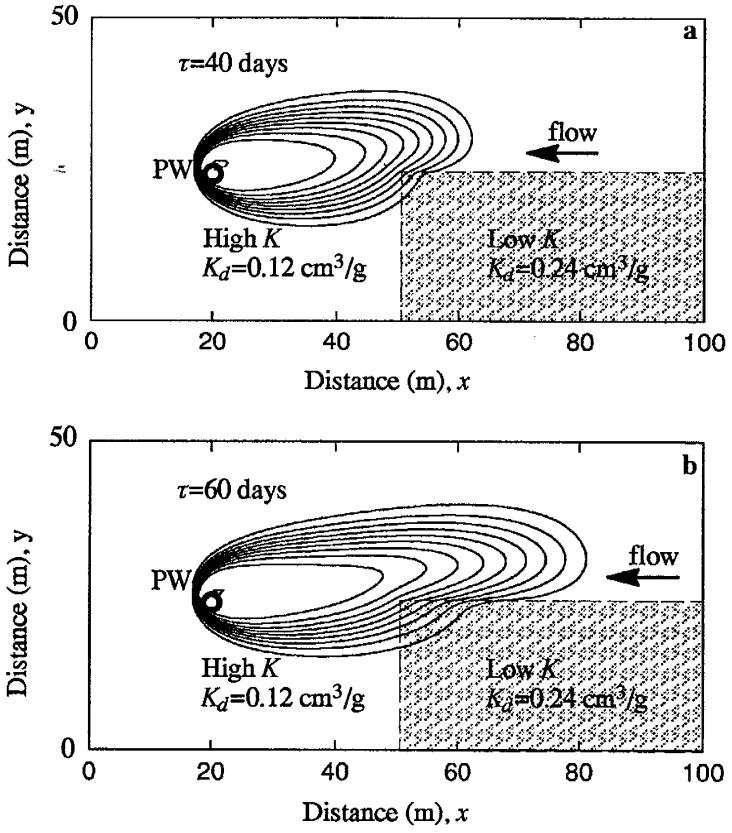

Figure 4.21. Two-dimensional aqueous phase travel time CDF for the case of non-equilibrium sorption. In the high K sub-domain: K=3.56 m/day, K_d=0.12 cm^{-3}/g (R=1.5), α=0.1 day^{-1} (time constant=10 days). In the low K sub-domain: K_2=1.78 m/day, K_d=0.24 cm^{-3}/g (R=2.0), α=0.1 day^{-1} (time constant=10 days). The outermost contour line represents 0.1, and the contour interval is 0.1. a-b show the travel time PDF for 40 days and 60 days, respectively.

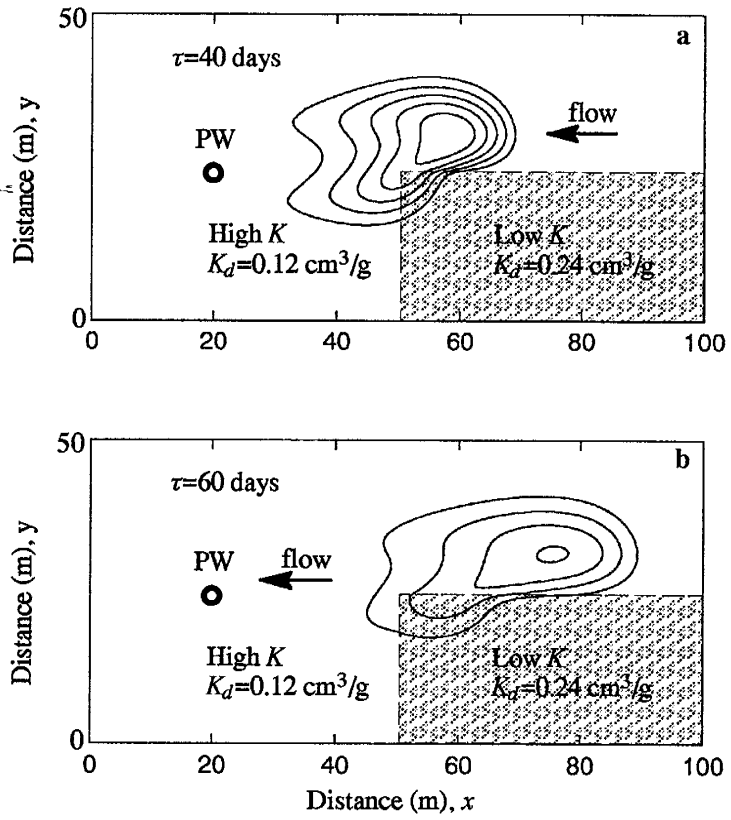

Figure 4.22. Two-dimensional location PDF for the aqueous phase in the case of non-equilibrium sorption. In the high K sub-domain: K_d=0.12 cm^{-3}/g (R=1.5), α=0.1 day^{-1} (time constant=10 days). In the low K sub-domain: K_d=0.24 cm^{-3}/g (R=2.0), α=0.1 day^{-1} (time constant=10 days). The outermost contour line represents 5.0E-4 m^{-2}, and the contour interval is 5.0E-4 m^{-2}. a-b show the location PDF for 40 days and 60 days, respectively.

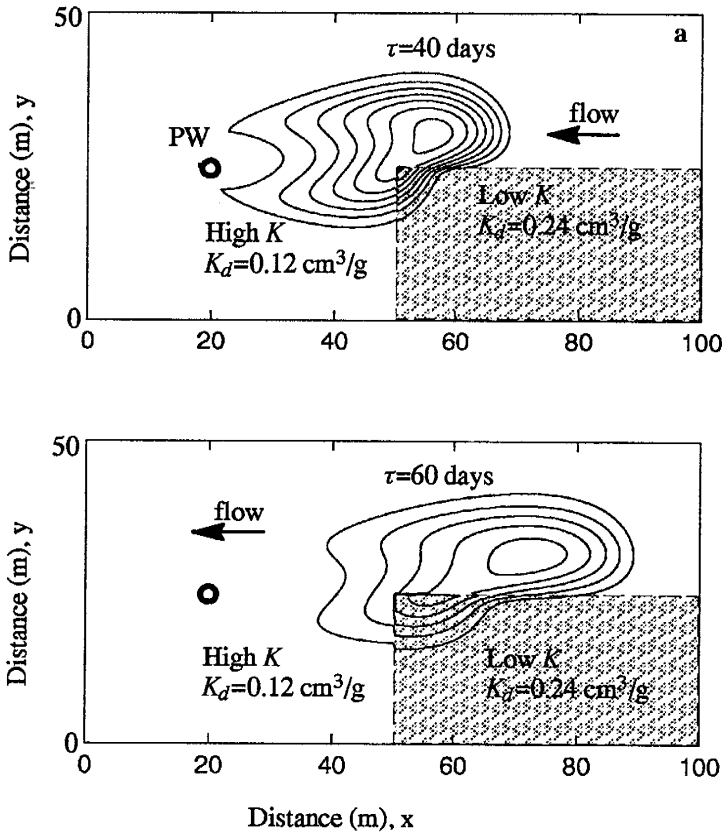

Figure 4.23. Two-dimensional total location PDF for the combined aqueous phase and sorbed phase in the case of non-equilibrium sorption. In the high K sub-domain: K_d=0.12 cm^{-3}/g (R=1.5), α=0.1day^{-1} (time constant=10 days). In the low K sub-domain: K_d=0.24 cm^{-3}/g (R=2.0), α=0.1 day^{-1} (time constant=10 days). The outermost contour line represents 5.0E-4 m^{-2}, and the contour interval is 5.0E-4 m^{-2}. a-b show the location PDF for 40 days and 60 days, respectively.

Compared to the location PDF in linear equilibrium sorption, the location PDFs have a wider distribution. Figure 4.23 shows the total location PDF for the combined aqueous phase and sorbed phase. Due to the combined influences of heterogeneity and sorption, the total location PDF has longer "tails" than the location PDF for the aqueous phase in Figure 4.22.

4.4 The Two-dimensional Backward-in-time Model in the Case of Natural Recharge

Natural recharge changes the groundwater flow and the mass transport. To begin with, the hydraulic head equation (4.1) is rewritten as:

$$\frac{\partial}{\partial x_i}\left(T_{ij}\frac{\partial h}{\partial x_j}\right)-\delta(\boldsymbol{X}-\boldsymbol{X}_1)Q_o + N = 0 \qquad (4.23)$$

where h is hydraulic head [L], T_{ij} is the second order aquifer transmissivity [L^2/T] tensor with i, j=1, 2, and Q_o is the pumping rate[L^3/T] at a location, $\boldsymbol{X}_1=(x_1,y_1)$. N is the natural recharge rate [L/T]. For the domain in Figure 4.1, the same boundary conditions for the steady state groundwater flow shown in equation (4.2) apply. The groundwater average velocity, $V_i=V_i(x,y)$, can be computed by Darcy's law.

For the same contaminant transport model as in the previous example, because of the natural recharge, the resident concentration $C^r(\boldsymbol{X},t)$ will be expressed as:

$$\frac{\partial C^r}{\partial t} = \frac{\partial}{\partial x_i}\left(D_{ij}\frac{\partial C^r}{\partial x_j}\right)-\frac{\partial}{\partial x_i}(V_i C^r) \qquad (4.24)$$

where $C^r=C^r(\boldsymbol{X},t)$ is the aqueous phase resident concentration in the aquifer. $V_i=V_i(x,y)$ is average velocity at $\boldsymbol{X}=(x,y)$. The boundary and initial conditions for equation (4.24) are expressed by equation (4.4).

For the domain of Figure 4.1, and a uniform natural recharge rate of N=0.005 m/day, the simulated heads are shown in Figure 4.24. Figure 4.24 indicates a groundwater flow divide through the domain along the y direction. The contamination released at (80,30) in the previous examples is not captured by the pumping well. In this example, it is supposed that the contamination was introduced into the aquifer's low conductivity zone, at location (66,

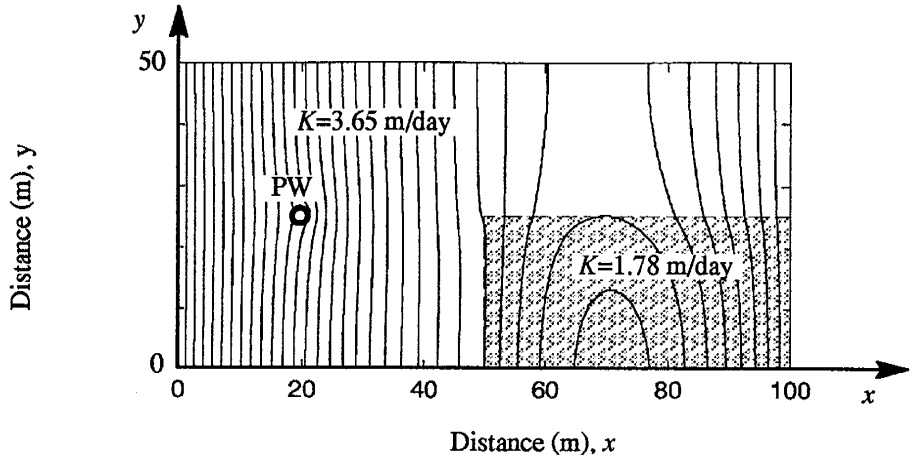

Figure 4.24. Two-dimensional hydraulic head contour in a heterogeneous aquifer with natural recharge. The pumping well (PW) is located at (20,25) with a pumping rate of Q_o=5.0 m^3/day. Constant heads: h_1=40 m at the left boundary, and h_2=50 m at the right boundary. The natural recharge rate is N=0.005 m/day. The contour interval is 0.5 m.

15). Figure 4.25 shows the contamination plume for three times: t=20 days, 40 days, and 60 days in the past. The contamination plume moves in a downstream direction and is only partially captured by the pumping well. Figure 4.25c shows that contamination not captured by the pumping well flows out through the left boundary. These results demonstrate the combined effects of advection, dispersion, aquifer heterogeneity, and natural recharge.

4.4.1 The Backward-in-time Model for Travel Time Probability

In the backward-in-time method, the travel time PDF is described by the advection-dispersion equation with a reversed flow problem ($V_i \rightarrow -V_i$) and recharge becoming discharge:

$$\frac{\partial f_\tau}{\partial \tau} = \frac{\partial}{\partial x_i}\left(D_{ij}\frac{\partial f_\tau}{\partial x_j} \right) + \frac{\partial}{\partial x_i}(V_i f_\tau) - \frac{N}{B\theta} f_\tau \qquad (4.25)$$

where $f_\tau = f_\tau(\tau \mid \boldsymbol{X})$ is the aqueous phase travel time PDF. After inserting (4.24) into (4.26), the travel time PDF can be rewritten as:

$$\frac{\partial f_\tau}{\partial \tau} = \frac{\partial}{\partial x_i}\left(D_{ij}\frac{\partial f_\tau}{\partial x_j} \right) + V_i\frac{\partial f_\tau}{\partial x_i} \qquad (4.26)$$

The boundary and initial conditions are expressed as in equation (4.7).

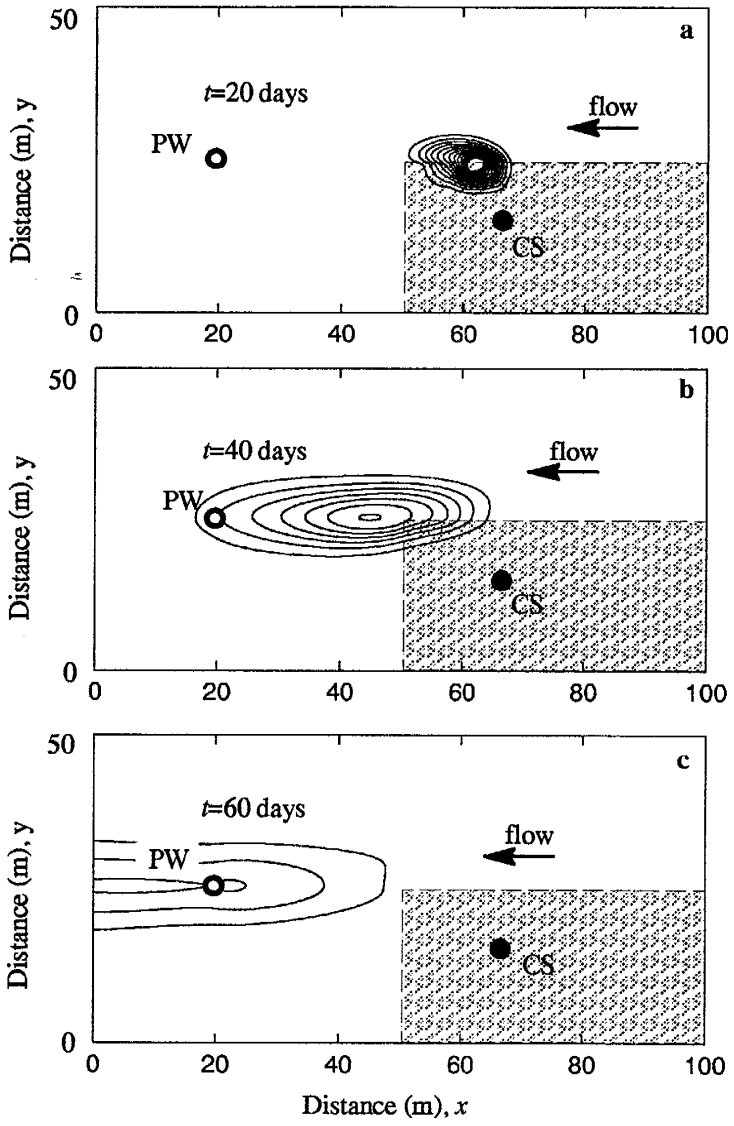

Figure 4.25. Two-dimensional resident concentration contour for the case of natural recharge in a heterogeneous aquifer. The contaminant source (CS) is located at (66,15), and the pumping well (PW) is located at (20,25) with a pumping rate of Q=5.0 m^3/day. The outermost contour line represents 0.004 mg/l, the contour interval is 0.004 mg/l. a–c show the plumes for 20, 40 and 60 days, respectively.

For natural recharge, the travel time cumulative distribution function CDF can also be expressed as equation (4.27) by replacing f_τ with F_τ along the same boundary and initial conditions shown in equation (4.9).

The simulation results are shown in Figures 4.26–4.28. Figure 4.26a and 4.26b represent the travel time PDF from locations: (66, 25) and (66, 15), respectively. The travel time PDF simulations from the backward–in–time model is in close agreement to the arrival time PDF simulations from two separate runs of a forward–in–time model. The highest travel time probability for the location (66, 25) is about 40 days, and the highest travel time probability for location (66, 15) is about 58 days. Because of the combined effects of recharge and heterogeneity, the travel time probability for location (66, 25) is much larger than that for location (66, 15), and the most possible travel time for location (66,25) is less than that for (66,15). Figure 4.27 pictures the travel time PDF for each of these possible former locations for two travel times: τ=40 days and 60 days. The travel time PDF distribution moves in an upgradient direction, spreads, and dilutes as travel time increases. It is moving in toward (66,15) from (66, 25). Under the influence of natural recharge and dispersion, some contaminants are not captured by the pumping well, especially for the locations that are far from the pumping well. Figure 4.27 also demonstrates that contamination observed in the pumping well came from the left side of the flow divide. Figure 4.28 plots the simulation results for the travel time CDF for the two times τ= 40 days and 60 days. The travel time cumulative distributions also show that the probability expands along the upgradient direction.

4.4.2 The Backward–in–time Model for Location Probability

In the case of natural recharge, location probability is not "discharged" in the backward–in–time problem. It can be expressed as:

$$\frac{\partial f_X}{\partial \tau} = \frac{\partial}{\partial x_i}\left(D_{ij}\frac{\partial f_X}{\partial x_j} \right) + \frac{\partial}{\partial x_i}(V_i f_X) \qquad (4.27)$$

where $f_X = f_X(X|\tau)$ is the location PDF. The boundary and initial conditions for the location PDF are the same as in the equation (4.11).

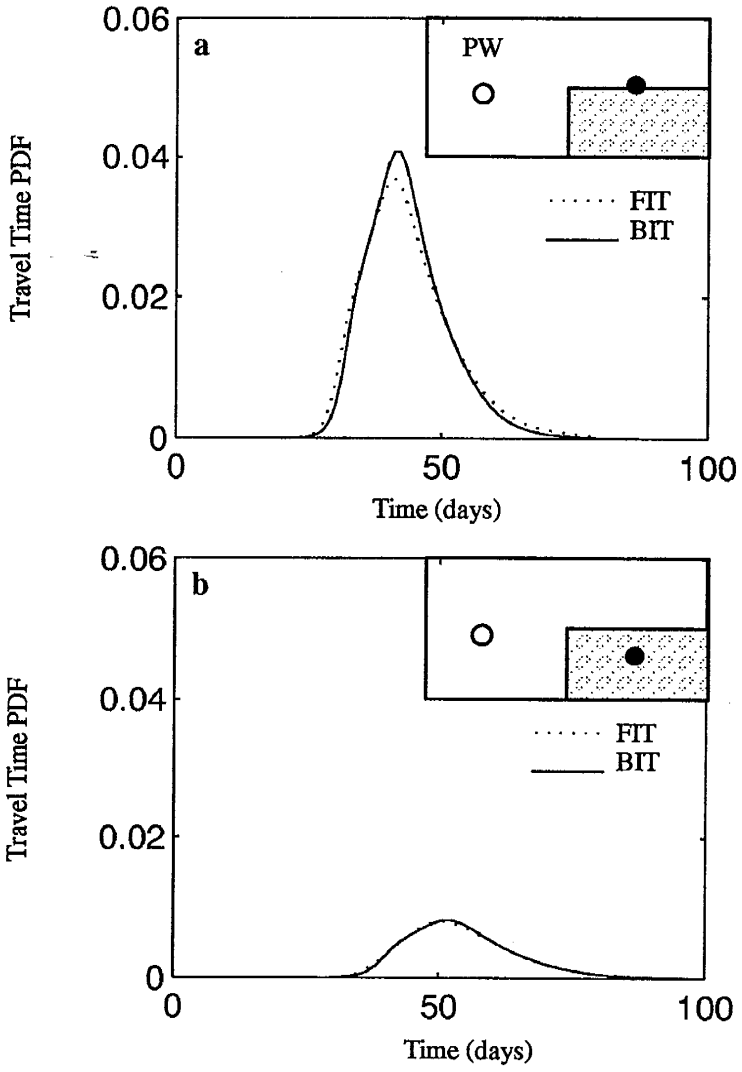

Figure 4.26. Diagram of the travel time PDF, $f_\tau(\tau|X)$ for natural recharge vs. time. a. Plots represent the travel time PDF for the source location at (66,25): the dotted line shows the forward-in-time (FIT) solution, and the solid line shows the backward-in-time (BIT) solution. b. Travel time PDF for the source location at (66,15).

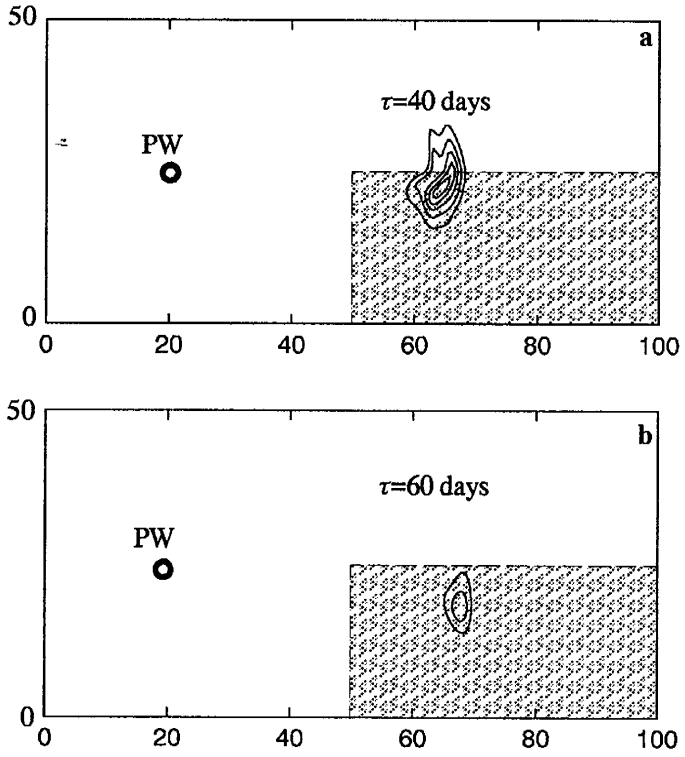

Figure 4.27. Two-dimensional travel time PDF for natural recharge in a heterogeneous aquifer. The natural recharge rate is N=0.005 m/day. The outermost contour line represents 0.01 day^{-1}, and the contour interval is 0.01 day^{-1}. a-b show the travel time PDF for 40 days and 60 days, respectively.

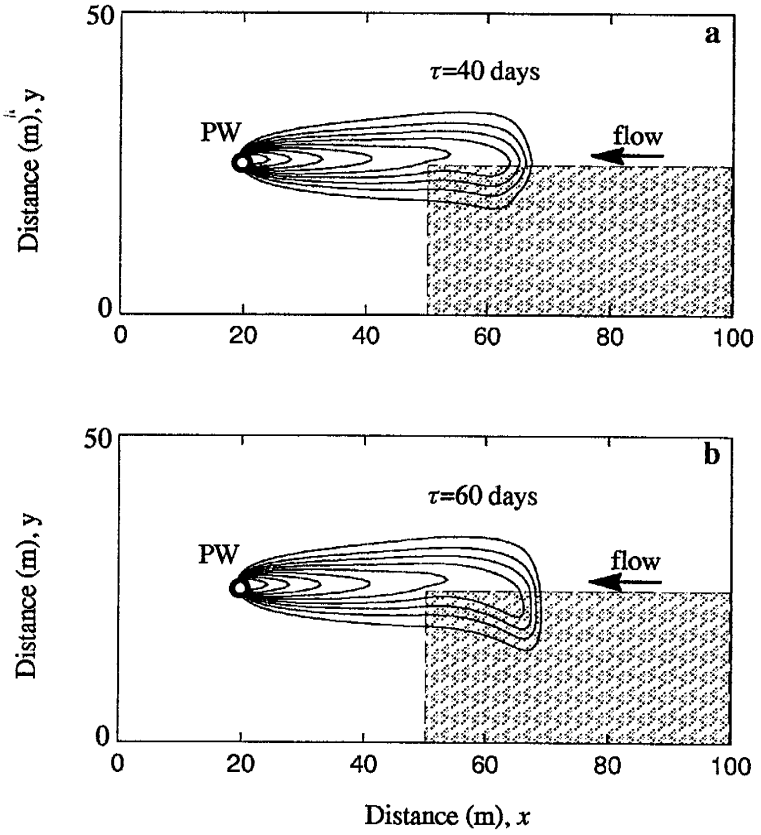

Figure 4.28. Two-dimensional travel time CDF in the heterogeneous aquifer with natural recharge. The natural recharge rate is N=0.005 m/day. The outermost contour line represents 0.1, and the contour interval value is 0.1. **a.** shows the travel time CDF for time less than 40 days. **b.** shows the travel time CDF for time less than 60 days.

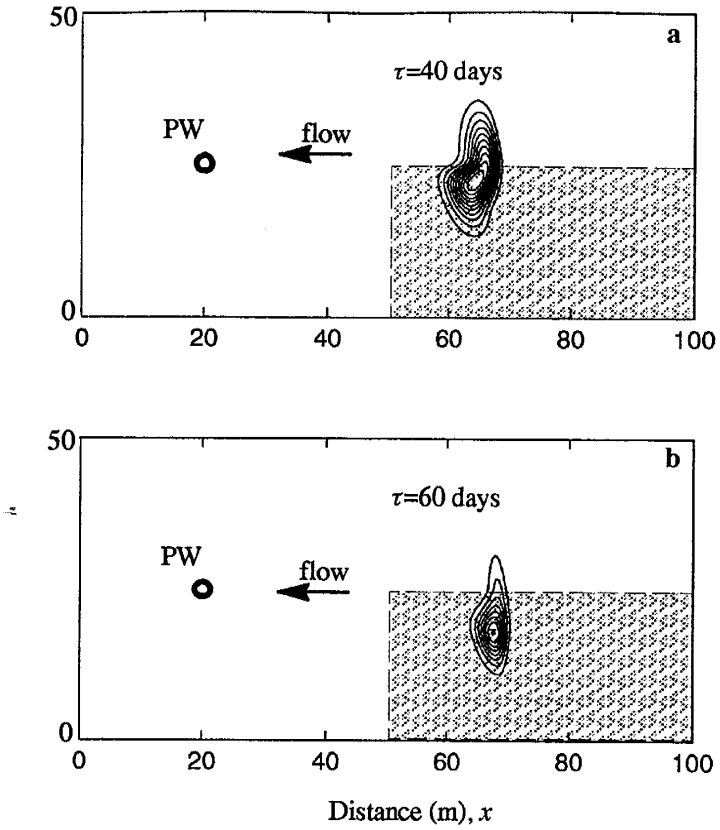

Figure 4.29. Two-dimensional location PDF in the heterogeneous aquifer with natural recharge. The natural recharge rate is N=0.005 m/day. The outermost contour line represents 0.002 m^{-2}, and the contour interval value is 0.002 m^{-2}. a. shows the location PDF in 40 days. b. shows the location PDF in time 60 days.

Figure 4.29 represents the simulated location PDFs for two given times: τ=40days and 60 days in the past. The most possible location for τ=40 days is located around the position (64,24), and the most possible location for τ=60 days is located around the position (64,18). The location PDF distributions demonstrate that the former location PDF moves upgradient. The possible former locations of the contamination only occur left of the flow divide.

5. APPLICATION TO THE BORDEN TRACER TEST

In the previous section, it has been demonstrated that the backward-in-time model can be adapted to a two-dimensional heterogeneous domain. As a further explanation of the usefulness of the backward-in-time PDEs model, this section will present its application to the Borden capture zone tracer test run by New Mexico Tech and the University of Waterloo, from 1992 to 1993. The author of this report did chemical analysis of water samples in the High Pressure Liquid Chromatographic (HPLC) Laboratory and tracer concentration interpretations. For the series of field tests, data were collected on tracer injection locations/times, and on tracer concentration as a function of time in both a pumping well and in monitoring wells. The flow field was well-monitored. Most data were published (Linderfelt, 1994; Linderfelt and Wilson, 1994; Linderfelt and Wilson 1995; Wilson and Linderfelt 1995). This report will use the concentrations observed from the first experiment to examine the backward-in-time model.

5.1 Tracer Transport Model in the Borden Tracer Test

The Borden site as shown in Figure 5.1 is located in Borden, Ontario, Canada. The Borden aquifer is an eight meter thick, unconfined sand aquifer which is underlain by a thick, silty clay deposit (Mackay et al., 1986; Linderfelt, 1994). The basic parameters, such as hydraulic conductivity, the dispersion coefficient, porosity, and the horizontal hydraulic gradient, were studied in previous research (Sykes, et al., 1982; Nwankwor et al., 1984; Sudicky, 1986; Sudicky et al., 1983; Mackay et al., 1986; Linderfelt, 1994). The basic parameters utilized in this research are listed in Table 5.1.

The regional hydraulic gradient, J_a, and flow direction angle, β, were frequently measured by Linderfelt et al. (Linderfelt, 1994; Linderfelt and Wilson 1995). The observations of gradient and flow direction shows that the groundwater flow changed with time (Wilson and Linderfelt, 1995). In this research, the experiment was broken into three time periods, with steady flow roughly assumed in each period, as shown in Table 5.1. This allowed us

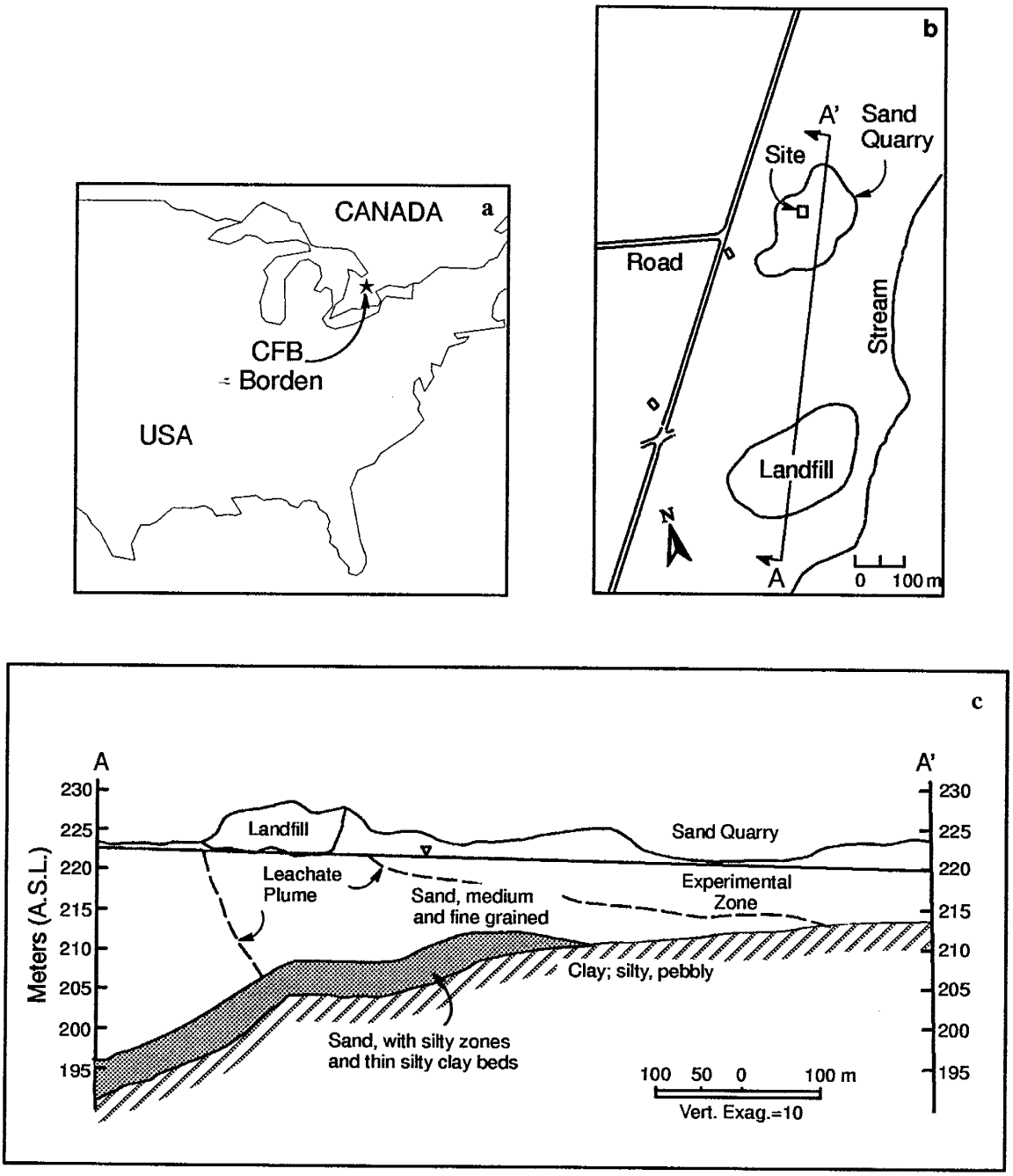

Figure 5.1. Map of the Borden site tracer test. **a.** Map of eastern USA and southern Ontario, Canada, showing Great Lakes region and location of CFB Borden; **b.** Plan view of the Borden site; **c.** Site cross-section (schematic) A–A' showing landfill, experimental zone, and local geologic features (after Linderfelt, 1994; Mackay et al., 1986).

to use the Laplace transform-in-time Galerkin finite element code. The regional ambient flow rate, q_a, can be computed by Darcy's law, $q_a=KBJ$. The average velocity in the tracer test site can be explained as (Linderfelt, 1994):

Table 5.1. The parameters for the backward-in-time model of the Borden site:

Parameters	Description
Domain	30 m x 30 m
Grid characteristics	Δx=0.2 m, Δy=0.2 m 22500 square elements, 22801 nodes.
Homogeneous and isotropic hydraulic conductivity	$K_x=K_y$=7.09 m/day*
Longitudinal dispersivity Lateral dispersivity	α_L = 0.08 m * α_T =0.001 m*
Porosity	0.33*
Aquifer thickness	7.3 m*
Gradient of the hydraulic head and direction	time (days): J_a β 0-66 4.1E-3, 25.4 67-118 3.8E-3, 9.0 118-124 2.9E-3, -3.5
Pumping well location	x=15, y=20m
Pumping rate	2.16 m^3/day*
Forward-in-time tracer transport: (1) initial condition (2) boundary conditions	 C^r=0 for t=0 $\partial C^r/\partial x_i$=0; all boundaries
Backward-in-time PDEs model: (1) initial condition	 f_τ=0 for t=0
(2) boundary conditions	third type boundary condition at the PW $\partial f_\tau/\partial x_i$=0; otherwise

* from Linderfelt, 1994.

$$V_x = \left[q_a \sin\beta - \frac{Q_o}{2\pi} \frac{x}{x^2 + y^2} \right] \frac{1}{\theta B} \tag{5.1a}$$

$$V_y = \left[q_a \sin\beta - \frac{Q_o}{2\pi} \frac{y}{x^2 + y^2} \right] \frac{1}{\theta B} \tag{5.1b}$$

where q_a is the ambient flow rate per unit of aquifer thickness [L^2/T], and Q_o is the pumping rate [L^3/T], x is positive to the east, y is positive to the north, β is the compass angle, and B is the thickness of the aquifer [L].

The first tracer test site, which consisted of one full penetrating extraction well, 15 injection wells, and 26 multilevel sampling wells, is shown in Figures 5.2 and 5.3. Figure 5.3 shows a schematic cross-section for the pumping well, injection well and multilevel sampler. The pumping well produced from the aquifer at a constant rate, 2.16m^3/day, for over four months. Eight different tracers were injected at 15 different locations upstream of the fully penetrating well. The injection mass and starting date are shown in Table 5.2. The groundwater samples collected in the pumping well were analyzed in the HPLC Lab at New Mexico Tech. The concentration data is replotted in this research and the concentration breakthrough curves of eight tracers are shown in Figure 5.4. The tracer concentrations are normalized by the total mass injected into the injection well, and the normalized curves are estimates of the arrival time probability of the tracers (Jury and Roth, 1990; Henley and Kumamoto, 1992). The normalized curves for the eight tracers are shown in Figures 5.5–5.11.

For the Borden site tracer test, the tracer transport forward-in-time simulation model is shown in Figure 5.12. The pumping well is located at (15,20) pumping at 2.16 m^3/day. The groundwater flows toward the northeast. One of eight tracers was injected into one or more injection wells, then the tracer moved downstream and possibly was captured by the pumping well some time later. Assuming two-dimensional flow, the tracer transport can be described by equation (4.3). The boundary and initial conditions for the simulation are shown in Table 5.1. The resident concentration is simulated using the Laplace transform-in-time Galerkin finite element method (Sudicky and McLaren, 1992). The normalization of concentrations in the pumping well or the arrival time PDFs for injection sites I5 and I8 are shown in Figure 5.13. Figure 5.13a and Figure 5.13b represent the arrival time PDF for injection sites I5 and I8, respectively. Figure 5.13c shows the arrival time PDF for two source locations where unit mass is introduced into the aquifer at I5 and I8 at the same time.

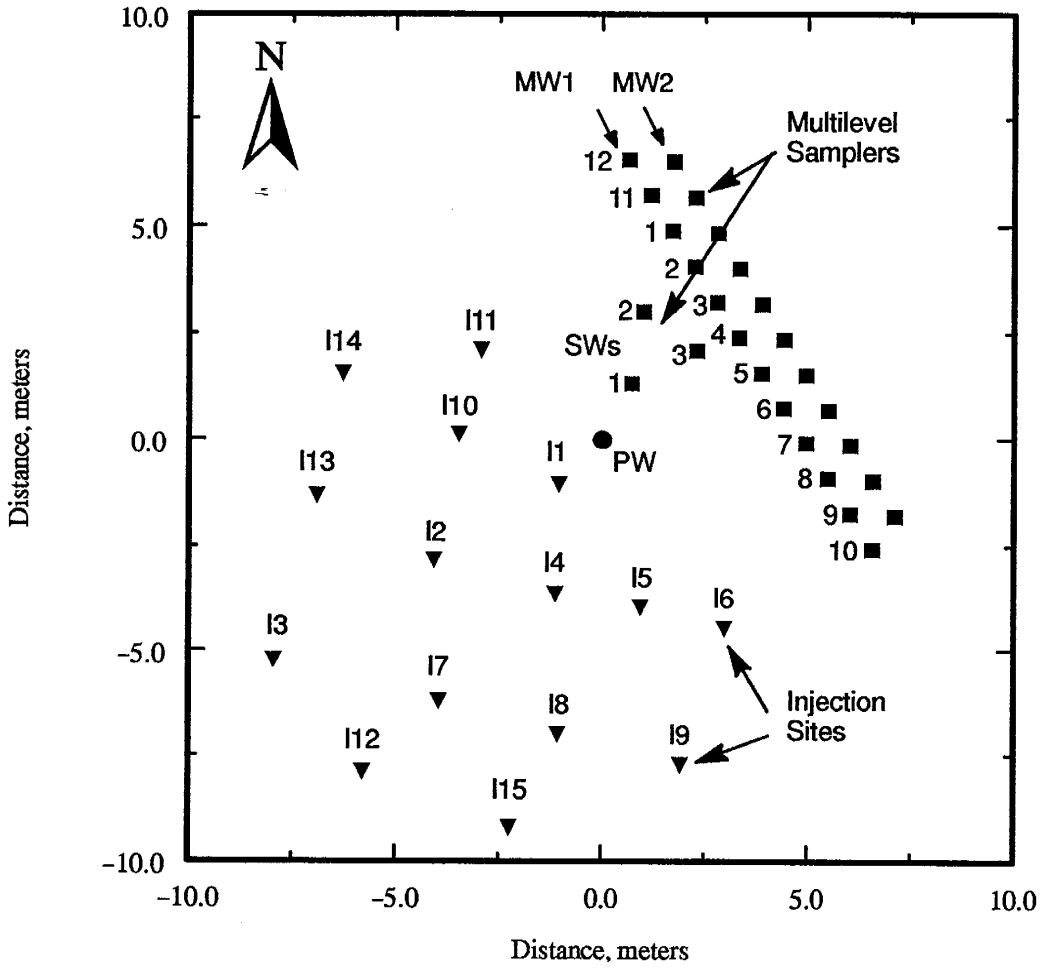

Figure 5.2 Plan view of the tracer test site showing location of injection sites, multilevel sampling wells (MW and SW) and the pumping well (PW) (after Linderfelt, 1994).

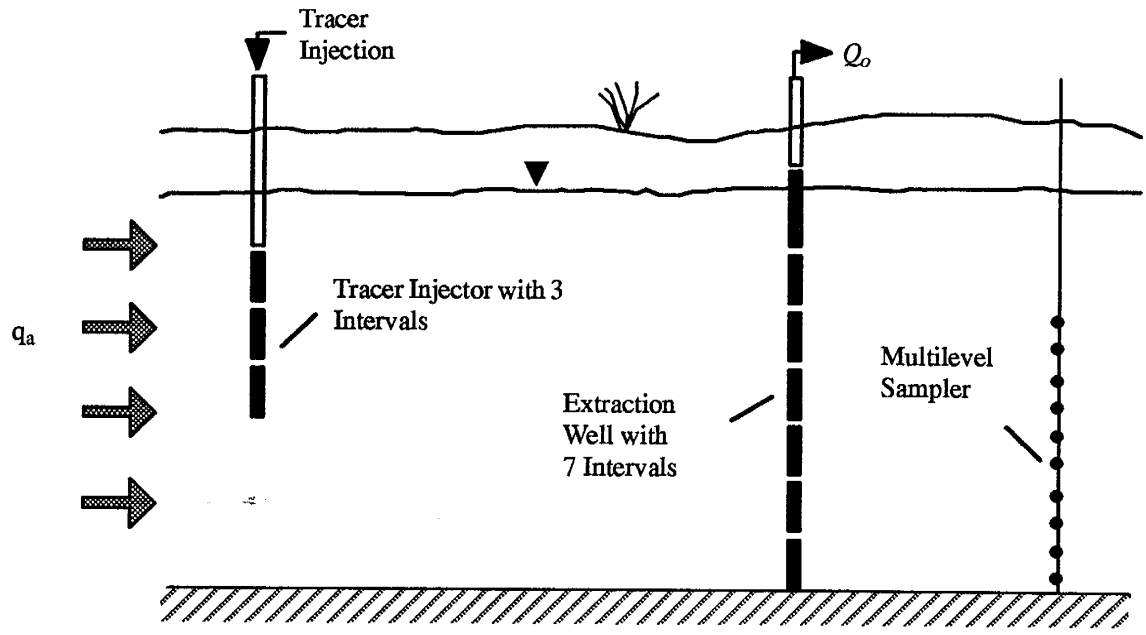

Figure 5.3. Schematic cross-section of the Borden tracer test with a fully penetrating pumping well (after Linderfelt, 1994).

Table 5.2. Tracer injection sites, dates and masses (after Linderfelt, 1994).

Injection Site	Injection Date, 1992		FBA, (g)
	Calender	Julian	
I1	July 1	0	o-TFMBA; 30.2
I2	July 1	0	m-TFMBA; 30.2
I3	July 6	5	3,4-DFBA; 60.4
I4	July 1	0	PFBA; 60.3
I5	July 1	0	2,3-DFBA; 60.4
I6	July 3	2	2,6-DFBA; 60.4
I7	July 6	5	3,5-DFBA; 60.3
I8	July 3	2	2,3-DFBA; 60.4
I9	July 3	2	PFBA; 30.2
I10	July 1	0	3,4-DFBA; 60.8
I11	July 3	2	3,5-DFBA; 60.4
I12	July 6	5	PFBA; 60.3
I13	July 3	2	o-TFMBA; 60.4
I14	July 6	5	m-TFMBA; 60.3
I15	July 6	5	2,6-DFBA; 30.2

Notes: DFBA - difluorobenzoic acid
TFMBA - trifluoromethylbenzoic acid
PFBA - pentafluorobenzoic acid

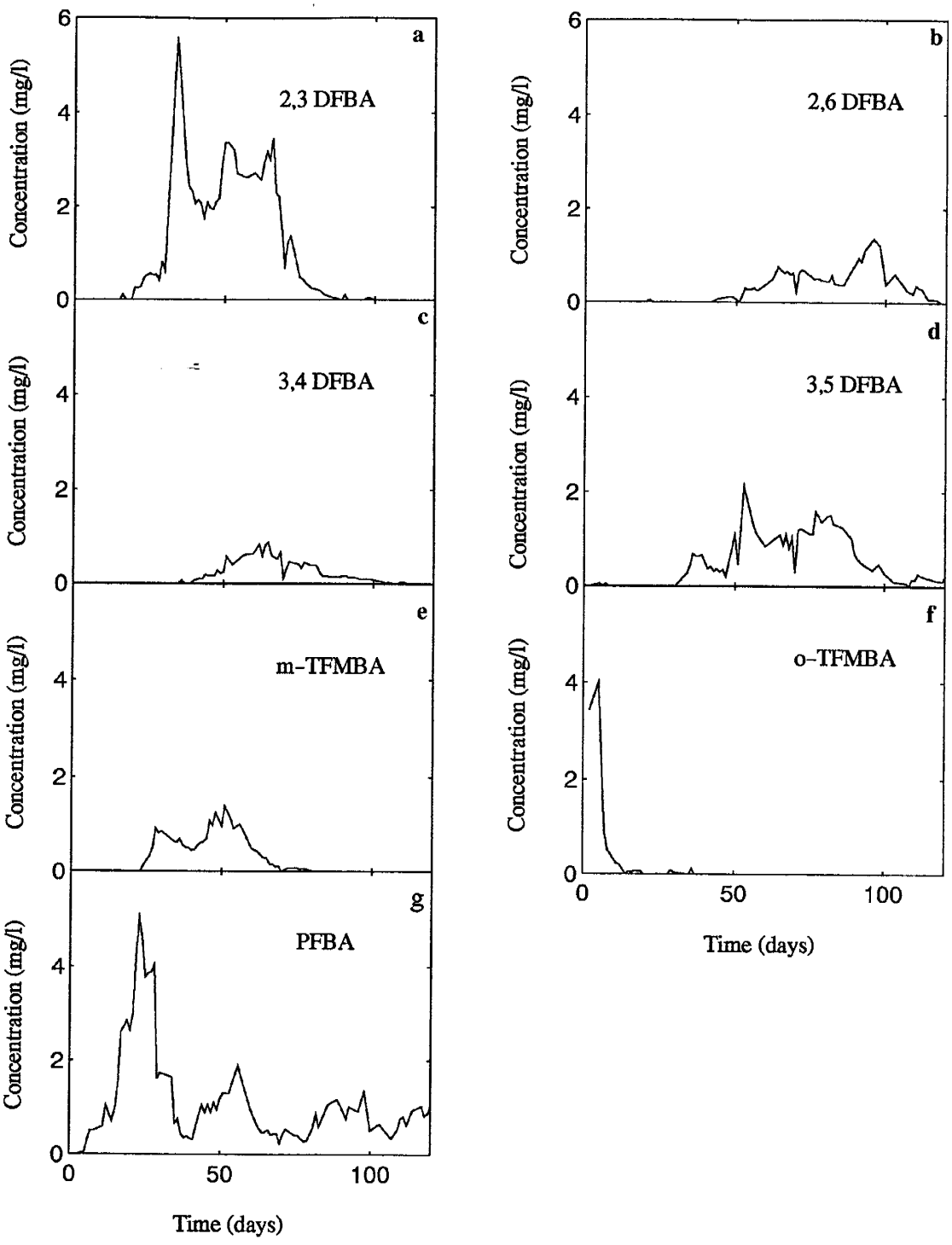

Figure 5.4. The measured concentration breakthrough curves from the pumping well for the 8 tracers at the Borden tracer test. The data was published by Linderfelt (1994).

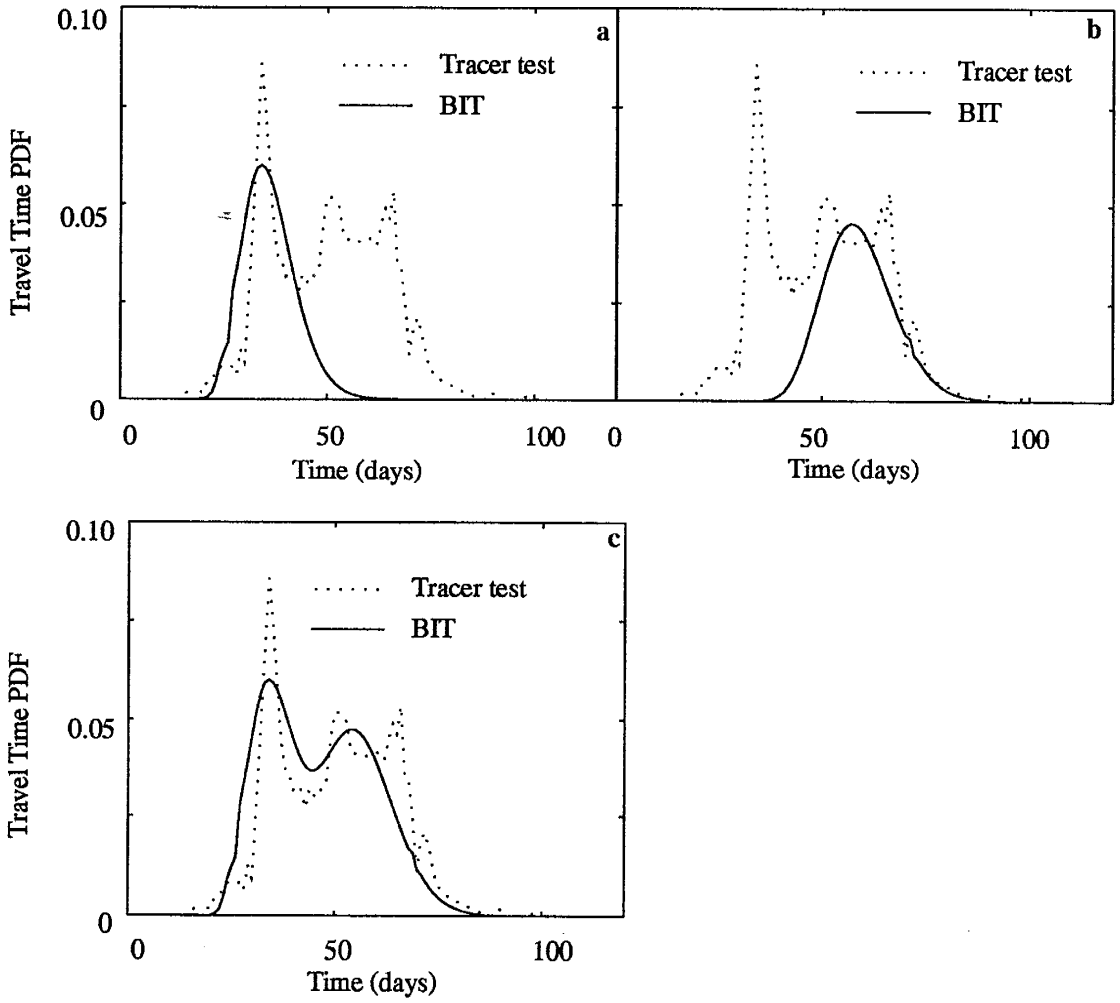

Figure 5.5. Simulations of the travel time PDFs from the backward-in-time (BIT) model and empirical arrival time PDF for the tracer 2,3 DFBA. a. Plots present the simulation from BIT model for injection well I5 (solid line), and 2,3 DFBA experimental breakthrough curves normalized by mass injected (dotted line); b. for injection well I8; c. for injection wells I5 and I8.

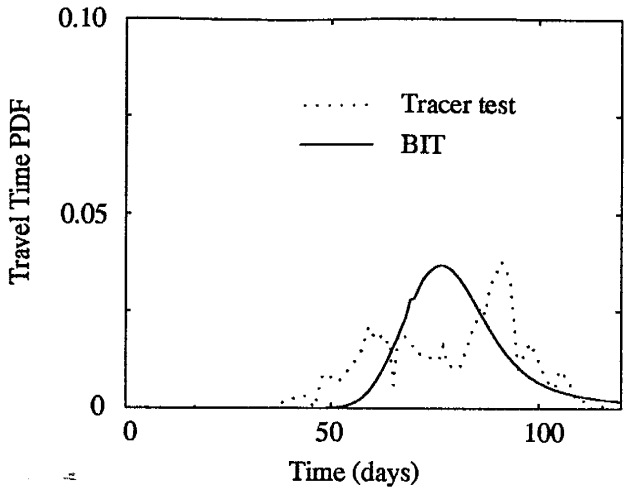

Figure 5.6. Simulations of the travel time PDF and arrival time PDF for the tracer 2,6 DFBA. The solid line presents the simulation from the backward-in-time (BIT) model for injection well I15, and the dotted line describes the tracer test.

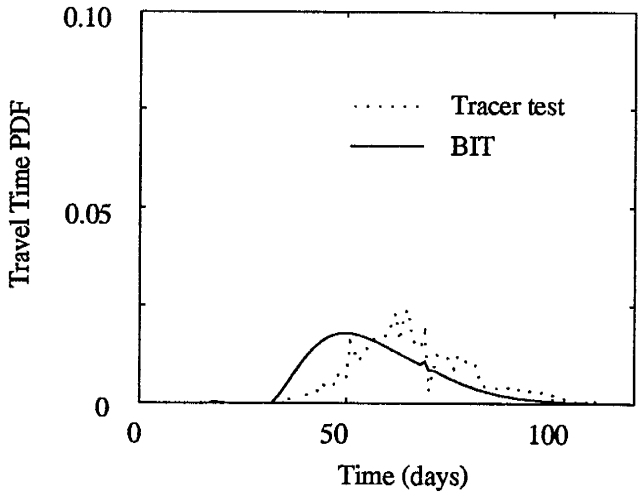

Figure 5.7. Simulations of the travel time PDFs and arrival time PDF of the tracer 3,4 DFBA. Solid line presents the simulation from the backward-in-time (BIT) model for injection well I10, and the dotted line describes the tracer test.

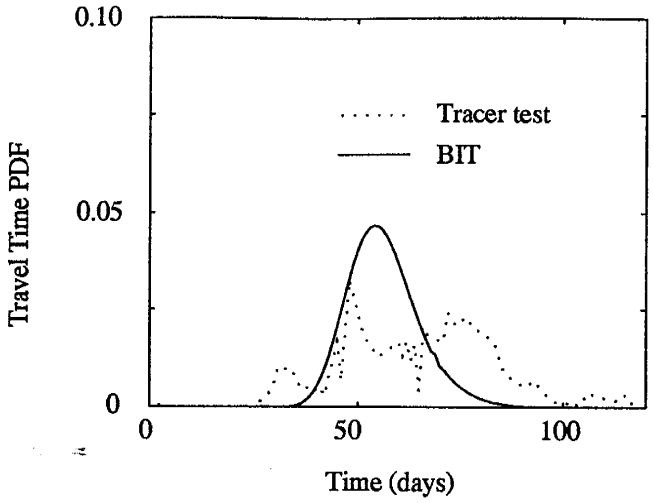

Figure 5.8. Simulations of the travel time PDF and arrival time PDF of the tracer 3,5 DFBA. The solid line presents the simulation from the backward-in-time (BIT) model for injection well, I7, and the dotted line describes the tracer test.

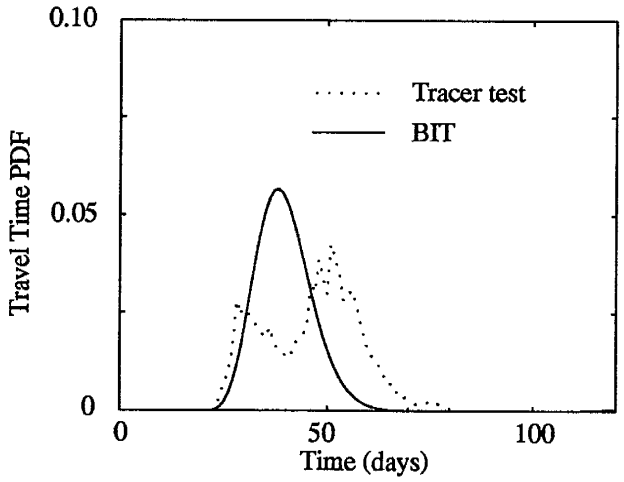

Figure 5.9. Simulations of the travel time PDF and arrival time PDF for the tracer m-TFMBA. The solid line presents the simulation from the backward-in-time (BIT) model for injection well I2, and the dotted line describes the tracer test.

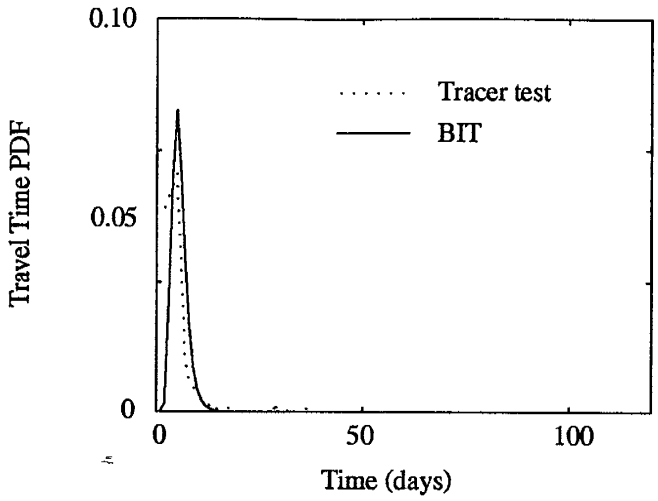

Figure 5.10. Simulations of the travel time PDF and arrival time PDF for the tracer o-TFMBA. The solid line presents the simulation from the backward-in-time (BIT) model for injection well I1, and the dotted line describes the tracer test.

5.2 Modeling Arrival Time of Tracers Using the Backward-in-time Method

For the domain in Figure 5.12, the travel time PDF in the backward-in-time model is expressed by equation (4.6). The boundary and initial conditions are given in Figure 5.12 and Table 5.1. Figure 5.13 demonstrates the travel time PDF simulations for injection sites I5 and I8 vs. travel time. Compared to the arrival time PDF simulated from the forward-in-time model, the travel time PDFs from the backward-in-time PDEs model are in close agreement to the arrival time PDFs. BIT travel time PDF simulations for the 15 injection sites are shown in Figures 5.5 - 5.11, and compared to the empirical data. Only previously published data are used. No additional calibration or curve fitting has been done.

The tracer 2,3-DFBA was injected into I5 and I8, and the concentration breakthrough curve observed from the pumping well is shown in Figure 5.4a. The normalized concentration is shown in Figure 5.5. The normalized curve illustrates the difficulty of separating three peaks from two injection wells. Simulations of travel time probability density functions for injection wells I5 and I8 are shown in Figure 5.5a and Figure 5.5b, respectively. Figure 5.5a

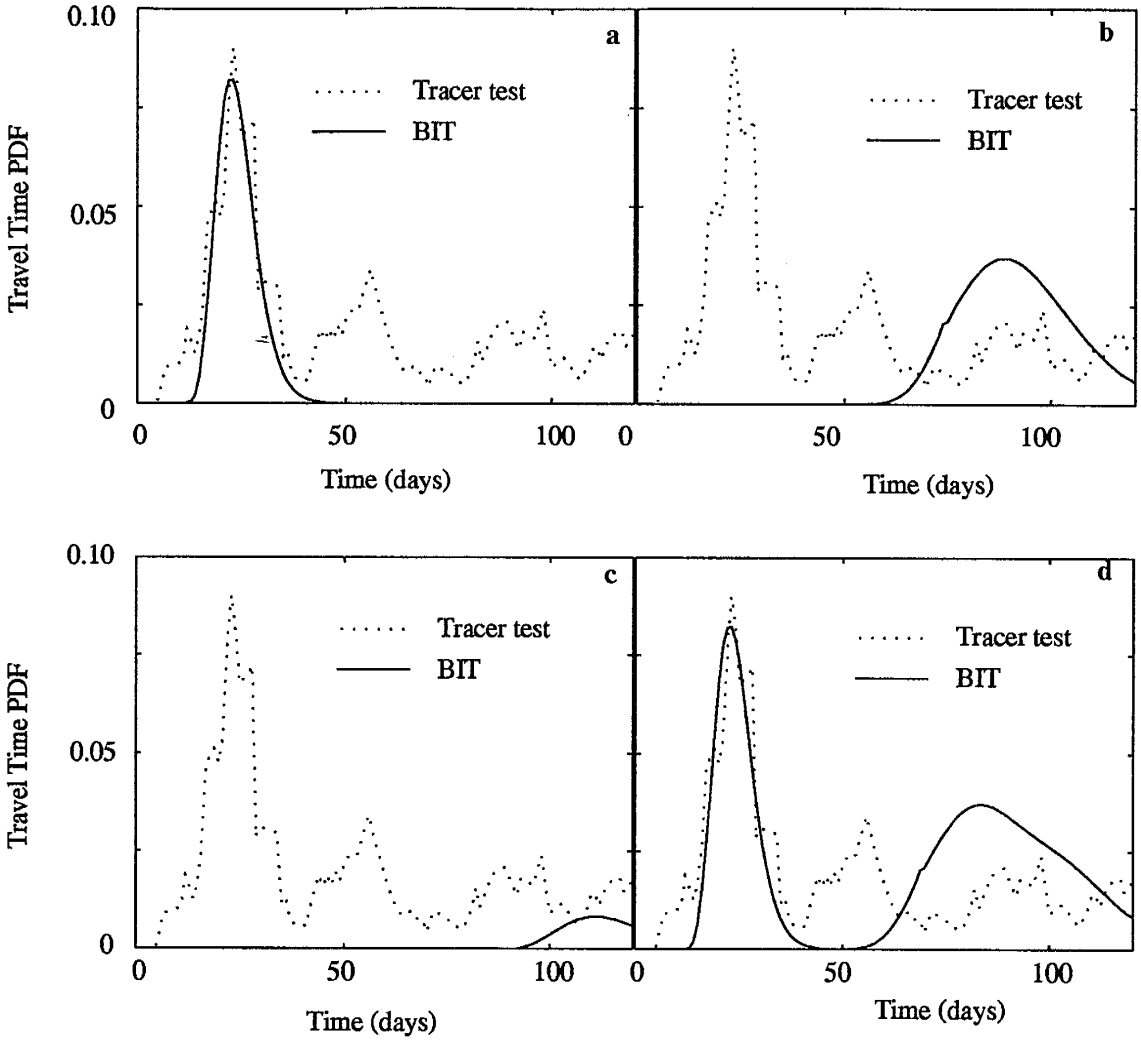

Figure 5.11. Simulations of the travel time PDF and arrival time PDF for the tracer PFBA. Plots present the arrival time PDF of PFBA (dotted line) and the travel time PDF from the backward-in-time (BIT) model for injection wells: **a.** I4; **b.** I12; **c.** I9; **d.** I4, I9, and I13.

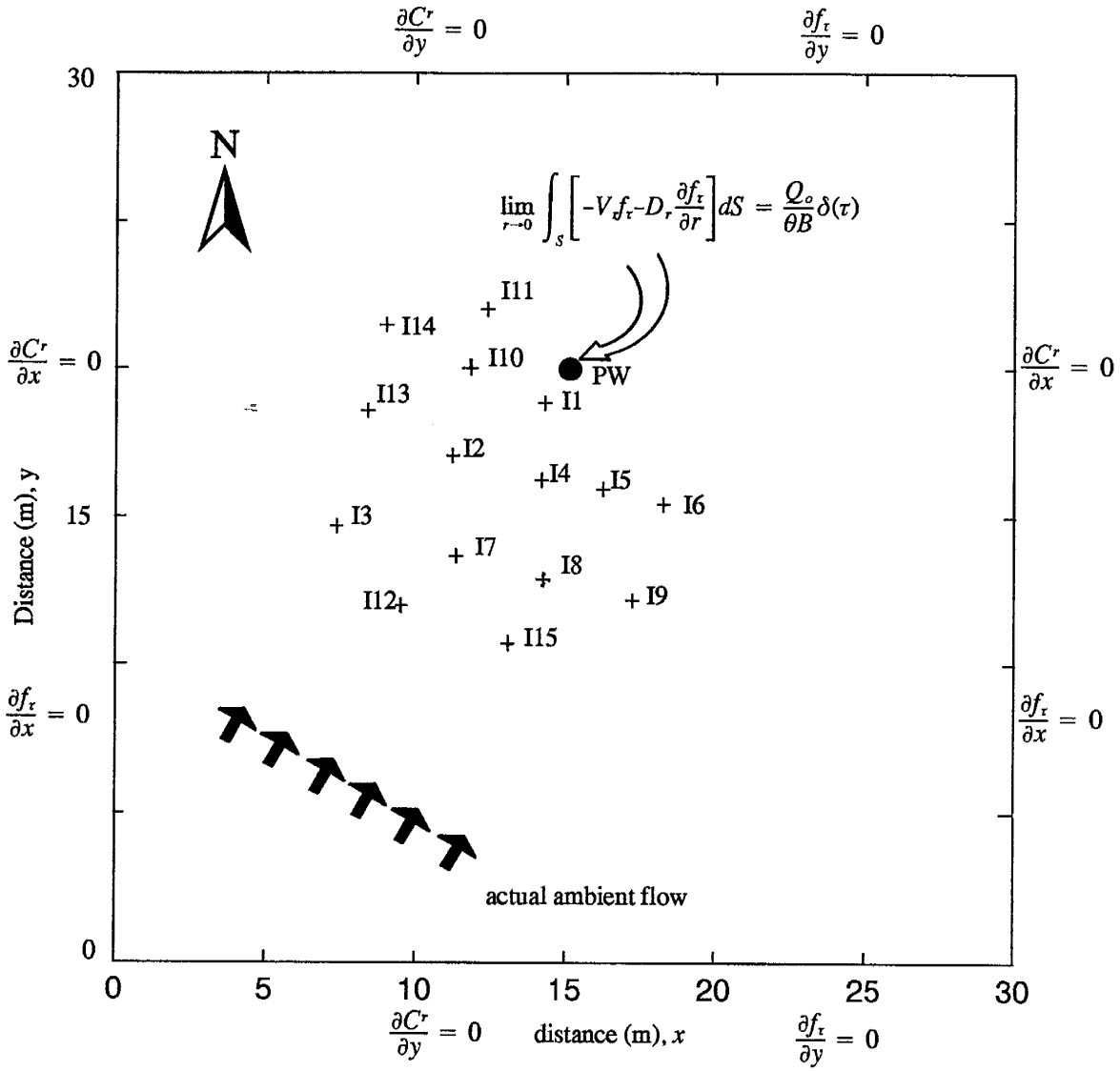

Figure 5.12. Illustration of the physical dimensions of a two-dimensional model at the Borden site. The domain is about 30 m in length and 30 m in width. A pumping well (PW) is located at (15,20), and the tracers are introduced in the injection wells. For forward-in-time mass transport, second type boundary conditions are used in all boundaries. For the backward-in-time PDEs model, the third type boundary condition is used at the pumping well, and second type boundary conditions are used in other boundaries.

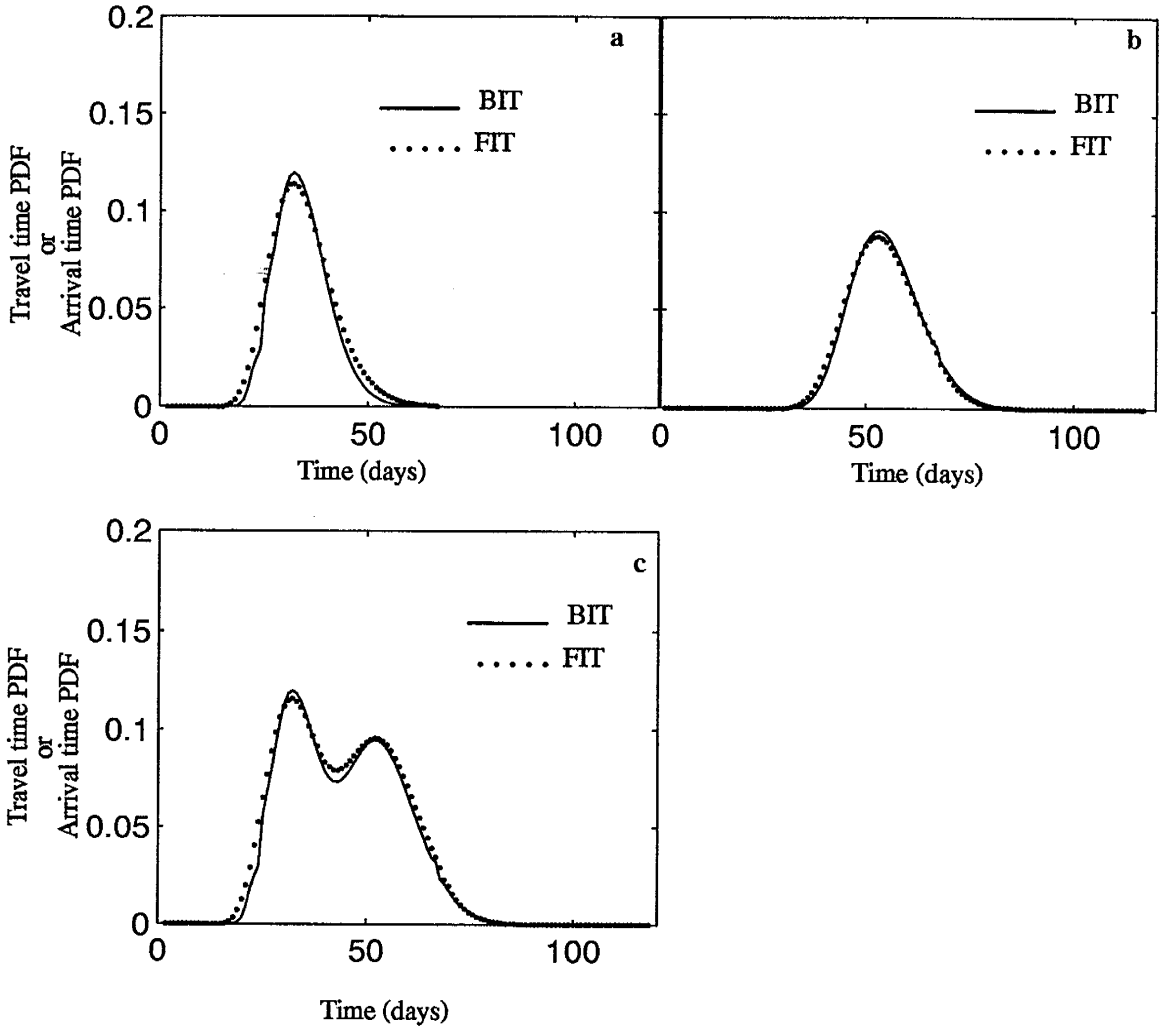

Figure 5.13. Simulations of the travel time PDFs from the backward-in-time (BIT) PDEs model and arrival time PDF from the forward-in-time (FIT) model in the Borden tracer test. **a.** Plots shows simulations for injection site I5. **b.** Plots show simulations for injection site I8; **c.** Plots show simulations for injection sites I5 and I8.

shows that the travel time was about 32 days from I5 to the pumping well, and that the simulation is very close to the first peak of the tracer 2,3 DFBA in shape. Figure 5.5b shows that the travel time is about 55 days from I8 to the pumping well, and that the simulation can be fitted to the last two peaks of tracer 2,3 DFBA. For the interpretation of tracer 2,3 DFBA, we need to consider the travel time probability for two or more injection wells. When the tracers were injected into wells at the same time, their arrival time probability can be computed by totalling their arrival time probabilities. Figure 5.5c presents the travel time probability for I5 and I8, which is very close to the empirical arrival time PDF of tracer 2,3 DFBA in shape. As a result, the first peak of tracer 2,3 DFBA represents the arrival time PDF for I5, and the last two peaks describe the arrival time PDFs for I8.

The tracer 2,6–DFBA was injected into I6 and I15, and the concentration breakthrough curve is shown in Figure 5.4b. The simulations for I6 and I15 demonstrate that the tracer from I6 was not captured by the pumping well. Figure 5.6 presents the the travel time probability for location I15. The estimated travel time from I15 to the pumping well is about 75 days. For the normalized concentration of 2,6–DFBA, the arrival time of the tracer ranged from 60 days to 95 days, with a most likely arrival time of 90 days. The comparison demonstrates that the simulations are reasonably close to the most likely arrival time.

The tracer 3,4 DFBA was injected into I3 and I10, and the tracer concentration breakthrough curve is shown in Figure 5.4c. Figure 5.7 shows that the most likely arrival time of 3,4 DFBA was about 60 days. The simulations show that the tracer 3,4 DFBA injected into I3 was not captured by the pumping well, as was also suggested by the forward–in–time model by Linderfelt (1994) and his tracer test interpretation. The most likely possible travel time is about 48 days which is 12 earlier days than the actual arrival time of 3,4 DFBA. Compared to the arrival time probability of the tracer 3,4 DFBA, the simulation is similar to the normalization of the tracer concentration in shape.

The tracer 3,5 DFBA was injected into I7 and I11, and its breakthrough curve is shown in Figure 5.4d. Figure 5.8 shows the most likely arrival time ranging from 50 days to 85 days. The simulations show that the tracer 3,5 DFBA injected into I11 was not captured by the pumping well, a fact also predicted by the forward–in–time model (Linderfelt, 1994). Figure 5.8 presents the travel time probability distribution for former location I7. The estimated travel time is about 55 days. The comparison of the simulation and tracer test demonstrates that the simulation is roughly similar to the empirical arrival times.

The tracer m–TFMBA was injected into I2 and I14, and its normalization is shown in Figure 5.9. The estimated arrival time ranges from 20 to 50 days. The simulations from the backward–in–time PDEs model illustrate that the tracer from I14 was not captured by the pumping well, and that the normalization in Figure 5.9 represents the arrival time probability from location I2 only. Simulations in the figure demonstrate that the most likely travel time from I2 to the pumping well is about 40 days, a value between the two peaks of the normalized concentration of m–TFMBA. The difference from the tracer test can be explained by the spatial variability of hydraulic conductivity (Linderfelt, 1994).

The tracer o–TFMBA was injected into I1 and I13, and the normalization of concentration is shown in Figure 5.10. The arrival time probability has one peak at about 5 days. The simulations illustrate that only the tracer from I1 was captured by the pumping well, and that the tracer from I13 flowed out through the multilevel sampler zone. The predicted travel time from I1 to the pumping well is about 4.5 days, which agrees with the arrival time of o–TFMBA.

The tracer p–TFMBA was injected into I4, I9 and I12. The concentration breakthrough curve and normalization are shown in Figure 5.4g and Figure 5.11, respectively. The empirical arrival time probability presents one high peak at about 20 days and three low peaks over a period of 50 days to 120 days. The simulations for the three injection wells are shown in Figure 5.11a, Figure 5.11b, and Figure 5.11c. Figure 5.11a shows that the travel time proba-

bility for I4 agrees with the first peak of p-TFMBA, and the most likely travel time is about 20 days from I4 to the pumping well. Figure 5.11b shows that the travel time probability for I12 has a range of 66 days to 90 days, which is close to the third peak of p-TFMBA. Figure 5.11c shows that the travel time probability for I9 is much less than for I4 or I12, and that the distribution is close to the last peak of p-TFMBA. Figure 5.11d shows that the total of the three travel time probabilities can be compared to the concentration normalization of p-TFMBA. As a result, the first high peak shows the arrival time PDF for I4, and the third low peak shows the arrival time PDF for I12. The last peak should represent the arrival time for I9. The second peak is probably also I12, which split off and arrived earlier because of aquifer heterogeneity.

5.3 Modeling the Capture Zone of the Tracer Test Using the Backward-in-time Method

We can obtain the travel time CDF map using the backward-in-time model. How can we examine the CDF map using the tracer test data? To begin with, we need to compute the cumulative distribution for the arrival time of the tracer for each injection site. The cumulative distribution can be obtained from the normalization of cumulative mass (Jury and Roth, 1990; Henley and Kumamoto, 1992). The cumulative mass of the tracer extracted from the pumping well can be computed using the concentration and pumping rate:

$$m_k = \sum_{i=1}^{k} C_i^f Q_o \Delta t_i \tag{5.2}$$

where m_k is the cumulative mass [M] for a time period less than t_k, C_i^f is the flux concentration [M/L^3] observed in time t_i from the pumping well, and Q_o is the pumping rate [L^3/T]. Linderfelt (1994) computed the total cumulative mass for eight types of tracer over the entire last period (to 124 days). The cumulative distribution for arrival time less than t can be computed by (Jury and Roth, 1990; Henley and Kumamoto, 1992):

$$P(t' < t|x) = \frac{m_k}{M} \tag{5.3}$$

where $P(t' < t|x)$ is the cumulative distribution for time less than t, and M is the total mass injected into the aquifer. In the tracer test, the cumulative distribution for 15 injection sites are computed by equations (5.2)–(5.3) and the simulation results are shown in Table 5.3.

Table 5.3. The cumulative distribution of arrival time for eight tracers:

Injection Well	CDF (t < 66days)	CDF (t < 117days)	CDF*(t < 124days)
I1	1.0	1.0	1.0
I2	0.95	0.97	0.97
I3	0.0	0.0	0.0
I4	1.0	1.0	1.0
I5	0.9	0.9	0.9
I6	0.0	0.03	0.03
I7	0.46	1.0	1.0
I8	0.8	1.0	1.0
I9	0.0	0.17	0.17
I10	0.34	0.61	0.32
I11	0.0	0.0	0.0
I12	0.20	0.96	0.96
I13	0.0	0.0	0.0
I14	0.0	0.0	0.0
I15	0.21	0.95	1.0

CDF* (t < 124 days) is the ratio of recovery mass to total injected mass, after Linderfelt (1994).

In the backward-in-time model, the cumulative distribution of the travel time, $F_\tau(\tau|x)$, for the Borden site can be expressed by equation (4.6), and the initial and boundary conditions can be expressed by equation (4.9). Simulations of the travel time CDFs in the Borden site are illustrated in Figures 5.14 and 5.15. Figure 5.14 presents the cumulative distribution for a travel time of less than 66 days. Figure 5.15 shows the cumulative distribution for travel time less than 117 days. The simulated capture zone extends upstream when the travel time increases.

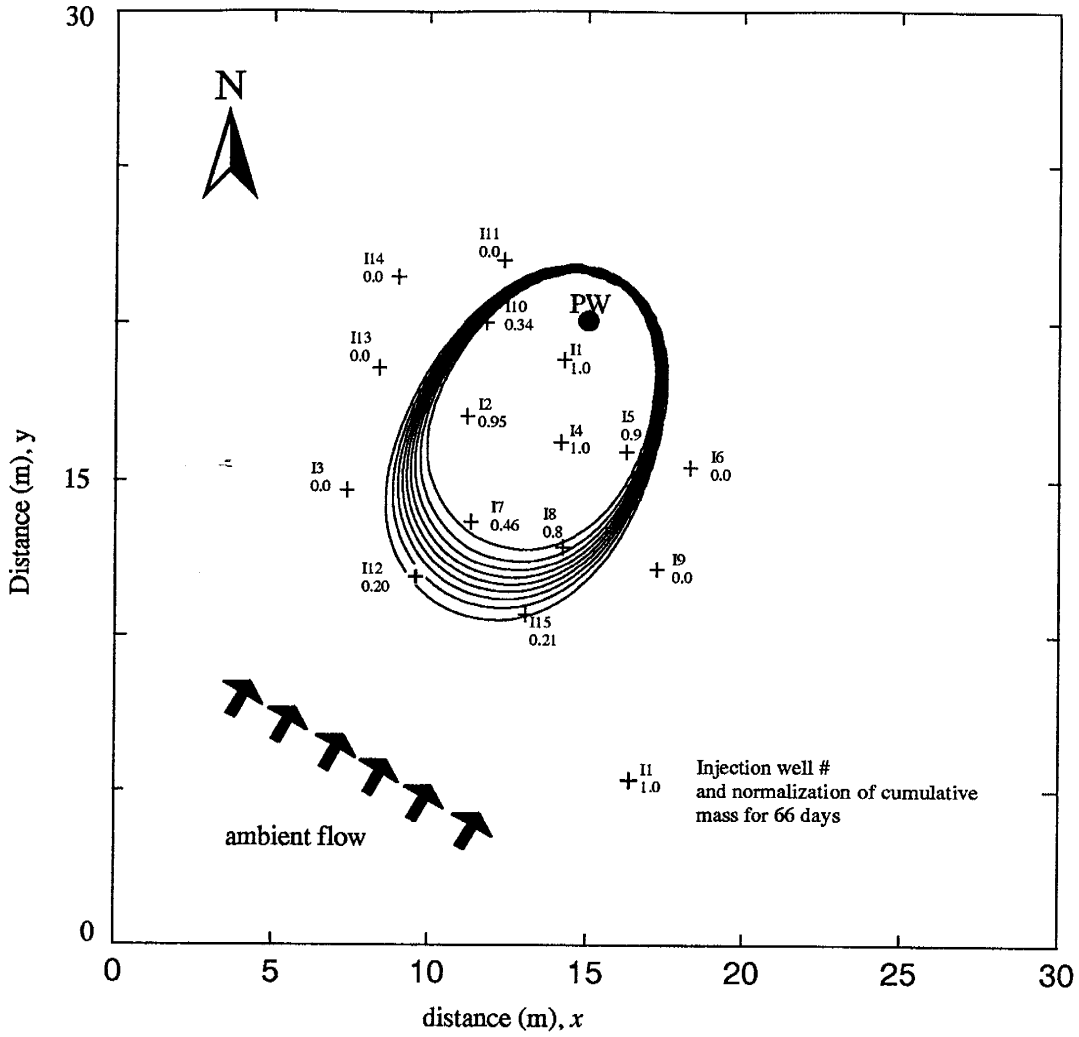

Figure 5.14. Simulations of the travel time cumulative distribution function (CDF) from the backward-in-time model, and normalization of the cumulative mass of 8 tracers for 66 days.

For 66 days, Figure 5.14 indicates that the injection wells I1, I2, I4, and I5, with greater than 0.9 actual recovery, are located in the area where the BIT simulations of travel time CDF predict recoveries greater than 0.9. I 8 is also in the zone, but actually had only 0.8 recovery. The injection wells I3, I6, I9, I11, I13 and I14, with no actual tracer recovery, are located where the simulations suggested zero recovery. Injection wells I12 and I15 had about 0.2 recovery and are located in the front of the predicted capture zone. The only data inconsistent

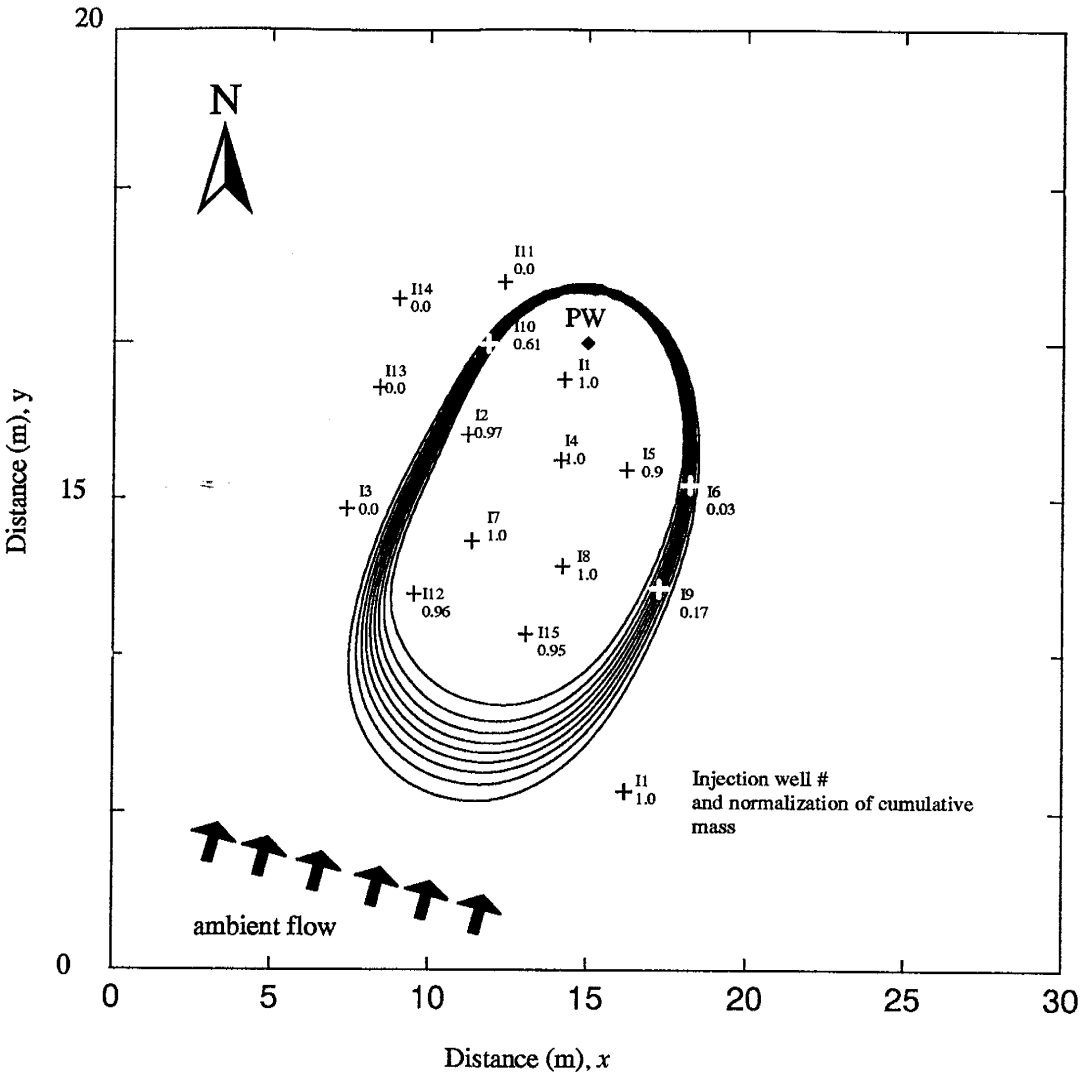

Figure 5.15. Simulations of the travel time cumulative distribution function (CDF) using the backward-in-time model and normalization of the cumulative mass of 8 tracers for 117 days.

with the BIT simulations is from I7, with 0.46 actual recovery vs. a simulated recovery of greater than 0.9. In general, the simulations demonstrate a good match to the tracer test.

Figure 5.15 presents the simulations and tracer cumulative distributions for travel time less than 117 days. Injection wells I1, I2, I4, I5, I7, I8, I12, I15 are located where the actual and simulated travel time CDFs are larger than 0.9. I3, I11, I13 and I14 are located where simulated recoveries were nil. I6, I9, and I10 are in the intermediate, dispersed zone, in both

the simulations and the data. The small differences could have been caused by the approximation of the transient flow field.

As a result, the backward–in–time method can be employed to predict the arrival time probability of a tracer, or to delineate the capture zone of the tracer test. The new model can also be utilized in assigning responsibility for observed contamination, pumping wellhead protection, and aquifer remediation.

6. CONCLUSIONS

This report examines a new hypothesis that the travel time and location probabilities of contamination can be directly formulated and solved from an advection–dispersion partial differential equation with reversed flow. The results of this research are expected to have applications for groundwater monitoring, remediation and water supply well head protection. The conclusions we have reached may be stated as follows:

(1) Using analytical solutions of one–dimensional backward–in–time models this work successfully tests the new hypothesis.

(2) The new hypothesis is extended to a two–dimensional model, and its results are compared to numerical simulations of a standard forward–in–time model.

(3) By proper selection of initial and boundary conditions at the pumping well, two types of maps for travel time probability and location probability can be obtained for both a one–dimensional and a two–dimensional model. The new appropriate boundary condition for the travel time probability is a third type boundary condition at the pumping well, and it is described by a delta function for the PDF or a unit one for the CDF. The new proper initial condition for the location PDF is a delta function distribution around the pumping well.

(4) In the backward–in–time problem, both travel time probability and location probability refer to conditional probabilities. Although the probability solutions are complicated by heterogeneity, chemical reaction and natural recharge, the relation of location and travel time probability is described by the Bayes theorem. The relation can be employed to transform one probability to the other.

(5) For the heterogeneity of conductivity and dispersion in a two–dimensional aquifer, the travel time and location probability are directly simulated from the backward–in–time partial differential equations. The travel time probability is successively compared to arrival time probabilities computed from forward–in–time simulations. Numerical simulations demonstrate that the highest probabilities tend to occur in the high permeable area. This re-

port presents an example for a given hydraulic conductivity distribution; however, the new model can also be used with the random fields of hydraulic conductivity.

(6) In the case of natural recharge, the travel time and location probability can be directly simulated by backward–in–time partial differential equations. For the travel time probability, the backward–in–time partial differential equation presents discharge of the probability under the reversing of groundwater flow. The simulations of the travel time probability demonstrate that the cumulative distribution becomes narrower and longer than it does for non–natural recharge. For the location probability, the backward–in–time partial differential equation does not present discharge of location probability while the groundwater flow is reversing.

(7) In the case of first order decay, some contaminants are lost before they reach the pumping well. The travel time probability and location probability, respectively, are computed from two different backward–in–time partial differential equations. For the travel time probability, the backward–in–time partial differential equation involves an exponential decay of travel time probability. For the location probability, estimation of the contaminant's origin location should not be impacted by first order decay, and the backward–in–time partial differential equation does not involve decay of the location probability.

(8) For the case of sorption in an aquifer, the travel time probability and location probability can be described for: the aqueous phase, the sorbed phase, and the combined aqueous and sorbed phases. Total probability for the combined phases is equal to the sum of the aqueous phase probability and the sorbed phase probability. In the new method, the probabilities can be directly solved from the backward–in–time partial differential equations, thereby accounting for either linear equilibrium sorption or non–equilibrium sorption. For linear equilibrium sorption, probabilities are retarded and reduced by the retardation factor. For non–equilibrium sorption, non–equilibrium sorption retards the expansion of probability

distributions, and the retardation is increased with the increasing equilibrium sorption coefficient and the larger mass transfer coefficient.

(9) The travel time PDF from the new backward-in-time method is employed to interpret the normalization of tracer concentration or arrival time probability in the Borden site capture zone tracer test. By running one backward-in-time simulation, we obtain the travel time probabilities for all injection sites. The simulations for most injection sites can match the tracer arrival time probability very well, especially, for the injection sites close to the pumping well.

(10) Using the backward-in-time model we delineate a travel time cumulative distribution map that can be employed to fit the observed time-dependent capture zone of the Borden tracer test.

(11) The new model can also be utilized in assigning responsibility for observed contamination, pumping wellhead protection, and aquifer remediation.

Recommendations For Future Work

During the course of this research it has been shown that the new hypothesis can be employed in a one-dimensional and two-dimensional model addressing dispersion, first order decay, sorption, heterogeneity, and natural recharge. Although time did not permit us to test a three-dimensional model and to apply the new model to the identification of the source location and release history, it is felt that future tasks as described below may be fruitful:

- Extend the backward-in-time method to the cases of double porosity (mobile-immobile pore space), non-Fickian dispersion, chemical production, multi-phase, and transient flow.
- Test the backward-in-time method's ability in a three-dimensional model.
- Extend the new method for the pumping well system to a monitoring well system.

- Use the new model to yield a joint probability for two or more observed concentrations from one pumping well or monitoring well, and to identify the source location or release history.

REFERENCES

Bear, J. 1972: Dynamics of Fluids in Porous Media, Elsevier, New York.

Bear, J. and A. Verruijt, 1987: Modeling Groundwater Flow and Pollution, Reidel, Norwell, 247–343.

Bagtzoglou, A. C., D. E. Dougherty, and A. F. B. Tompson, 1992: Application of particle methods to reliable identification of groundwater pollution sources. Water Resources Management, Vol. 6, 15–23.

Brusseau, M.L., R.E. Jessup, and P.S.C. Rao, 1992: Modeling solute transport influenced by multiprocess nonequilibrium and transformation reactions. Water Resources Research, Vol. 28, No. 1, 175–182.

Cacuci, D.G., 1981: Sensitivity theory for nonlinear systems, I, nonlinear functional analysis approach. J. Math. Phys., Vol. 22, No. 12, 2973–2802.

Carrera, J. and S.P. Neuman, 1985: Estimation of aquifer parameters under transient and steady state conditions, 2. Uniqueness, stability and solution algorithms. Water Resources Research, Vol. 22, No. 2, 211–227.

Chandrasekhar, S., 1942: Stochastic problems in physics and astronomy. Reviews of Modern Physics, Vol. 15, No. 1, 1–43.

Chock, D.P. and S.L. Winkler, 1994: A particle grid air quality modeling approach: 1. The dispersion aspect. J. of Geophysical Research, Vol. 99, No. D1, 1019–1031.

Chin, D. and P.V.K. Chittaluru, 1994: Risk management in wellhead protection. J. Water Resources Planning and Management, Vol. 120, No. 3, 293–315.

Dagan, G., 1984: Solute transport in heterogeneous porous formations. J. Fluid Mech., Vol. 145, 151–177.

Dagan, G., and V. Nguyen, 1989: A comparison of travel time and concentration approaches to modeling transport by groundwater. J. Contam. Hydrol., Vol. 4, 79–91.

Environmental Protection Agency, 1990: WHPA: An integrated semi-analytical model for the delineation of wellhead protection areas. Office of Ground-water Protection, Washington, D.C.

Freyberg, D., 1986: A natural gradient experiment on solute transport in a sand aquifer. 2. Spatial moments and advection and dispersion of nonreactive tracers. Water Resources Research, Vol. 22, 2031-2046.

Gleati, G. and Gambolati G., 1989: On boundary conditions and point sources in the finite element integration of the transport equation. Water Resources Research, Vol. 25, No. 5, 847-856.

Gorelick, S. M., B. Evans and I. Remson, 1983: Identifying sources of groundwater contamination: an optimization approach. Water Resource Research, Vol. 19, No. 3, 779-790.

Ghez, R., 1987: A Primer of Diffusion Problems, Wiley, New York.

Hathhorn, W. E., R. J. Charbeneau, 1994: Stochastic fluid travel times in heterogeneous porous media. J. Hydraulic Engineering, Vol. 120, No. 2, 133-145.

Henley, E. J. and H. Kumamoto, 1992: Probabilistic risk assessment: Reliability engineering, design, and analysis. IEEE Press, New York, 245-264.

Jury, W.A. and F. Roth, 1990: Transfer functions and solute movement through soils. Birkhauser, Boston.

Jury, W.A., G. Sposito, and R.E. White, 1986: A transfer function model of solute movement through soil. 1. Fundamental Concepts. Water Resources Research, Vol. 22, 243-247.

Kreft, A. and A. Zuber, 1978: On the physical meaning of the dispersion equation and its solution for different initial and boundary conditions. Chem. Eng. Soc., Vol. 33, 1471-1480.

Linderfelt, W.R., 1994: Field study of capture zones in a shallow sand aquifer. Ph. D. thesis, New Mexico Tech, Socorro, NM.

Linderfelt, W.R., J.L. Wilson, 1995: Capture zone delineation: models and experiments, Draft EPA Completion Report, CR-818019-091-0, U.S. Envionmental Protection Agency, R.S. Kerr Lab., Ada, Ok.

Linderfelt, W.R., J.L. Wilson, and S. Leppert, 1989: Capture zones for wellhead protection: Effect of time dependent pumping, saturated thickness, and uncertain parameters. Presented at Fall Meeting, American Geophysical Union, San Francisco.

Lindstrom, F.T. and L. Boersma, 1989: Analytical solutions for convective-dispersive transport in confined aquifers with different initial and boundary conditions. Water Resources Research, Vol. 25, No. 1, 241-255.

Liu, J. and J.L. Wilson, 1994: Backward travel time and location probabilities for non-equilibrium sorption. Abstract, EOS, Vol. 75, No. 44, 293.

Liu, J. and J.L. Wilson, 1995: Modeling travel time and source location probabilities in two-dimensional heterogeneous aquifer. Proceedings of 5th Annual WERC Technology Develop Conference, Las Cruces, New Mexico, 59-67.

Macky, D.M., D.L. Freyberg, P.V. Roberts and J.A. Cherry, 1986: A natural gradient experiment on solute transport in a sand aquifer. 1. Approach and overview of plume movement, Water Resources Research, Vol. 22, No. 13, 2017-2029

Parker, J. C., and P.M. Jardine, 1986: Effects of heterogeneous adsorption behavior on ion transport. Water Resources Research, Vol. 22, No. 8, 1334-1140.

Parker, J. C., and M. Th. Van Genuchten, 1984: Flux-averaged and volume-averaged concentrations in continuum approaches to solute transport. Water Resources Research, Vol. 20, 866-872.

Provencher, S.W., 1982: A constrained regularization method for inverting data represented by linear algebraic or integral equations. Compu. Phys. Commun., Vol. 27, 213-227.

Schafer–Perini, A. L. and J. L. Wilson. Efficient and accurate front tracking for two–dimensional groundwater flow models. Water Resources Research, Vol. 27, No. 7, 1471–1485, 1991.

Segol, G., 1993: Classic groundwater simulations: Proving and improving numerical models. PTR Prentice Hall, New Jersey.

Shafer, J.M., 1987a: Reverse Pathline Calculation of Time Related Capture Zones in Non–Uniform Flow. Groundwater, Vol. 25, No. 3, 282–289.

Shafer, J.M., 1987b: GWPATH: Interactive ground–water flow path analysis. Bulletin 69, Illinois Department of Energy and Natural Resources.

Skaggs, T.H. and Z.J., Kabala, 1994: Recovering the release history of a groundwater contaminant. Water Resources Research, Vol. 30, No. 1, 71–79.

Soong, T.T., 1972: Random Differential Equations in Engineering, Academic Press, New York.

Small, M.J. and J.R. Mullar, 1987: Long term pollutant degradation in the unsaturated zone with stochastic rainfall infiltration. Water Resources Research, Vol. 23, 2246–2256.

Sposito, G. and W.A. Jury, 1988: The solute lifetime probability density function for solute movement in the subsurface zone. J. Hydrol., Vol. 102, 503–518.

Sudicky, E. A. and R. G. McLaren, 1991: User's guide for FRACTRAN: An efficient simulator for two–dimensional, saturated groundwater flow and solute transport in porous or discretely–fractured porous formations. Waterloo Centrer for Groundwater Research, University of Waterloo, Ontario, Canada.

Sudicky, E. A. and R. G. McLaren, 1992: The Laplace transform Galerkin technique for large–scale simulation of mass transport in discretely fracture porous formations. Water Resource Research, Vol. 28, No. 2, 499–513.

Toride, N., F.J. Leij, and M.T. van Genuchten, 1993: A comprehensive set of analytical solutions for nonequilibrium solute transport with first–order decay and zero–order production. Water Resources Research, Vol. 29, No. 7, 2167–2182.

Tiedeman, C. and S.M. Gorelick, 1993: Analysis of uncertainty in optimal groundwater contaminant capture design. Water Resources Research, Vol. 29, No. 7, 2139–2153.

Tikhonov, A.N., and V.Y. Arsenin, 1977: Solutions of Ill–Posed Problems, Winston and Sons, New York.

Uffink, G.J.M., 1988: Modeling of solute transport with the random walk method. in Groundwater Flow and Quality Modeling, E. Custodo, A. Gurgui, and J.P.L. Ferreira (eds) D. Reidel Publishing Company, Boston.

Uffink, G.J.M., 1989: Application of Kolmogrorov's backward equation in random walk simulations of groundwater contaminant transport. in Contaminant Transport in Groundwater, Kobus and Kinzelbach (eds), Balkema, Rotherdam.

Van Genuchten, M. Th. and W. J. Alves, 1982: Analytical solutions of the one–dimensional convective–dispersive solute transport equation. U.S. Dept. of Agriculture, Tech. Bull. No. 1661.

Van Genuchten, M. Th. and P. J. Wierenga, 1976: Mass transfer studies in sorbing porous media. 1. Analytical solution. Soil Sci. Soc. Am. J., Vol. 40, 473–480.

Varljen, M.D. and J.M. Shafer, 1992: Assessment of uncertainty in time–related capture zones using conditional simulation of hydraulic conductivity. Ground Water, Vol. 19, No. 5, 737–748.

Wagner, B. J., 1992: Simultaneous parameter estimation and contaminant source characterization for coupled groundwater flow and contaminant transport modeling. J. Hydrology, Vol. 135, 272–302.

Weiss, G.H., 1983: Random walks and their applications. American Science, Vol. 71, 65–71.

Wilson, J.L, 1993: Induced infiltration in aquifers with ambient flow. Water Resource Research, Vol. 29, No. 10, 3503–3512.

Wilson, J.L. and W.R. Linderfelt, 1991: Groundwater quality in pumping wells located near surface water bodies. Tech. Comp. Rpt. 261, New Mexico Water Resour. Res. Inst., Las Cruses, New Mexico November.

Wilson J.L. and W.R. Linderfelt, 1995: Field tracer experiment design problems at the Borden site. Proc. from the 2nd Tracer Workshop, Univ. of Texas at Austin, November 14–15, 1994, T. Bjornstad & G.A. Pope, Eds, Rpt. IFE/KR/E–95/002, Inst. for Energy Technology, Kjeller, Norway, 11–21.

Wilson, J.L. and J. Liu, 1994: Backward tracking to find the source of pollution. Proceedings of 4th Annual WERC Technology Develop Conference, Las Cruces, New Mexico.

Wilson, J.L. and J. Liu, 1995: Backward to find the source of pollution. in Waste–management: From Risk to Reduction, R. Bahda (Ed.), ECM Press, Albuquerque, New Mexico, 181–199.

Wilson, J.L and S. Rao, 1992: The backward–in–time advection–dispersion problem. Abstr., EOS, Vol. 73, No. 14, 134.

APPENDIX A: THE ANALYTICAL SOLUTIONS OF ONE-DIMENSIONAL MODELS

A1. Solution of the Resident Concentration in Advection and Dispersion

The resident concentration of contamination, $C^r(x, t)$, is described by the one-dimensional advection and dispersion governing equation:

$$\frac{\partial C^r}{\partial t} = D\frac{\partial^2 C^r}{\partial x^2} + V\frac{\partial C^r}{\partial x} \tag{A1.1}$$

For the example in Figure 2.1, the boundary and initial conditions are:

$$\frac{\partial C^r}{\partial x} = 0 \ at \ x = 0 \ ; \tag{A1.2a}$$

$$C^r = 0, \ as \ x \rightarrow \infty \tag{A1.2b}$$

$$C^r(x, t) = \frac{M}{\theta}\delta(x-x_o), \ for \ t = 0 \tag{A1.2c}$$

The Laplace transform in time ($t \rightarrow p$) of resident concentration is written as:

$$L[C^r(x,t)] = \hat{C^r}(x,p) = \int_0^\infty C^r(x,t)e^{-pt}dt \tag{A1.3a}$$

$$L\left[\frac{\partial C^r}{\partial t}\right] = p\hat{C^r} - C^r(t = 0) \tag{A1.3b}$$

$$L\left[\frac{\partial C^r}{\partial x}\right] = \frac{\partial \hat{C^r}}{\partial x} \tag{A1.3c}$$

$$L\left[\frac{\partial^2 C^r}{\partial x^2}\right] = \frac{\partial^2 \hat{C^r}}{\partial x^2} \tag{A1.3d}$$

where $\hat{C^r}(x,p)$ is the Laplace transform of resident concentration. Equations (A1.1) and (A1.2) can be rewritten as:

$$D\frac{\partial^2 \hat{C^r}}{\partial x^2} + V\frac{\partial \hat{C^r}}{\partial x} - p\hat{C^r} + \frac{M}{\theta}\delta(x-x_o) = 0 \tag{A1.4}$$

with boundary conditions:

$$\frac{\partial \hat{C^r}}{\partial x} = 0 \ at \ x = 0 \ ; \tag{A1.5a}$$

$$\hat{C^r} = 0, \ as \ x \rightarrow \infty \tag{A1.5b}$$

The double Laplace transform-in-time ($t \rightarrow p$) and space ($x \rightarrow s$) of the resident concentration is:

$$\tilde{C}^r(s,p) = \int_0^\infty \int_0^\infty C^r(x,t)e^{-pt}e^{-sx}dtdx = \int_0^\infty \hat{C}^r(x,p)e^{-sx}dx \qquad \text{(A1.6)}$$

The double Laplace transform-in-time-space of equations (A1.4) and (A1.5) can be rewritten as:

$$\tilde{C}^r(s,p) = \frac{1}{D(s_2-s_1)}\left[\frac{Ds_2\hat{C}^r(0) + V\hat{C}^r(0) - \frac{M}{\theta}e^{-sx_o}}{s-s_2} - \frac{Ds_1\hat{C}^r(0) + V\hat{C}^r(0) - \frac{M}{\theta}e^{-sx_o}}{s-s_1}\right] \qquad \text{(A1.7)}$$

where:

$$s_1 = -\frac{V}{2D}(1+\xi); \quad s_2 = -\frac{V}{2D}(1-\xi); \quad \xi = \sqrt{1+\frac{4pD}{V^2}} \qquad \text{(A1.8)}$$

After inverting the Laplace transform-in-space the Laplace transform in time is expressed as:

$$\hat{C}^r(x,p) = \frac{M}{\theta}\frac{1}{V\xi}e^{-\frac{V}{2D}(x-x_o)}e^{-\frac{V}{2D}(x-x_o)\xi} + \frac{M}{\theta}\frac{1}{V\xi}e^{-\frac{V}{2D}(x-x_o)}e^{-\frac{V}{2D}(x+x_o)\xi} - \frac{M}{\theta}\frac{1}{V\xi(1+\xi)}e^{-\frac{V}{2D}(x-x_o)}e^{-\frac{V}{2D}(x+x_o)\xi} \qquad \text{(A1.9)}$$

The solution of the resident concentration after inversing this Laplace transform is:

$$C^r(x,t) = \frac{1}{\sqrt{4\pi Dt}}\frac{M}{\theta}exp\left[\frac{-(x-x_o+Vt)^2}{4Dt}\right]\left\{1 + exp\left(\frac{-x_o x}{Dt}\right)\right\} - \frac{V}{2D}\frac{M}{\theta}exp\left[\frac{Vx_o}{D}\right]erfc\left[\frac{(x+x_o+Vt)}{\sqrt{4Dt}}\right] \qquad \text{(A1.10)}$$

A2. Solution of Travel Time Probability in Advection and Dispersion

The travel time probability density function $f_\tau(\tau/x)$ is described by the backward-in-time (BIT) partial differential equation:

$$\frac{\partial f_\tau}{\partial \tau} = D\frac{\partial^2 f_\tau}{\partial x^2} - V\frac{\partial f_\tau}{\partial x} \qquad \text{(A2.1)}$$

For the example in Figure 2.1, the appropriate boundary and initial conditions can be written as:

$$Vf_\tau - D\frac{\partial f_\tau}{\partial x} = V\delta(t), \ at\ x = 0 \tag{A2.2a}$$

$$f_\tau(\tau|x) = 0, \ at\ x \to \infty \tag{A2.2b}$$

$$f_\tau(\tau|x) = 0, \ for\ \tau = 0 \tag{A2.2c}$$

The Laplace transform–in–time of travel time PDF in equation (A2.1) can be rewritten as:

$$D\frac{\partial^2 \hat{f}_\tau}{\partial x^2} - V\frac{\partial \hat{f}_\tau}{\partial x} - p\hat{f}_\tau = 0 \tag{A2.3}$$

And the equation (A2.2) can be rewritten as:

$$V\hat{f}_\tau - D\frac{\partial \hat{f}_\tau}{\partial x} = V, \ at\ x = 0 \tag{A2.4a}$$

$$\hat{f}_\tau(\tau|x) = 0, \ at\ x \to \infty \tag{A2.4b}$$

The solution of the Laplace transform in time can be solved from equations (A2.3) and (A2.4):

$$\hat{f}_\tau(x,p) = \frac{2}{1+\xi} exp\left(\frac{Vx}{2D}\right) exp\left(-\frac{Vx\xi}{2D}\right) \tag{A2.5a}$$

$$\xi = \sqrt{1 + \frac{4pD}{V^2}} \tag{A2.5b}$$

After inverting the Laplace transform, the solution of the travel time PDF $f_\tau(\tau|x)$ is expressed as:

$$f_\tau(\tau|x) = \frac{V}{\sqrt{\pi D\tau}} \ exp\left[\frac{-(x-V\tau)^2}{4D\tau}\right] - \frac{V^2}{2D} exp\left[\frac{Vx}{D}\right] erfc\left[\frac{x+V\tau}{\sqrt{4D\tau}}\right] \tag{A2.6}$$

For the same example, the cumulative probability distribution of travel time, $F_\tau(\tau|x)$, is described by equation (A2.1) replacing f_τ with F_τ along boundary and initial conditions:

$$F_\tau - \frac{D}{V}\frac{\partial F_\tau}{\partial x} = 1, \ at \ x = 0 \tag{A2.7a}$$

$$F_\tau(\tau|x) = 0, \ at \ x \to \infty \tag{A2.7b}$$

$$F_\tau(\tau|x) = 0, \ for \ \tau = 0 \tag{A2.7c}$$

The Laplace transform of travel time CDF, $F_\tau(\tau|x)$, leads to:

$$D\frac{\partial^2 \hat{F_\tau}}{\partial x^2} - V\frac{\partial \hat{F_\tau}}{\partial x} - p\hat{F_\tau} = 0 \tag{A2.8}$$

Equation (A2.7) can be rewritten as:

$$V\hat{F_\tau} - D\frac{\partial \hat{F_\tau}}{\partial x} = \frac{V}{p}, \ at \ x = 0 \tag{A2.9a}$$

$$\hat{F_\tau}(\tau|x) = 0, \ at \ x \to \infty \tag{A2.9b}$$

The solution of the Laplace transform-in-time can be solved from equations (A2.8) and (A2.9):

$$\hat{F_\tau}(x,p) = \frac{2}{(1+\xi)p} exp\left(\frac{Vx}{2D}\right) exp\left(-\frac{Vx\xi}{2D}\right) \tag{A2.10a}$$

$$\xi = \sqrt{1 + \frac{4pD}{V^2}} \tag{A2.10b}$$

After inversing the Laplace transform, the solution of the travel time CDF $F_\tau(\tau|x)$ is:

$$F_\tau(\tau|x) = \frac{V\tau}{\sqrt{\pi D\tau}} \ exp\left[\frac{(x-V\tau)^2}{4D\tau}\right] + \frac{1}{2}\left\{erfc\left[\frac{(x-V\tau)}{\sqrt{4D\tau}}\right]\right\}$$

$$-\left[\frac{D + Vx + V^2\tau}{2D}\right]\left\{exp\left[\frac{Vx}{D}\right] erfc\left[\frac{(x+V\tau)}{\sqrt{4D\tau}}\right]\right\} \tag{A2.11}$$

A3. Solution of Location Probability in Advection and Dispersion

Location probability density function, $f_x(x|\tau)$ is described by the equation:

$$\frac{\partial f_x}{\partial \tau} = D\frac{\partial^2 f_x}{\partial x^2} - V\frac{\partial f_x}{\partial x} \tag{A3.1}$$

For the example in Figure 2.1, the appropriate boundary and initial conditions can be written as:

$$Vf_x - D\frac{\partial f_x}{\partial x} = 0, \quad at\ x = 0 \tag{A3.2a}$$

$$f_x(x|\tau) = 0, \quad at\ x \to \infty \tag{A3.2b}$$

$$f_x(x|\tau) = \delta(x), \quad for\ \tau = 0 \tag{A3.2c}$$

The Laplace transform-in-time of travel time PDF, $f_\tau(\tau|x)$, leads to:

$$D\frac{\partial^2 \hat{f}_x}{\partial x^2} - V\frac{\partial \hat{f}_x}{\partial x} - p\hat{f}_x + \delta(x) = 0 \tag{A3.3}$$

Equation (A3.2) can be rewritten as:

$$V\hat{f}_x - D\frac{\partial \hat{f}_x}{\partial x} = 0, \quad at\ x = 0 \tag{A3.4a}$$

$$\hat{f}_x(x,p) = 0, \quad at\ x \to \infty \tag{A3.4b}$$

The double Laplace transform-in-time-space from equations (A3.3) and (A3.4) can be written as:

$$\tilde{f}_x(s,p) = \frac{1}{D(s_2 - s_1)}\left[\frac{Ds_2\hat{f}_x(0) - 1}{s - s_2} - \frac{Ds_1\hat{f}_x(0) - 1}{s - s_1}\right] \tag{A3.5}$$

where:

$$s_1 = \frac{V}{2D}(1 - \xi); \quad s_2 = \frac{V}{2D}(1 + \xi); \quad \xi = \sqrt{1 + \frac{4pD}{V^2}} \tag{A3.6}$$

After inversing the Laplace transform-in-space, the Laplace transform in time is:

$$\hat{f}_x(x,p) = \frac{1}{D(s_2 - s_1)}\left[e^{s_2 x}(Ds_2\hat{f}_x(0) - 1) - e^{s_1 x}(Ds_1\hat{f}_x(0) - 1)\right] \tag{A3.7}$$

As $x \to \infty$, $(Ds_2\hat{f}_x(0) - 1) = 0$, so that the Laplace transform in time can be rewritten as:

$$\hat{f}_x(x,p) = \frac{1}{D(s_2 - s_1)}\left[-e^{s_1 x}\left(\frac{s_1 - s_2}{s_2}\right)\right] \tag{A3.8}$$

This can be simplified to:

$$\hat{f}_x(x,p) = \frac{2}{(1 + \xi)V} exp\left(\frac{Vx}{2D}\right) exp\left(-\frac{Vx\xi}{2D}\right) \tag{A3.9}$$

So that the solution of the location PDF is derived as:

$$f_x(x|\tau) = \frac{1}{\sqrt{\pi D\tau}}\ exp\left[\frac{-(x - V\tau)^2}{4D\tau}\right] - \frac{V}{2D} exp\left[\frac{Vx}{D}\right] erfc\left[\frac{x + V\tau}{\sqrt{4D\tau}}\right] \tag{A3.10}$$

Location cumulative distribution function, $F_x(x|\tau)$, is described by equation (A3.1), replacing f_x with F_x along boundary and initial conditions:

$$F_x(x|\tau) = 0, \ at \ x = 0 \tag{A3.11a}$$

$$F_x(x|\tau) = 0, \ at \ x \rightarrow \infty \tag{A3.11b}$$

$$F_x(x|\tau) = 1, \ for \ \tau = 0 \tag{A3.11c}$$

The Laplace transform of location CDF leads to:

$$D\frac{\partial^2 \hat{F}_x}{\partial x^2} - V\frac{\partial \hat{F}_x}{\partial x} - p\hat{F}_x + 1 = 0 \tag{A3.12}$$

The Laplace transform of equation (A3.11) can be rewritten as:

$$\hat{F}_x = 0, \ at \ x = 0 \tag{A3.13a}$$

$$\hat{F}_x(x|\tau) = 0, \ at \ x \rightarrow \infty \tag{A3.13b}$$

Solution of the Laplace transform–in–time is solved from equations (A3.12)–(A3.13) by:

$$\hat{F}_x(x,p) = \frac{1}{p} - \frac{1}{p}\left\{exp\left[\frac{Vx}{2D}\left(1 - \sqrt{1 + \frac{4Dp}{V^2}}\right)\right]\right\} \tag{A3.13}$$

which can be inversed to give the CDF:

$$F(x|t) = 1 - \frac{1}{2}\left\{erfc\left[\frac{(x-Vt)}{\sqrt{4Dt}}\right] + exp\left[\frac{Vx}{D}\right]erfc\left[\frac{(x+Vt)}{\sqrt{4Dt}}\right]\right\} \tag{A3.14}$$

A4. Solution of Resident Concentration for the Case of Non–equilibrium Sorption:

For non–equilibrium sorption, the resident concentration can be described by:

$$\frac{\partial C^r}{\partial t} + \frac{\partial C_s^r}{\partial t} = D\frac{\partial^2 C^r}{\partial x^2} + V\frac{\partial C^r}{\partial x} \tag{A4.1a}$$

$$\frac{\partial C_s^r}{\partial t} = \alpha\left[\frac{K_d \rho_b}{\theta} C^r - C_s^r\right] \tag{A4.1b}$$

The initial and boundary conditions for the example in Figure 2.1 can be expressed by:

$$\frac{\partial C^r}{\partial x} = 0 \ at \ x = 0 \tag{A4.2a}$$

$$C^r = 0, \ as \ x \rightarrow \infty \tag{A4.2b}$$

$$C^r = \frac{M}{\theta}\delta(x\text{-}x_o), \ for \ t = 0 \tag{A4.2c}$$

$$C_s^r = 0, \ \text{for } t = 0 \tag{A4.2d}$$

The double Laplace transform-in-time-space is described by:

$$\tilde{C}^r = \frac{1}{D(s_2\text{-}s_1)}\left[\frac{Ds_2\hat{C}^r(0) + V\hat{C}^r(0)\text{-}B_1e^{-x_o s}}{D(s\text{-}s_2)(s\text{-}s_1)}\right] \tag{A4.3}$$

$$s_1 = -\frac{V}{2D}(1 + \xi) \qquad s_2 = -\frac{V}{2D}(1\text{-}\xi)$$

$$\xi = \sqrt{\frac{V^2 + 4ADp}{V^2}} \qquad A = \left[1 + \frac{\varrho_b K_d \alpha}{\theta(p + \alpha)}\right]$$

$$B_1 = \frac{M}{\theta}\left[1 + \frac{\varrho_b K_d \alpha}{\theta(p + \alpha)}\right]$$

After inversing the Laplace transform-in-space, the Laplace transform-in-time is:

$$\hat{C}^r = \frac{M}{\theta}\frac{exp(s_2(x\text{-}x_o))}{V\xi}\left[1\text{-}U_{(x\text{-}x_o)}\right]\text{-}\frac{M}{\theta}\frac{exp(s_1(x\text{-}x_o))}{V\xi}\left[\frac{s_2}{s_1}exp(\frac{\text{-}V\xi x_o}{D})\text{-}U_{(x\text{-}x_o)}\right] \tag{A4.4a}$$

$$\hat{C}_s^r = \frac{\alpha K_d \varrho_b}{(\alpha + p)\theta}\hat{C}^r \tag{A4.4b}$$

$$U_{(x\text{-}x_o)} = \begin{cases} 0 \ at \ x \leq x_o \\ 1 \ at \ x > x_o \end{cases}$$

$$s_1 = -\frac{V}{2D}(1 + \xi) \qquad s_2 = -\frac{V}{2D}(1\text{-}\xi)$$

$$A = \left(1 + \frac{\varrho K_d \alpha}{\theta(p + \alpha)}\right) \qquad \xi = \sqrt{\frac{V^2 + 4ADp}{V^2}}$$

Using the inversing method of the Laplace transform in time (Toride, al et., 1993; Lindstrom and Boersma, 1989), the analytical solution of A4.4 can be written:

$$C = \frac{M}{\theta} exp(-(A_o + \alpha)t) \left\{ g_o(t) \int_0^t I_1\left[2(B_o(t-\tau)\tau)^{1/2}\right] g_o(\tau) d\tau \right\} \tag{A4.5}$$

$$g_o(t) = \frac{1}{\sqrt{4\pi Dt}} exp\left(-\frac{(x-x_o + Vt)^2}{4Dt}\right)\left\{1 + exp\left(\frac{Vx_o}{D}\right)\right\} - \frac{V}{2D} exp\left(\frac{Vx_o}{D}\right) erfc\left(\frac{x + x_o + Vt}{\sqrt{4Dt}}\right)$$

$$A_o = \frac{\varrho_b K_d \alpha}{\theta} - \alpha \qquad B_o = \frac{\varrho_b K_d \alpha}{\theta}$$

where I_1 is the Bessel function of order one.

A5. Solution of Travel Time Probability for the Case of Non-equilibrium Sorption:

For non-equilibrium sorption, the travel time PDFs can be expressed as:

$$\frac{\partial f_\tau}{\partial \tau} + \frac{\partial g_\tau}{\partial \tau} = D\frac{\partial^2 f_\tau}{\partial x^2} - V\frac{\partial f_\tau}{\partial x} \tag{A5.1a}$$

$$\frac{\partial g_\tau}{\partial \tau} = \alpha\left(\frac{\varrho_b K_d}{\theta} f_\tau - g_\tau\right) \tag{A5.1b}$$

For the example in Figure 2.1, the initial and boundary conditions in the one-dimensional domain are described by:

$$Vf_\tau - D\frac{\partial f_\tau}{\partial x} = V\delta(\tau), \ at\ x = 0 \tag{A5.2a}$$

$$f_\tau = 0, \ as\ x \to \infty \tag{A5.2b}$$

$$f_\tau = 0, \ for\ \tau = 0 \tag{A5.2c}$$

$$g_\tau = 0, \ \text{for}\ \tau = 0 \tag{A5.2d}$$

Using the Laplace transform in time of (A5.1) and (A5.2), we can obtain:

$$\hat{f}_\tau(x,p) = \frac{2exp(\frac{Vx}{2D})exp(-\frac{Vx}{2D}\xi)}{(1+\xi)} \tag{A5.3a}$$

$$\hat{g_\tau} = \frac{\alpha \varrho_b K_d}{\theta(\alpha + p)}\hat{f_t} \tag{A5.3b}$$

$$\xi = \sqrt{\frac{V^2 + 4ADp}{V^2}} \qquad A = \left[1 + \frac{\varrho_b K_d \alpha}{\theta(p+\alpha)}\right]$$

Using the reversing method of the Laplace transform (Toride, al et., 1993; Lindstrom and

Boersma, 1989), the solution of the travel time PDF can be written:

$$f_t(t|x) = exp(-(A_o + \alpha)t) \left\{ f_o(t) \int_0^t I_1\left[2(B_o(t-\tau)\tau)^{1/2}\right] f_o(\tau)d\tau \right\} \qquad \text{(A5.4)}$$

$$f_o(t) = \frac{V}{\sqrt{\pi Dt}} exp\left(-\frac{(x-Vt)^2}{4Dt}\right) - \frac{V2}{2D} exp\left(\frac{Vx}{D}\right) erfc\left(\frac{x+Vt}{\sqrt{4Dt}}\right)$$

$$A_o = \frac{\varrho_b K_d \alpha}{\theta} - \alpha \qquad\qquad B_o = \frac{\varrho_b K_d \alpha}{\theta}$$

where I_1 is the Bessel function of order one.

This thesis is accepted on behalf of the faculty
of the Institute by the following committee:

John L. Wilson

Advisor

Allan Gutjahr

Jon M. McCord

Robert S. Bowman

August 3, 1995

Date

I release this document to the New Mexico Institute of Mining and Technology.

Student's Signature

August 15, 1995

Date